UNIVERSITÄT OSNABRÜCK

Symmetry assisted exact and approximate determination of the energy spectra of magnetic molecules using irreducible tensor operators

Dissertation (kumulativ)

zur Erlangung des Grades
eines Doktors der Naturwissenschaften (Dr. rer. nat.)

dem Fachbereich Physik der Universität Osnabrück
vorgelegt von

Dipl.-Phys. Roman Schnalle

Osnabrück, im September 2009

Symmetry assisted exact and approximate determination of the energy spectra of magnetic molecules using irreducible tensor operators

Dissertation (cumulative)

Roman Schnalle*
Universität Osnabrück, Fachbereich Physik, D-49069 Osnabrück, Germany
(Dated: October 15, 2009)

In this work a numerical approach for the determination of the energy spectra and the calculation of thermodynamic properties of magnetic molecules is presented. The work is focused on the treatment of spin systems which exhibit point-group symmetries. Ring-like and archimedean-type structures are discussed as prominent examples. In each case the underlying spin quantum system is modeled by an isotropic Heisenberg Hamiltonian. Its energy spectrum is calculated either by numerical exact diagonalization or by an approximate diagonalization method introduced here. In order to implement full spin-rotational symmetry the numerical approach at hand is based on the use of irreducible tensor operators. Furthermore, it is shown how an unrestricted use of point-group symmetries in combination with the use of irreducible tensor operators leads to a reduction of the dimensionalities – a block-diagonal form of the Hamilton matrices – as well as to additional information about the physics of the systems. By exemplarily demonstrating how the theoretical foundations of the irreducible tensor operator technique can be realized within small spin systems the technical aspect of this work is covered. These considerations form the basis of the computational realization that was implemented and – in combination with high performance computing – used in order to get insight into the investigated systems.

PACS numbers: 75.10.Jm,75.50.Xx,75.40.Mg,75.50.Ee

Contents

I. Introduction 3
A. Numerical exact diagonalization 4

II. Theoretical foundations 5
A. Spin Hamiltonian of magnetic molecules 5
1. The calculation of thermodynamic observables 7
B. Irreducible tensor operator method 7
1. Coupling of angular momenta and Wigner-nJ symbols 8
2. Irreducible tensor operators 10
3. Matrix elements of irreducible tensor operators 11
C. Point-group symmetries in Heisenberg spin systems 11
D. On bipartite and frustrated spin systems 13

III. Guide to publications 15
A. Numerical exact diagonalization of archimedean-type molecules 15
1. Symmetry assisted complete evaluation of energy spectra using irreducible tensor operators 15
2. Frustration effects in antiferromagnetic molecules 15
B. Approximate diagonalization of bipartite and frustrated magnetic molecules 16

IV. Summary and conclusion 16

V. Outlook 17

Acknowledgments 17

References 18

Appendix 21

A. Realization of the irreducible tensor operator technique 21
1. The construction of basis states 21
2. The Heisenberg Hamiltonian expressed as irreducible tensor operator 22
a. Non-Heisenberg contributions to the Hamiltonian 23
3. Matrix elements - decoupling 25
4. Using point-group symmetries 26
5. The calculation of general recoupling coefficients 28
a. Binary trees 29
b. Graph theoretical solution - Yutsis graphs 31
6. Irreducible tensor operator technique and high performance computing 35

B. Pre-prints of publications 39
1. Phys. Rev. B **79**, 104419 (2009) 39
2. Cond. Mat. Phys. **12**, 331 (2009) 49
3. Polyhedron **28**, 1620 (2009) 61

I. INTRODUCTION

The synthesis of one of the first magnetic molecular compounds, Mn_{12},[4] drastically influenced the investigations of magnetic molecules. They turned from being exclusively reserved to magnetochemistry to being subject to a much broader community. No other compound than Mn_{12} has been, to such an extent, theoretically and experimentally studied throughout the years.[5,6,7,8] Nowadays, magnetic molecules serve as a common basis for scientists working in a crossover regime between chemistry, physics, and material sciences. In recent years a huge amount of magnetic molecules have been synthesized that differ in size and structure. While there exist small molecules that only contain a few interacting paramagnetic ions which are responsible for their magnetic properties, the largest magnetic molecules – built up from polyoxometalate coordination chemistry[9,10,11] – contain up to several dozens of it. From a geometrical point of view it seems that chemists are able to synthesize, starting from a huge variety of well adapted ligands, molecules that are formed as desired by theory.[12] Referring to large molecular compounds, their paramagnetic ions, i.e. spins, are often arranged in a highly symmetrical way. Some of them form ringlike structures[13,14,15,16,17] whereas a different class appears as so-called archimedean-type molecules[18,19,20], i.e. molecules in which the spins occupy the vertices of archimedean solids (cf. App. B).

The range of possible applications for magnetic molecules is widespread. Their fascinating properties have led to envisioning future applications in various fields. Magnetic molecules are promising building blocks to be used, for instance, in refrigerators[21,22,23] or displays[24], as well as in biomedicine[25,26]. By using single-molecule magnets as a representation of one bit in magnetic storage devices it would be possible to increase the storage density far beyond the superparamagnetic limit. Additionally, the field of quantum information processing was heavily influenced by magnetic molecules in the last decades. Leuenberger and Loss proposed the application of single-molecule magnets as spin qubits.[27,28,29,30] Here, recent progress was achieved by linking two ringlike molecular units via a tunable coupling that can be switched by electron paramagnetic resonance pulses.[31] Also very recently magnetic molecules gave reason to their use in molecular spintronics.[32]

Most future applications are closely related to a ground state with non-vanishing magnetic moment. Nonetheless, even if the ground-state spin vanishes due to antiferro- or ferrimagnetic couplings, magnetic molecules are still of high interest, especially for theoretical considerations. Since the intermolecular interactions are often negligible, magnetic molecules offer the possibility to investigate objects that cannot be described as single particles nor as solids. They represent mesoscopic systems that illustrate, due to their size, the transition from simple paramagnets to bulk magnets. Furthermore, with increasing size of the spin the intersection between the quantum mechanical and the classical regime becomes accessible.

As already briefly mentioned, the thermodynamic properties of magnetic molecules are determined by the non-vanishing magnetic moments of the present ions. Their moments arise from summarized contributions of unpaired electrons that are supposed to be localized at the atomic centers. Therefore, an effective modelling of magnetic molecules can be obtained by using interacting spin systems. Mostly, magnetic molecules are described by the Heisenberg model with nearest-neighbor interactions and additional anisotropy terms.[33,34] Whether the isotropic exchange of the Heisenberg term is dominant or the anisotropy terms which are often reduced to a single-ion anisotropy, is clearly dependent on the specific sample. In this context, it has been shown that very often antiferromagnetic molecules can be well described by an isotropic Heisenberg Hamiltonian.[35]

Due to the fact that magnetic molecules are described using interacting spin systems, it is not surprising that the investigations of antiferromagnetic molecules are not exclusively pushed on by means of molecular magnetism. A large impact can be ascribed to investigations that have aimed at the understanding of extended one-, two-, and three-dimensional highly frustrated systems, i.e. magnets in the more common sense. In this regard, a special importance is attached to the term *frustration* that leads to unusual magnetic properties (see Sec. II D and App. B 3). Archimedean-type molecules, for instance, can be seen as zero-dimensional realizations of the Kagomé lattice that has been studied intensively as a paradigm of highly frustrated magnetism in recent years.[36,37,38,39,40]

In general, investigating magnetic molecules corresponds to the determination of the energy spectrum – or at least parts of it – of the spin Hamiltonian that describes the system under consideration (see Sec. II A). To this end, solutions of the stationary Schrödinger equation have to be found. The determination of the energy spectrum can either be exact or approximate depending on whether additional approximations have to be introduced within the method. It is called exact if a solution can be found without further restrictive assumptions. Of course, exact solutions to a simplified spin Hamiltonian imply approximations to the original description.

There are certainly many ways to investigate molecular spin systems, analytical and numerical ones. However, analytical solutions can only be found very rarely in the field of molecular magnetism. Since the Hilbert space of the system grows exponentially with its size, i.e. the number of spins, an analytical solution can only be found if the system is small and symmetries are present.[41,42,43]

As an alternative, very powerful numerical methods have been developed in order to determine the energy spectrum of spin systems. They are in principle independent of the specific model that is used to describe a system, but, from a more global point of view, they are sometimes restricted by aspects of dimensionality or

occurring frustration. In addition, a very general restriction that is common for all methods is imposed by limited hardware resources.

Although there exist several techniques like classical spin dynamics[44,45,46] or Monte Carlo[47,48,49,50] that have contributed a lot to the understanding of magnetic molecules, only the most often used numerical techniques relying on purely quantum mechanical considerations shall be mentioned. In general, the available methods can be divided into stochastic and wavefunction-based approaches. A compact overview about diverse numerical techniques that are frequently used in the field of frustrated spin systems – either of classical or quantum mechanical nature – is given in Ref. 51.

Quantum Monte Carlo[52,53], for instance, evaluates the expectation values of certain observables by means of stochastics. It does not explicitly provide the energy spectrum or the eigenfunctions of the system. The key idea is to map the quantum mechanical partition function on a form with probabilistic interpretation.[53,54] After a proper form of the partition function has been found, the stochastic evaluation is performed. However, such a form cannot always be found. In frustrated systems negative probabilities appear which prevent the stochastic evaluation. This limitation is referred to as negative sign problem.[55]

Density matrix renormalization group[56,57] (DMRG) and numerical exact diagonalization, the latter is subject to this work, are based on the use of wavefunctions. They deliver information about the spectrum and the corresponding eigenfunctions, but they suffer from other restrictions.

In the case of DMRG, the application is more or less limited to one-dimensional systems providing only a few low-lying energy levels and eigenstates. DMRG calculations are based on a proper truncation of the Hilbert space with respect to the accuracy of a certain target state. To this end, the system is divided into two subunits, i.e. blocks. The central idea of DMRG is that calculations which are performed on a single block take information into account that has been obtained from the super block, i.e. the composition of the blocks. The number of interactions between the blocks has to be small in order to yield a reasonable convergence of the calculated energies of the whole system.[58,59] For this reason, the application of the DMRG technique to one-dimensional spin systems with nearest-neighbor interactions is favored.[60] Whenever higher-dimensional systems are investigated, they are mapped on quasi one-dimensional systems. Unfortunately, even if the initial system only includes nearest-neighbor interactions, this mapping usually results in long-range interactions and therefore in numerical limitations.

Numerical exact diagonalization is probably the most powerful technique in order to investigate magnetic molecules. It uses the unmodified Hamiltonian and is not limited to any particular class of systems. Unfortunately, if the full spectrum is to be calculated, numerical exact diagonalization can only be applied to rather small systems due to the exponential growth of the Hilbert space (see Sec. I A).

The present work therefore deals with symmetry considerations that enlarge the range of applicability of numerical exact diagonalization in the field of molecular magnetism. To this end, the underlying framework for the combined use of full spin-rotational and point-group symmetries, i.e. spin-permutational symmetry, is developed and discussed. The incorporation of point groups is particularly not restricted to special groups. In contrast, a scheme has been developed that makes a general use of point groups possible. Complementary, an approximate diagonalization is presented that also benefits from the simultaneous incorporation of spin-rotational and point-group symmetries. The reason for the investigation of ring-like and archimedean-type molecules is twofold motivated. On the one hand, it is demonstrated that with the help of the developed technique the energy spectra of those systems that have been beyond the computational limits before can now be calculated. On the other hand, the approximate diagonalization is applied in order to investigate its quality.

The determination of the complete energy spectra of large spin systems, as done in the work at hand, has only been possible with the help of irreducible tensor operators. The formulation of the spin Hamiltonian in terms of irreducible tensor operators is shown to be essential in order to reduce the dimensions of the resulting matrices to a feasible size for today's high performance computers. Within the irreducible tensor operator approach the basis is chosen such that its states reflect – a priori – full spin-rotational symmetry. As a result, the incorporation of point-group symmetries becomes a very challenging task.

This work is organized as follows. In the remaining part of Sec. I an overview of the numerical exact diagonalization technique is given. Section II provides theoretical foundations that help to understand the work which is summarized in Sec. III and has been published in Refs. 1, 2 and 3. Section IV comprises a summary of the whole work while in Sec. V a brief outlook is given. In App. A the technical details directly related to the realization of the irreducible tensor operator technique are developed. Additionally, those graph-theoretical considerations are presented that allow the incorporation of point-group symmetries. Appendix B contains pre-prints of the published articles.

A. Numerical exact diagonalization

The determination of the energy spectrum of a system described by a Hamiltonian $\underset{\sim}{H}$ corresponds to finding the solutions of the stationary Schrödinger equation

$$\underset{\sim}{H}|\phi\rangle = E|\phi\rangle \ , \tag{1}$$

where E refers to the energy eigenvalue of the eigenstate $|\phi\rangle$ of $\underset{\sim}{H}$. Finding these solutions is equivalent to finding a diagonal matrix representation of $\underset{\sim}{H}$. The elements of a general, non-diagonal Hamilton matrix $\mathbf{H}$ are given by $H_{ij} = \langle i|\underset{\sim}{H}|j\rangle$ where the states $|i\rangle$ with $i = 1, \ldots, \dim \mathcal{H}$ form a basis of the corresponding Hilbert space $\mathcal{H}$.

Now, a diagonal form of $\mathbf{H}$ can be found by a unitary transformation according to

$$\mathbf{H}_{\text{diag}} = \mathbf{U}^{\dagger}\mathbf{H}\mathbf{U} \ . \tag{2}$$

The columns of the matrix $\mathbf{U}$ then represent the eigenvectors, i.e. eigenstates of $\mathbf{H}$, and the diagonal elements of $\mathbf{H}_{\text{diag}}$ the corresponding eigenvalues. If the determination of $\mathbf{U}$ and $\mathbf{H}_{\text{diag}}$ is performed numerically, the method is referred to as *numerical exact diagonalization*. In this case the obtained eigenvectors and eigenvalues are exact with respect to the numerical precision of floating-point operations that is influenced by the computer architecture the calculations are performed on.

Irrespective of the particular choice of the basis, the total dimension of the Hilbert space for a system of N identical spins s is $\dim \mathcal{H} = (2s+1)^N$. As one can see, the dimension grows exponentially with the number of participating spins. Without further reduction for larger systems, this immediately restricts the possibility of exactly calculating the full energy spectrum of the Hamiltonian. A reduction of the dimension can be achieved by block-factorizing the Hamilton matrix. Due to missing transition elements, each block can then be diagonalized separately (cf. Sec. II B 1). The possible factorization of the Hamilton matrix results from the invariance of the Hamiltonian under certain symmetry operations. An extensive description of the role of symmetries in Heisenberg spin systems is given throughout this work. It should be mentioned here that an appropriate choice of the basis, which takes the symmetries of the Hamiltonian into account, leads to a block-diagonal form of the Hamilton matrix without further calculations (see App. A 1).

Having calculated the complete energy spectrum of the Hamiltonian by means of a numerical exact diagonalization, all spectroscopic, dynamic, and thermodynamic properties can be obtained, irrespective of the temperature (cf. Sec. II A 1). However, sometimes only the low-temperature behavior of the system is of interest. In this case, the whole spectrum does not need to be calculated since only a few low-lying energy levels are thermally populated. Algorithms performing the evaluation of these low-lying eigenvalues together with the respective eigenstates have been developed by Lanczos[61] as well as Davidson[62] and can be found in various linear algebra packages. Using these algorithms molecular systems can be investigated that contain up to 10^9 states.

Nevertheless, in the work at hand the term numerical exact diagonalization always refers to the evaluation of the complete energy spectrum of the system because the field and temperature dependence of thermodynamic observables up to room temperature is investigated.

II. THEORETICAL FOUNDATIONS

This section deals with a brief overview of the theoretical background which is required for a complete understanding of the papers described in Sec. III and listed in App. B.

A. Spin Hamiltonian of magnetic molecules

The research field of molecular magnetism deals with the investigation of the magnetic properties of chemical compounds composed of a number of ions that reaches from only a few up to dozens of it. For the modelling of the molecule, at least, it does not play any role how the chemical compound looks like in detail. Furthermore, only those ions are taken into account which possess unpaired electrons and thus a non-vanishing magnetic moment. Since the molecules which come up in the form of a crystal or powder sample are often quite well separated from each other by their ligands, inter-molecular interactions can be neglected in most cases. Additionally, the electrons can usually be seen as being localized so that both features lead to a simplified sketch of the chemical compound, namely a spin system. The interactions between different spins of the system then depend of course on the chemical surrounding and stem from direct exchange or super-exchange[63] via chemical bridges.

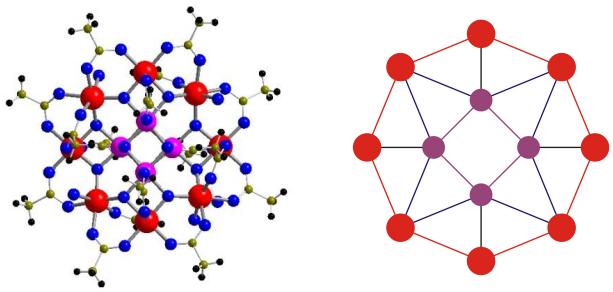

FIG. 1: Simplification of the chemical structure of the Mn_{12} compound (l.h.s., picture taken from Ref. 64) to the corresponding spin system for the same molecule (r.h.s.). The different colorings of the edges refer to possibly different exchange parameters extracted from the chemical structure.

Figure 1 shows such a simplification for the Mn_{12} compound the investigation of which stimulated the whole research field of molecular magnetism.

A general Hamiltonian that models magnetic molecules could be

$$\underset{\sim}{H} = \underset{\sim}{H}_{\text{exchange}} + \underset{\sim}{H}_{\text{Zeeman}} \ , \tag{3}$$

where, to be more specific, in a system of N spins, i.e.

$i, j = 1, \ldots, N$, the two terms take the forms

$$\underset{\sim}{H}_{\text{exchange}} = \sum_{i,j} \underset{\sim}{\mathbf{s}}(i) \cdot \mathbf{J}_{ij} \cdot \underset{\sim}{\mathbf{s}}(j) \ , \tag{4}$$

$$\underset{\sim}{H}_{\text{Zeeman}} = g\mu_B \underset{\sim}{\mathbf{S}} \cdot \vec{B} \ . \tag{5}$$

$\underset{\sim}{H}_{\text{exchange}}$ describes the exchange interaction between two single-spin vector operators $\underset{\sim}{\mathbf{s}}(i)$ and $\underset{\sim}{\mathbf{s}}(j)$.[34] The quantity $\mathbf{J}_{ij}$ is a second rank cartesian tensor containing the corresponding exchange parameters. $\underset{\sim}{H}_{\text{Zeeman}}$ couples the total spin $\underset{\sim}{\mathbf{S}} = \sum_i \underset{\sim}{\mathbf{s}}(i)$ to an external magnetic field $\vec{B}$. In general, the coupling to an external field could be anisotropic, but here it is assumed to be well described by an isotropic term.

Now, the exchange term in Eq. (4) can be transformed into a more familiar form by decomposing the tensor $\mathbf{J}_{ij}$ into irreducible cartesian tensors.[65] This decomposition yields

$$\underset{\sim}{H}_{\text{exchange}} = \underset{\sim}{H}_{\text{Heisenberg}} + \underset{\sim}{H}_{\text{antisymmetric}} + \underset{\sim}{H}_{\text{anisotropy}}$$

with the resulting terms given by

$$\underset{\sim}{H}_{\text{Heisenberg}} = -\sum_{i,j} J_{ij} \underset{\sim}{\mathbf{s}}(i) \cdot \underset{\sim}{\mathbf{s}}(j) \ , \tag{6}$$

$$\underset{\sim}{H}_{\text{antisymmetric}} = \sum_{i,j} \vec{G}_{ij} \cdot [\underset{\sim}{\mathbf{s}}(i) \times \underset{\sim}{\mathbf{s}}(j)] \ , \tag{7}$$

$$\underset{\sim}{H}_{\text{anisotropy}} = \sum_{i,j} \underset{\sim}{\mathbf{s}}(i) \cdot \mathbf{D}_{ij} \cdot \underset{\sim}{\mathbf{s}}(j) \ . \tag{8}$$

Here, $\vec{G}_{ij}$ is a vector containing the antisymmetric exchange parameters[66] and $[\underset{\sim}{\mathbf{s}}(i) \times \underset{\sim}{\mathbf{s}}(j)]$ is a vector product. $\mathbf{D}_{ij}$ is a traceless symmetric tensor that describes anisotropic exchange between the interacting spin components. In general, commutation relations of $\underset{\sim}{H}_{\text{anisotropy}}$ and $\underset{\sim}{H}_{\text{antisymmetric}}$ with $\underset{\sim}{S}^z$ and $\underset{\sim}{\mathbf{S}}^2$ do not hold leading to a loss of good quantum numbers S and M. In contrast, the Heisenberg Hamiltonian in Eq. (6) is completely isotropic. The interaction strength for each pair of spins is given by the coupling constant J_{ij} with $J_{ij} < 0$ referring to an antiferromagnetic and $J_{ij} > 0$ to a ferromagnetic coupling.

For the sake of completeness, it has to be mentioned that the anisotropic exchange in Eq. (8) contains a contribution that is referred to as single-ion anisotropy. With $i = j$ and $\mathbf{D}_{ii}$ in diagonal form in a local frame, Eq. (8) turns into

$$\begin{aligned} \underset{\sim}{H}_{\text{single-ion}} = \sum_i \Bigg\{ & D_i \left[\left(\underset{\sim}{\mathbf{s}}^{z'}(i)\right)^2 - \frac{1}{3}\underset{\sim}{\mathbf{s}}^2(i) \right] \\ & + E_i \left[\left(\underset{\sim}{\mathbf{s}}^{x'}(i)\right)^2 - \left(\underset{\sim}{\mathbf{s}}^{y'}(i)\right)^2 \right] \Bigg\} \ , \end{aligned} \tag{9}$$

where the right hand side of the equation is quadratic in the spin operators.[67] In Eq. (9) a slightly simplified form is given with only two independent parameters $D_i = D_{ii}^{z'z'} - 1/2(D_{ii}^{x'x'} + D_{ii}^{y'y'})$ and $E_i = 1/2(D_{ii}^{x'x'} - D_{ii}^{y'y'})$. Here, the condition $|D_i| > |E_i|$ defines the local z'-direction that is pointing along the major principal axis.

Up to now the description of magnetic molecules was chosen to be of a rather general kind. However, molecular systems are often modeled using assumptions that simplify the Hamiltonian of the system drastically, i.e. reduce the parameter space one has to work in, in order to compare theoretical and experimental results. In this work any interaction within the Hamilton operator leading to anisotropy is not considered. This work exclusively focuses on the investigation of systems which can be described by the isotropic Heisenberg Hamiltonian of Eq. (6).

The commutators of the square of the total spin $\underset{\sim}{\mathbf{S}}$ and its z-component $\underset{\sim}{S}^z$ with $\underset{\sim}{H}_{\text{Heisenberg}}$ vanish, i.e

$$\left[\underset{\sim}{H}_{\text{Heisenberg}}, \underset{\sim}{S}^z\right] = 0 \ , \quad \left[\underset{\sim}{H}_{\text{Heisenberg}}, \underset{\sim}{\mathbf{S}}^2\right] = 0 \ . \tag{10}$$

Additionally regarding $\left[\underset{\sim}{\mathbf{S}}^2, \underset{\sim}{S}^z\right] = 0$ the total magnetic quantum number M and the quantum number of the total spin S serve as good quantum numbers and a simultaneous eigenbasis of $\underset{\sim}{S}^z$, $\underset{\sim}{\mathbf{S}}^2$ and $\underset{\sim}{H}_{\text{Heisenberg}}$ can be found.

A well adapted basis is then given by states of the form $|\alpha\, S\, M\rangle$ which can be constructed according to a vector-coupling scheme (see App. A 1). These states are already eigenstates of $\underset{\sim}{\mathbf{S}}^2$ and $\underset{\sim}{S}^z$ and α denotes a set of additional quantum numbers resulting from the coupling of the single spins $\underset{\sim}{\mathbf{s}}(i)$ to the total spin $\underset{\sim}{\mathbf{S}}$.

Due to Eqs. (10) the matrix elements of the Heisenberg Hamiltonian $\langle \alpha'\, S'\, M' | \underset{\sim}{H}_{\text{Heisenberg}} | \alpha\, S\, M \rangle$ between states with different S and M vanish, leading to a block-factorized Hamilton matrix in which each block can be diagonalized separately. In the case of absent anisotropies the field dependence of the energies induced by the Zeeman term in Eq. (5) can easily be added without further complicate calculations. This is because the external field can always be defined to point in the z-direction, so that the Zeeman term commutes with $\underset{\sim}{H}_{\text{Heisenberg}}$, $\underset{\sim}{\mathbf{S}}^2$ and $\underset{\sim}{S}^z$. Then M still serves as a good quantum number, and the effect of the external field $\vec{B} = B \cdot \vec{e}^z$ on eigenstates of $\underset{\sim}{H}_{\text{Heisenberg}}$ results in a simple field dependence of the energy eigenvalues E_i according to

$$E_i(B) = E_i + g\mu_B B M_i \ . \tag{11}$$

This way thermodynamical properties depending on the temperature T and the external magnetic field $\vec{B}$ can easily be calculated from the energy spectrum of the investigated magnetic molecule once the energies E_i are known.

Since the systems which are investigated exhibit a highly symmetric chemical structure which is also reflected in the corresponding spin system, the Heisenberg

Hamiltonian further simplifies to

$$\underset{\sim}{H}_{\text{Heisenberg}} = -J \sum_{<i,j>} \underset{\sim}{\mathbf{s}}(i) \cdot \underset{\sim}{\mathbf{s}}(j) \ . \tag{12}$$

The summation is running over pairs $< i, j >$ of nearest neighbors of single-spin vector operators $\underset{\sim}{\mathbf{s}}$ at sites i and j counting each pair only once. Since the exchange parameter J is assumed to be the same for every spin-spin interaction, Eq. (12) is a special case of Eq. (6) with $J_{ij} = J \ \forall < i, j >$. The systems investigated in the papers of App. B all represent antiferromagnetic molecules, and thus for the exchange parameter $J < 0$ is assumed.

1. *The calculation of thermodynamic observables*

In this section basic formulas for the thermodynamic observables calculated in the papers of App. B shall be given. Throughout this work all systems are modeled using an isotropic Heisenberg Hamiltonian. As already mentioned, defining the external field to point in the z-direction results in a simultaneous eigenbasis $\{|\phi_i\rangle\}$ of $\underset{\sim}{H}_{\text{Heisenberg}}$ and $\underset{\sim}{H}_{\text{Zeeman}}$ with energy eigenvalues of $\underset{\sim}{H} = \underset{\sim}{H}_{\text{Heisenberg}} + \underset{\sim}{H}_{\text{Zeeman}}$ given by Eq. (11).

Assuming thermal equilibrium, the expectation value of a general observable $\underset{\sim}{O}$ is given by the Boltzmann statistics of the canonical ensemble and takes the form

$$\langle \underset{\sim}{O} \rangle = \frac{1}{Z(T,B)} \operatorname{Tr}\left\{ \underset{\sim}{O} e^{-\beta \underset{\sim}{H}} \right\} \ , \tag{13}$$

where $\beta = 1/(k_{\text{B}}T)$ and Z is known as the partition function. The partition function is defined as

$$Z(T,B) = \operatorname{Tr}\left\{ e^{-\beta \underset{\sim}{H}} \right\} = \sum_i e^{-\beta E_i(B)} \ , \tag{14}$$

with the trace being taken over eigenstates $|\phi_i\rangle$ of $\underset{\sim}{H}$ in order to find an expression for Z as a sum containing the field-dependent energy eigenvalues $E_i(B)$ of Eq. (11).

The magnetization of a molecule is proportional to the expectation value of the magnetic moment, i.e. for $\vec{B} = B \cdot \vec{e}^{\,z}$ it depends on $\langle \underset{\sim}{S}^z \rangle$. This relationship results in the expression

$$\begin{aligned} M(T,B) &= -g\mu_{\text{B}} \langle \underset{\sim}{S}^z \rangle \\ &= -\frac{g\mu_{\text{B}}}{Z} \operatorname{Tr}\left\{ \underset{\sim}{S}^z e^{-\beta \underset{\sim}{H}} \right\} \\ &= -\frac{g\mu_{\text{B}}}{Z} \sum_i M_i \ e^{-\beta E_i(B)} \ . \end{aligned} \tag{15}$$

Here, it was used that both, the Hamiltonian $\underset{\sim}{H}$ as well as the z-component of the total spin $\underset{\sim}{S}^z$, take diagonal form if represented within the basis $\{|\phi_i\rangle\}$.

The magnetic susceptibility is now given by

$$\begin{aligned} \chi(T,B) &= \frac{\partial M(T,B)}{\partial B} \\ &= -g\mu_{\text{B}} \frac{\partial}{\partial B} \langle \underset{\sim}{S}^z \rangle \\ &= (g\mu_{\text{B}})^2 \beta \left(\langle (\underset{\sim}{S}^z)^2 \rangle - \langle \underset{\sim}{S}^z \rangle^2 \right) \\ &= (g\mu_{\text{B}})^2 \beta \left\{ \frac{1}{Z} \sum_i M_i^2 \ e^{-\beta E_i(B)} \right. \\ &\qquad \left. - \left(\frac{1}{Z} \sum_i M_i \ e^{-\beta E_i(B)} \right)^2 \right\} \ . \end{aligned} \tag{16}$$

While the magnetization and the magnetic susceptibility are evaluated using the first and the second moment of $\underset{\sim}{S}^z$, the internal energy $U(T,B)$ as well as the specific heat $C(T,B)$ are deduced from the first and the second moment of the Hamiltonian $\underset{\sim}{H}$. They take a very similar form, yielding, although not evaluated in the papers listed in App. B, for the internal energy

$$\begin{aligned} U(T,B) &= \langle \underset{\sim}{H} \rangle \\ &= \frac{1}{Z} \sum_i E_i(B) \ e^{-\beta E_i(B)} \end{aligned} \tag{17}$$

and for the specific heat

$$\begin{aligned} C(T,B) &= \frac{\partial U(T,B)}{\partial T} \\ &= \frac{1}{k_{\text{B}}T^2} \left\{ \frac{1}{Z} \sum_i (E_i(B))^2 \ e^{-\beta E_i(B)} \right. \\ &\qquad \left. - \left(\frac{1}{Z} \sum_i E_i(B) \ e^{-\beta E_i(B)} \right)^2 \right\} \ . \end{aligned} \tag{18}$$

B. Irreducible tensor operator method

The determination of the matrix elements of the Heisenberg Hamiltonian is achieved with the help of irreducible tensor operators throughout this work. To this end, it is necessary to reformulate the spin vector-operators in terms of irreducible tensor operators and to subsequently use tensorial algebra. In this regard the underlying theory is clearly based on group as well as representation theory. At this point it would probably not make sense to introduce all group-theoretical tools which lead to a complete understanding of the technical implementations in the papers of App. B. Several textbooks provide deep knowledge about these topics and the author would like to refer to those.[65,68,69,70,71,72] Nevertheless, at least the origin of appearing concepts and formulations shall be explained with an existing fundamental understanding of abstract group and representation theory being assumed.

1. Coupling of angular momenta and Wigner-nJ symbols

As a first step the coupling of two general angular momenta $\underset{\sim}{\mathbf{j}}_1$ and $\underset{\sim}{\mathbf{j}}_2$ shall be discussed. Regarding this, the work at hand mainly refers to the use of definitions and name conventions that have been introduced by Wigner.[68]

The vector coupling rule for the addition of angular momentum, known from elementary atomic physics, states that the resulting angular momenta $\underset{\sim}{\mathbf{J}}$ can be characterized by a quantum number J. J assumes all values

$$|j_1 - j_2|, |j_1 - j_2| + 1, \ldots, j_1 + j_2 - 1, j_1 + j_2 \ , \qquad (19)$$

where j_1 and j_2 denote the quantum numbers of the angular momenta $\underset{\sim}{\mathbf{j}}_1$ and $\underset{\sim}{\mathbf{j}}_2$. Equation (19) is also referred to as triangular condition for the coupling of two angular momenta.

From a group-theoretical point of view the eigenstates $|j\,m\rangle$ of $\underset{\sim}{j}^z$ and $\underset{\sim}{\mathbf{j}}^2$ span a $(2j+1)$-dimensional irreducible representation $D^{(j)}$ of the group R_3, i.e. the group of all rotations within three-dimensional space. Keeping this in mind, the above vector addition rule Eq. (19) is equivalent to

$$D^{(j_1)} \otimes D^{(j_2)} = \sum_{J=|j_1-j_2|}^{j_1+j_2} D^{(J)} \ . \qquad (20)$$

According to this equation, the direct product between two irreducible representations of the dimensions $(2j_1 + 1)$ and $(2j_2 + 1)$, which is in general reducible, decays into $(2J+1)$-dimensional irreducible representations with respect to J.

Now, the operators $\underset{\sim}{D}^{(j_1)}(R)$ and $\underset{\sim}{D}^{(j_2)}(R)$ are considered that are associated with an arbitrary coordinate rotation R of R_3 and operate in the Hilbert spaces spanned by $|j_1\,m_1\rangle$ and $|j_2\,m_2\rangle$. What does Eq. (20) mean to the direct product $\mathbf{D}^{(j_1)}(R) \otimes \mathbf{D}^{(j_2)}(R)$ of the corresponding matrix representations? The product can be transformed into a block-diagonal form $\mathbf{U}(R)$ by a unitary matrix $\mathbf{A}$, i.e.

$$\mathbf{D}^{(j_1)}(R) \otimes \mathbf{D}^{(j_2)}(R) = \mathbf{A}^\dagger \mathbf{U}(R) \mathbf{A} \ , \qquad (21)$$

where $\mathbf{U}(R)$ has the form

$$\mathbf{U}(R) = \begin{bmatrix} \mathbf{D}^{(|j_1-j_2|)}(R) & \mathbf{0} & \ldots & \mathbf{0} \\ \mathbf{0} & \mathbf{D}^{(|j_1-j_2|+1)}(R) & \ldots & \mathbf{0} \\ \vdots & \vdots & \ldots & \vdots \\ \mathbf{0} & \mathbf{0} & \ldots & \mathbf{D}^{(j_1+j_2)}(R) \end{bmatrix} .$$

The matrices $\mathbf{D}^{(J)}(R)$ appearing therein comprise matrix elements with respect to those functions that span the irreducible representations $D^{(J)}$ in Eq. (20).

The determination of the elements of the transformation matrix $\mathbf{A}$ has been a central task in the theory of group representations. The elements of $\mathbf{A}$ are the so-called *Clebsch-Gordan coefficients* $C^{j_1\,j_2\,J}_{m_1\,m_2\,M}$. They appear in a more familiar form as scalar products between a state of the form $|j_1\,j_2\,J\,M\rangle$ and the product states $|j_1\,m_1\,j_2\,m_2\rangle$ leading to the decomposition

$$\begin{aligned} |j_1\,j_2\,J\,M\rangle &= \sum_{m_1,m_2} \langle j_1\,m_1\,j_2\,m_2 | j_1\,j_2\,J\,M\rangle \, |j_1\,m_1\,j_2\,m_2\rangle \\ &= \sum_{m_1,m_2} C^{j_1\,j_2\,J}_{m_1\,m_2\,M} |j_1\,m_1\,j_2\,m_2\rangle \ . \end{aligned} \qquad (22)$$

The Clebsch-Gordan coefficients therefore relate two different orthonormal sets of basis vectors. It should be emphasized that these sets are obviously not orthogonal to each other because they span the same space. The Clebsch-Gordan coefficients are non-zero only if the vector addition rule from Eq. (19) and simultaneously the equation $m_1 + m_2 = M$ hold. A very important symmetry of the Clebsch-Gordan coefficients is

$$C^{j_1\,j_2\,J}_{m_1\,m_2\,M} = (-1)^{j_1+j_2-J} C^{j_2\,j_1\,J}_{m_2\,m_1\,M} \ , \qquad (23)$$

with $(-1)^{j_1+j_2-J} = \pm 1$ according to Eq. (19).

In order to reveal the symmetry properties of the Clebsch-Gordan coefficients, they are reformulated in a straightforward manner. A proper reformulation leads to the *Wigner coefficients* or *Wigner-3J symbols*

$$\begin{pmatrix} j_1 & j_2 & J \\ m_1 & m_2 & M \end{pmatrix} ,$$

which are related to the Clebsch-Gordan coefficients by

$$\begin{pmatrix} j_1 & j_2 & J \\ m_1 & m_2 & M \end{pmatrix} = (-1)^{j_1-j_2-M} (2J+1)^{-\frac{1}{2}} \, C^{j_1\,j_2\,J}_{m_1\,m_2\,-M} \ . \qquad (24)$$

The relation between Clebsch-Gordan coefficients and the Wigner-3J symbols from Eq. (24) directly leads to non-zero values of the Wigner-3J symbols only if $m_1 + m_2 + M = 0$ holds and the vector addition rule from Eq. (19) is fulfilled.

Expressed in terms of Wigner-3J symbols the symmetry property of the Clebsch-Gordan coefficients given in Eq. (23) takes the form

$$\begin{pmatrix} j_1 & j_2 & J \\ m_1 & m_2 & M \end{pmatrix} = (-1)^{j_1+j_2+J} \begin{pmatrix} j_2 & j_1 & J \\ m_2 & m_1 & M \end{pmatrix} \ . \qquad (25)$$

Thus, the Wigner-3J symbols are invariant under an even number of permutations of the columns whereas under a single permutation they obey Eq. (25). A further evaluation of the symmetry properties of the Clebsch-Gordan coefficients yields an additional symmetry of the Wigner-3J symbols, i.e.

$$\begin{pmatrix} j_1 & j_2 & J \\ m_1 & m_2 & M \end{pmatrix} = (-1)^{j_1+j_2+J} \begin{pmatrix} j_1 & j_2 & J \\ -m_1 & -m_2 & -M \end{pmatrix} \ . \qquad (26)$$

So far the coupling of only two angular momenta has been considered. A procedure similar to the one which has led to the Wigner-3J symbols now leads to the occurence of *Wigner-6J symbols*. In the case of a coupling of three angular momenta, $\underset{\sim}{\mathbf{J}} = \underset{\sim}{\mathbf{j}}_1 + \underset{\sim}{\mathbf{j}}_2 + \underset{\sim}{\mathbf{j}}_3$, a basis can be constructed in which the representations of the operators $\underset{\sim}{\mathbf{J}}^2$ and $\underset{\sim}{J}^z$ as well as $\underset{\sim}{\mathbf{j}}_1^2$, $\underset{\sim}{\mathbf{j}}_2^2$, and $\underset{\sim}{\mathbf{j}}_3^2$ are diagonal. Obviously, there exists a certain freedom of choice in the construction of this basis. The resulting $\underset{\sim}{\mathbf{J}}$ can be constructed in three different ways, namely

$$\underset{\sim}{\mathbf{J}} = (\underset{\sim}{\mathbf{j}}_1 + \underset{\sim}{\mathbf{j}}_2) + \underset{\sim}{\mathbf{j}}_3 \ , \tag{27}$$

$$\underset{\sim}{\mathbf{J}} = \underset{\sim}{\mathbf{j}}_1 + (\underset{\sim}{\mathbf{j}}_2 + \underset{\sim}{\mathbf{j}}_3) \ , \tag{28}$$

$$\underset{\sim}{\mathbf{J}} = (\underset{\sim}{\mathbf{j}}_1 + \underset{\sim}{\mathbf{j}}_3) + \underset{\sim}{\mathbf{j}}_2 \ . \tag{29}$$

This leads to three different basis sets, each with the square of one of the operators $\underset{\sim}{\mathbf{j}}' = \underset{\sim}{\mathbf{j}}_1 + \underset{\sim}{\mathbf{j}}_2$, $\underset{\sim}{\mathbf{j}}'' = \underset{\sim}{\mathbf{j}}_2 + \underset{\sim}{\mathbf{j}}_3$, and $\underset{\sim}{\mathbf{j}}''' = \underset{\sim}{\mathbf{j}}_1 + \underset{\sim}{\mathbf{j}}_3$ given in a diagonal form. The matrix elements of the unitary transformation matrix which connects two of these sets of basis states can be found as scalar products between states belonging to two different *coupling schemes*. Expressing a state belonging to a coupling scheme resulting from a coupling according to Eq. (27) in terms of states belonging to the scheme resulting from Eq. (28) yields

$$\begin{aligned} &|j_1\, j_2\, j_{12}\, j_3\, J\, M\rangle = \\ &\sum_{j_{23}} \langle j_1\, j_2\, j_3\, j_{23}\, J | j_1\, j_2\, j_{12}\, j_3\, J\rangle\, |j_1\, j_2\, j_3\, j_{23}\, J\, M\rangle \ , \end{aligned} \tag{30}$$

with the quantum numbers j_{12} and j_{23} referring to $\underset{\sim}{\mathbf{j}}'^2$ and $\underset{\sim}{\mathbf{j}}''^2$, respectively.

Scalar products of the kind found in Eq. (30) – often called *recoupling coefficients* – are independent of any magnetic quantum number. They can be evaluated by decomposing the vector-coupling states into a sum of product states with the help of an extended version of Eq. (22). For example, the decomposition of the ket on the left hand side of the aforementioned recoupling coefficients yields

$$\begin{aligned} &|j_1\, j_2\, j_3\, j_{23}\, J\, M\rangle = \\ &\sum_{m_1, m_2, m_3} \langle j_1\, m_1\, j_2\, m_2\, j_3\, m_3 | j_1\, j_2\, j_3\, j_{23}\, J\, M\rangle \\ &\qquad \times |j_1\, m_1\, j_2\, m_2\, j_3\, m_3\rangle \ . \end{aligned} \tag{31}$$

The scalar products in Eq. (31), i.e. the matrix elements of the transformation matrix that connects the vector-coupling state with the product states, are called in analogy to the former name convention *generalized Clebsch-Gordan coefficients* $C^{j_1\, j_2\, j_3\, j_{23}\, J}_{m_1\, m_2\, m_3\, m_{23}\, M}$ for the coupling of three angular momenta. They can be simplified to a product of Clebsch-Gordan coefficients according to

$$C^{j_1\, j_2\, j_3\, j_{23}\, J}_{m_1\, m_2\, m_3\, m_{23}\, M} = \sum_{m_{23}} C^{j_2\, j_3\, j_{23}}_{m_2\, m_3\, m_{23}} \cdot C^{j_1\, j_{23}\, J}_{m_1\, m_{23}\, M} \ . \tag{32}$$

As one can see, generating generalized Clebsch-Gordan coefficients for the coupling of more than three angular momenta and – in addition – an expression of it in terms of Clebsch-Gordan coefficients is then a straightforward task. Here it should be mentioned that according to Eq. (32) generalized Clebsch-Gordan coefficients can also be expressed as a sum over products of Wigner-3J symbols using the relation from Eq. (24). Coefficients of this kind are then called *generalized Wigner coefficients* (cf. A 5 b).[73]

The recoupling coefficients that appear in Eq. (30) can now be reformulated in terms of Wigner-6J symbols in order to reveal their symmetry properties. For the transition between the basis sets belonging to j_{12} and j_{23} the corresponding Wigner-6J symbol is related to the recoupling coefficient by[68]

$$\begin{aligned} &\begin{Bmatrix} j_1 & j_2 & j_{12} \\ j_3 & J & j_{23} \end{Bmatrix} = (-1)^{j_1+j_2+j_3+J} (2j_{12}+1)^{-\frac{1}{2}} \\ &\quad \times (2j_{23}+1)^{-\frac{1}{2}} \langle j_1\, j_2\, j_3\, j_{23}\, J | j_1\, j_2\, j_{12}\, j_3\, J\rangle \ . \end{aligned} \tag{33}$$

Equations (31) and (32) directly show that a Wigner-6J symbol can be expressed as a sum over products of Clebsch-Gordan coefficients or, by using Eq. (24), over products of Wigner-3J symbols.

For the sake of completeness, also the Wigner-9J symbols[68] shall be given which result as elements of the transition matrices when recoupling four angular momenta. For example the transition between two different sets of basis states yields a Wigner-9J symbol like

$$\begin{aligned} &\begin{pmatrix} j_1 & j_2 & j_{12} \\ j_3 & j_4 & j_{34} \\ j_{13} & j_{24} & J \end{pmatrix} = \\ &[(2j_{12}+1)(2j_{34}+1)(2j_{13}+1)(2j_{24}+1)]^{-\frac{1}{2}} \\ &\quad \times \langle j_1\, j_2\, j_{12}\, j_3\, j_4\, j_{34}\, J | j_1\, j_3\, j_{13}\, j_2\, j_4\, j_{24}\, J\rangle \ . \end{aligned} \tag{34}$$

A very comprehensive overview of algebraic expressions for Wigner-nJ symbols as well of their symmetry properties is given in Ref. 74. Regarding the use of Wigner symbols in connection with irreducible tensor operators, here only a graphical visualization of the triangular conditions for a Wigner-6J symbol is shown. The Wigner-6J symbol is nonzero only if for certain triads of quantum numbers the triangular condition (Eq. (19)) holds. For which combination of quantum numbers of angular momenta the triangular condition has to be valid in order to yield a nonzero Wigner-6J symbol, is visualized graphically in Fig. 2.

Since a Wigner-9J symbol can be written as a sum over products of Wigner-6J symbols[74], these triangular conditions play an important role in reducing the computational effort when matrix elements of the Heisenberg Hamiltonian are calculated using irreducible tensor operators.

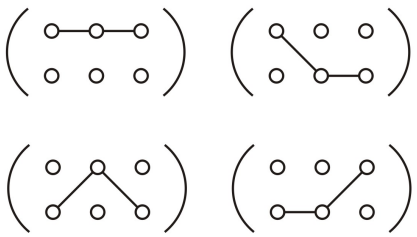

FIG. 2: Graphical visualization of the four triangular conditions occurring in a Wigner-6J symbol which have to be valid in order to yield a nonzero result.

2. *Irreducible tensor operators*

An irreducible tensor operator $\underset{\sim}{\mathbf{T}}^{(k)}$ of rank k is defined by the transformation properties of its components q under a general coordinate rotation R according to

$$\underset{\sim}{D}(R)\underset{\sim}{T}_q^{(k)}\underset{\sim}{D}^{-1}(R) = \sum_{q'} \underset{\sim}{T}_{q'}^{(k)} D_{qq'}^{(k)}(R) \ . \tag{35}$$

Here $\underset{\sim}{D}(R)$ again denotes the operator associated with the coordinate rotation R. The subscripts q as well as q' take the values $-k, -k+1, \ldots, k$. By $D_{qq'}^{(k)}(R)$ the matrix elements of the previously (Eq. (21)) used matrices $\mathbf{D}^{(k)}(R)$ – also called *Wigner rotation matrices* – are denoted.

The case $k = 0$ in Eq. (35) directly leads to what is called a *scalar operator*. As can easily be seen, a scalar operator is invariant under coordinate rotation, i.e. with $D_{00}^{(0)}(R) = 1$

$$\begin{aligned} \underset{\sim}{D}(R)\underset{\sim}{T}^{(0)}\underset{\sim}{D}^{-1}(R) &= \underset{\sim}{T}^{(0)} D_{00}^{(0)}(R) \\ &= \underset{\sim}{T}^{(0)} \ . \end{aligned} \tag{36}$$

In analogy to the states which span the irreducible representation $D^{(1)}$ of R_3 and which are said to behave under coordinate rotations like the components of a vector the irreducible tensor operator $\underset{\sim}{\mathbf{T}}^{(1)}$ is called a *vector operator*. For example, the components of a first-rank irreducible tensor operator $\underset{\sim}{\mathbf{s}}^{(1)}$ derived from the cartesian components of the spin vector operator are given by

$$\begin{aligned} \underset{\sim}{s}_0^{(1)} &= \underset{\sim}{s}^z \ , \\ \underset{\sim}{s}_{\pm 1}^{(1)} &= \mp\sqrt{\frac{1}{2}}\left(\underset{\sim}{s}^x \pm i\underset{\sim}{s}^y\right) \ . \end{aligned} \tag{37}$$

Stressing the analogy between the behavior of states and irreducible tensor operators under coordinate rotations, the role of the components $\underset{\sim}{T}_q^{(k)}$ in Eq. (35) has to be specified. The components of the irreducible tensor operator $\underset{\sim}{\mathbf{T}}^{(k)}$ of rank k serve as a basis and therefore span the $(2k+1)$-dimensional irreducible representation $D^{(k)}$ of the rotation group R_3.

For comparison, consider a group $\mathcal{G}$ and its irreducible representations $\Gamma(\mathcal{G})$. The direct product of the irreducible representations $\Gamma^{(i)}$ and $\Gamma^{(j)}$ separately spanned by two sets of basis vectors is given by $\Gamma^{(i)} \otimes \Gamma^{(j)}$. It is reducible (cf. Eq. (20)) if linear combinations of the product functions can be found which transform as basis functions for an irreducible representation. This concept can – in a one-to-one correspondence – be extended to tensor operators since they behave like the above mentioned functions. As a result, the direct product of two irreducible tensor operators spanning $D^{(k_1)}$ and $D^{(k_2)}$ can be decomposed into irreducible representations spanned by linear combinations of the products $\underset{\sim}{T}_{q_1}^{(k_1)}\underset{\sim}{T}_{q_2}^{(k_2)}$. The coefficients of these linear combinations are the Clebsch-Gordan coefficients of Eq. (22).

Formally, the direct product of two irreducible tensor operators is given by

$$\left\{\underset{\sim}{\mathbf{T}}^{(k_1)} \otimes \underset{\sim}{\mathbf{T}}^{(k_2)}\right\}_q^{(k)} = \sum_{q_1,q_2} C_{q_1\, q_2\, q}^{k_1\, k_2\, k}\, \underset{\sim}{T}_{q_1}^{(k_1)}\underset{\sim}{T}_{q_2}^{(k_2)} \ , \tag{38}$$

where possible values of the resulting rank k can be determined in analogy to the vectorial coupling of spins and are given by $k = |k_1 - k_2|, |k_1 - k_2| + 1, \ldots, k_1 + k_2$. Equation (38) is a fundamental expression for the application of the irreducible tensor operator method within a numerical exact diagonalization routine. It leads to the desired formulation of the spin Hamiltonian in terms of irreducible tensor operators.

As an example, the coupling of the first rank irreducible tensor operators $\underset{\sim}{\mathbf{U}}^{(1)}$ and $\underset{\sim}{\mathbf{V}}^{(1)}$ according to Eq. (38) shall be presented here. Considering a compound irreducible tensor operator with $k = 0$, the coupling results in

$$\begin{aligned} &\left\{\underset{\sim}{\mathbf{U}}^{(1)} \otimes \underset{\sim}{\mathbf{V}}^{(1)}\right\}^{(0)} = \\ &\qquad \frac{1}{\sqrt{3}}\left(\underset{\sim}{U}_1^{(1)}\underset{\sim}{V}_{-1}^{(1)} - \underset{\sim}{U}_0^{(1)}\underset{\sim}{V}_0^{(1)} + \underset{\sim}{U}_{-1}^{(1)}\underset{\sim}{V}_1^{(1)}\right) \ , \end{aligned} \tag{39}$$

where for the Clebsch-Gordan coefficients the equation $C_{q_1\, q_2\, 0}^{1\, 1\, 0} = 1/\sqrt{3} \cdot (-1)^{1-q_1}\delta_{q_1,q_2}$ was used.[74] Expressing the spherical components of $\underset{\sim}{\mathbf{V}}^{(1)}$ and $\underset{\sim}{\mathbf{U}}^{(1)}$ in terms of the cartesian components in analogy to Eq. (37) yields

$$\begin{aligned} &\left\{\underset{\sim}{\mathbf{U}}^{(1)} \otimes \underset{\sim}{\mathbf{V}}^{(1)}\right\}^{(0)} = \\ &\qquad -\frac{1}{\sqrt{3}}\left(\underset{\sim}{U}^x\underset{\sim}{V}^x + \underset{\sim}{U}^y\underset{\sim}{V}^y + \underset{\sim}{U}^z\underset{\sim}{V}^z\right) \ , \end{aligned} \tag{40}$$

which is, apart from the prefactor, the scalar product of the cartesian vector operators $\underset{\sim}{\mathbf{U}}$ and $\underset{\sim}{\mathbf{V}}$.

Finally, the problem of coupling irreducible tensor operators is identical to the coupling of angular momenta. Thus, from a mathematical point of view an advantage when using irreducible tensor operators is that one can adapt the mathematical approaches for coupling angular momenta and that one can refer to them.

3. Matrix elements of irreducible tensor operators

In the case of an irreducible tensor operator $\underset{\sim}{\mathbf{T}}^{(k)}$ the matrix elements of this operator can be calculated according to the *Wigner-Eckart theorem* as it is done in App. B. For the sake of consistence, the Wigner-Eckart theorem shall be given here once more. It states for matrix elements with respect to spin states of the form $|\alpha\, S\, M\rangle$ that

$$\begin{aligned}&\langle \alpha\, S\, M|\underset{\sim}{T}{}^{(k)}_q|\alpha'\, S'\, M'\rangle = \\ &\quad (-1)^{S-M}\langle \alpha\, S||\underset{\sim}{\mathbf{T}}^{(k)}||\alpha'\, S'\rangle \begin{pmatrix} S & k & S' \\ -M & q & M' \end{pmatrix} .\end{aligned} \tag{41}$$

The matrix element is apart from a phase factor decoupled into a Wigner-3J symbol and a quantity $\langle \alpha\, S||\underset{\sim}{\mathbf{T}}^{(k)}||\alpha'\, S'\rangle$ called the *reduced matrix element* of the irreducible tensor operator $\underset{\sim}{\mathbf{T}}^{(k)}$. The proof of Eq. (41) is given in standard textbooks about group theory and quantum mechanics.[65,72] However, the physical meaning of this theorem and the consequences for the use within the irreducible tensor operator method shall be briefly discussed here.

First of all, it should be mentioned that the Wigner-Eckart theorem relies on the transformation properties of the appearing wave functions and operators. Furthermore, since the reduced matrix element is completely independent of any magnetic quantum number, the Wigner-Eckart theorem separates the physical part of the matrix element – the reduced matrix element – from the purely geometrical part reflected by the Wigner-3J symbol. The value of the reduced matrix element depends on the particular form of the tensor operator and the states (cf. App. A 3) whereas the Wigner-3J symbol only depends on rotational symmetry properties. If a zero-rank ($k = 0$) irreducible tensor operator is assumed, the Wigner-3J symbol in Eq. (41) directly reflects that there is no transition between states $|\alpha\, S\, M\rangle$ with different S or M. The matrix of the Heisenberg Hamiltonian from Eq. (12), which can be written as a zero-rank irreducible tensor operator (see App. A 2), therefore takes block-diagonal form without further calculations.

According to Eq. (41) the calculation of the matrix element of an irreducible tensor operator is directly related to the calculation of the reduced matrix element of this operator. The reduced matrix element of an irreducible tensor operator $\underset{\sim}{\mathbf{s}}^{(k)}$ with $k = 0, 1$, acting on a basis function of a single spin, can be derived from the evaluation of the Wigner-Eckart theorem. It yields the expressions

$$\langle s||\underset{\sim}{\mathbf{s}}^{(0)}||s\rangle = \langle s||\underset{\sim}{\mathbb{1}}||s\rangle = (2s+1)^{\frac{1}{2}} , \tag{42}$$

$$\langle s||\underset{\sim}{\mathbf{s}}^{(1)}||s\rangle = [s\,(s+1)\,(2s+1)]^{\frac{1}{2}} , \tag{43}$$

where the zero-rank irreducible tensor operator of a single spin $\underset{\sim}{\mathbf{s}}^{(0)}$ is given by the unity operator $\underset{\sim}{\mathbb{1}}$ and the components of $\underset{\sim}{\mathbf{s}}^{(1)}$ by Eq. (37).

Using Eq. (38) in combination with the Wigner-Eckart theorem in Eq. (41) and a decomposition of states $|\alpha\, S\, M\rangle$ into product states according to Eq. (22), one obtains the expression[75]

$$\begin{aligned}&\langle \alpha_1\, s_1\, \alpha_2\, s_2\, S||\left\{\underset{\sim}{\mathbf{T}}^{(k_1)} \otimes \underset{\sim}{\mathbf{T}}^{(k_2)}\right\}^{(k)}_q ||\alpha'_1\, s'_1\, \alpha'_2\, s'_2\, S'\rangle = \\ &\quad [(2S+1)\,(2S'+1)\,(2k+1)]^{\frac{1}{2}} \begin{pmatrix} s_1 & s'_1 & k_1 \\ s_2 & s'_2 & k_2 \\ S & S' & k \end{pmatrix} \\ &\quad \times \langle \alpha_1\, s_1||\underset{\sim}{\mathbf{T}}^{(k_1)}||\alpha'_1\, s'_1\rangle\langle \alpha_2\, s_2||\underset{\sim}{\mathbf{T}}^{(k_2)}||\alpha'_2\, s'_2\rangle .\end{aligned} \tag{44}$$

This is the reduced matrix element of a compound irreducible tensor operator of rank k which consists of the direct product of two irreducible tensor operators of general ranks k_1 and k_2.

Equation (44) is the basic formula for calculating reduced matrix elements of irreducible tensor operators composed of single-spin tensor operators as they appear in the Heisenberg Hamiltonian. By a successive application every irreducible tensor operator of that kind can be decoupled into a series of phase factors, Wigner-9J symbols and the reduced matrix elements of single-spin tensor operators (cf. Eq. (37)). The successive application of Eq. (44) is often called *decoupling procedure* since the compound tensor operator that describes the system under consideration is decoupled so that its reduced matrix element can be calculated (see App. A 3).

C. Point-group symmetries in Heisenberg spin systems

Magnetic molecules, especially those of an archimedean type, are often – not only from a scientific point of view – perceived to be of a special beauty (cf. Fig. 3). Certainly, this view is closely related to the high symmetry which can be found in the chemical structures and is referred to as point-group symmetry.[76] Point-group symmetries do not only contribute to the beauty of magnetic molecules, but they are also very instrumental in characterizing the energy levels of the spectra and thus in extracting physical information from the underlying spin system. Furthermore, in App. B it is shown that a numerical exact diagonalization often remains impossible unless point-group symmetries are used in order to reduce the dimensionalities of the Hamilton matrices.

It must be emphasized that there is a clear difference between a group of symmetry operations in real space that map the molecule on itself and the corresponding group of symmetry operations in a many-body spin system. Since from a physical point of view a magnetic molecule is described by a system of interacting spins with a certain coupling graph (cf. r.h.s of Fig. 1), the term point-group refers rather to a group of symmetry operations on this coupling graph than to operations

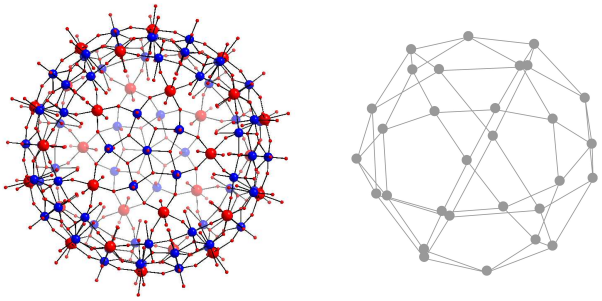

FIG. 3: Sketch of the $\{Mo_{72}Fe_{30}\}$ molecule (l.h.s., picture taken from Ref. 20). The underlying spin system exhibits the structure of an icosidodecahedron, i.e. possesses icosahedral (I_h) point-group symmetry (r.h.s.).

in real space. As a direct result, the group-theoretical characterization is also rather based on the symmetry of the coupling graph than on the molecular symmetry. Of course, since the number of appearing coupling constants as well as their strengths are estimated from the chemical structure of the molecule, there is a close connection between the symmetries of the molecule and the corresponding coupling graph but not necessarily a one-to-one correspondence.

In Heisenberg spin systems point-group symmetries can be included by mapping the symmetry operations on spin permutations. In order to emphasize this, the term spin-permutational symmetry instead of point-group symmetry is often used. However, in the work at hand the term point-group symmetry is used although the symmetry is always incorporated by mapping the point-group operations on spin permutations. In context to this, it has to be mentioned that in systems which include anisotropies the incorporation of point-group symmetries is much more complicated since rotations in real space have to be performed.[75]

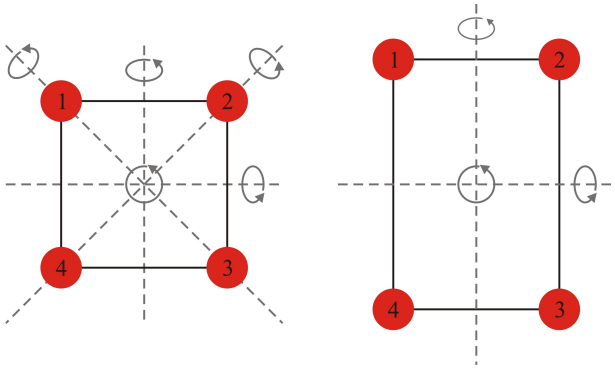

FIG. 4: Coupling graph of a square of identical spins s with D_4 symmetry axes (l.h.s) and a rectangle with D_2 symmetry axes (r.h.s.).

Figure 4 exemplarily shows the coupling graphs of a square and a rectangle consisting of identical spins s with the symmetry axes of D_4 and D_2 being indicated. The rectangle can be seen as resulting from the square – a system of four interacting spins with only one coupling constant J – by introducing a second coupling constant of a different strength J' between spin pairs $< 1, 4 >$ and $< 2, 3 >$. In this case the coupling strength is indicated by the length of the coupling paths between the spins. The introduction of the second coupling constant then results in a reduction of the point-group symmetry from D_4 to D_2.

The point-group operations on the spin system can be identified with permutations of the spins that leave the Hamiltonian invariant.[77] Such a permutation is represented by an operator $\underset{\sim}{G}(R_i)$ of the point-group $\mathcal{G}$ for which the commutation relation

$$\left[\underset{\sim}{H}_{\text{Heisenberg}}, \underset{\sim}{G}(R_i)\right] = 0 \tag{45}$$

holds, where $i = 1, \ldots, h$ numbers the symmetry operations up to the order h of $\mathcal{G}$.

The theory of group representations now provides the theoretical background for the use of point-group symmetries. The irreducible representations $\Gamma^{(n)}$ of a point-group $\mathcal{G}$ can be used to classify the energy eigenstates of $\underset{\sim}{H}_{\text{Heisenberg}}$ and to block-factorize the Hamilton matrices. The dimensionalities of the resulting subspaces, i.e. blocks, can be calculated with only little information. The irreducible matrix representations $\mathbf{\Gamma}^{(n)}(R_i)$ of the group elements, i.e. the permutation operators, are somewhat arbitrary concerning the choice of the underlying basis. Thus, these elements are represented by their character, i.e. the trace of the particular matrix representation. The character $\chi^{(n)}(R_i)$ is invariant under unitary transformations and is in general given by

$$\chi^{(n)}(R) = \operatorname{Tr} \mathbf{\Gamma}^{(n)}(R) = \sum_{\lambda=1}^{l_n} \Gamma^{(n)}(R)_{\lambda\lambda} \ , \tag{46}$$

where l_n denotes the dimension of the n-th irreducible representation $\Gamma^{(n)}$.

A given character table of $\mathcal{G}$ now enables one to calculate the dimensions of the resulting blocks within the Hamilton matrix, i.e. the dimensions of the subspaces $\mathcal{H}(S, M, \Gamma^{(n)})$. Character tables for various point-groups can be found in almost every textbook about the theory of group representations. The author would like to refer to these concerning the construction of character tables.[68,72,78]

In order to calculate the dimensions of the subspaces $\mathcal{H}(S, M, \Gamma^{(n)})$, the reducible matrix representations $\mathbf{G}(R_i)$ of the operators $\underset{\sim}{G}(R_i)$ have to be considered. With $l, m = 1, \ldots, \dim \mathcal{H}(S, M)$ the matrix elements of these matrices are given by

$$G(R_i)_{lm} = \langle \alpha_l \, S \, M | \underset{\sim}{G}(R_i) | \alpha_m \, S \, M \rangle \ ,$$

where the subscripts attached to α indicate that specific basis states are considered. The decomposition of the

character $\chi(R_i) = \sum_{ll} G(R_i)_{ll}$ with respect to the irreducible representations n of $\mathcal{G}$ then yields

$$\chi(R_i) = \sum_n a_n \chi^{(n)}(R_i) \ . \tag{47}$$

Using the great orthogonality theorem[72], the above equation results in the expression

$$\begin{aligned} a_n &= \dim \mathcal{H}(S, M, \Gamma^{(n)}) \\ &= \frac{1}{h} \sum_k N_k [\chi^{(n)}(\mathcal{C}_k)]^* \chi(\mathcal{C}_k) \ , \end{aligned} \tag{48}$$

where a_n gives the multiplicity of the irreducible representation $\Gamma^{(n)}$ that is contained in the reducible representation $\mathbf{G}(\mathcal{C}_k)$. $\mathcal{C}$ refers to the classes which the group elements can be divided in. Each class contains equivalent operations, for example n-fold rotations, which are linked by the same group operation and thus hold the same character. N_k denotes the number of elements of $\mathcal{C}_k$.

From Eq. (48) the dimensions of the subspaces $\mathcal{H}(S, M, \Gamma^{(n)})$ can be calculated, but no information about the basis states that span these Hilbert spaces is given. The required symmetrized basis states can be determined by the application of the projection operator[72]

$$\mathcal{P}^{(n)}_{\kappa\kappa} = \frac{l_n}{h} \sum_i [\Gamma^{(n)}(R_i)_{\kappa\kappa}]^* \underset{\sim}{G}(R_i) \ . \tag{49}$$

This operator projects our that part of a function $|\phi\rangle$ which belongs to the κ-th row of the irreducible representation $\Gamma^{(n)}$. A subsequent application of the operator in Eq. (49) on basis states, for example of the form $|\alpha\, S\, M\rangle$, is called the *basis-function generating machine*.[72]

Although Eq. (49) provides the information required to construct symmetrized basis states that serve as a basis for the irreducible representations of $\mathcal{G}$, it is important to notice that the matrices of $\Gamma^{(n)}$ have to be known completely. Of course, this does not cause a problem as long as $\mathcal{G}$ entirely consists of one-dimensional irreducible representations. However, if more-dimensional irreducible representations appear, it is often more convenient to use the projection operator

$$\mathcal{P}^{(n)} = \sum_\kappa \mathcal{P}^{(n)}_{\kappa\kappa} = \frac{l_n}{h} \sum_i [\chi^{(n)}(R_i)]^* \underset{\sim}{G}(R_i) \tag{50}$$

that only requires information which can be extracted from the character table of $\mathcal{G}$. The operator of Eq. (50) projects out that part of a function $|\alpha\, S\, M\rangle$ which belongs to the irreducible representation $\Gamma^{(n)}$, irrespective of the row. As a consequence one has to orthonormalize resulting functions – for example by a *Gram-Schmidt orthonormalization* – in order to obtain the correct symmetrized basis functions (cf. App. A 4).

D. On bipartite and frustrated spin systems

The terms bipartite or non-bipartite, i.e. frustrated, spin system are frequently used in the field of molecular magnetism. In this section a very basic understanding of the physical meaning of these terms shall be developed. First of all, it should be mentioned that, whenever a spin system is classified according to appearing or non-appearing frustration, this view is mostly driven by a purely classical picture of the system. The classical description of a spin system can be seen as the limit of the quantum mechanical description for $s \to \infty$. Although the range of validity of the classical description is not entirely clear, often both, quantum mechanically and classically motivated descriptions, are used to extract physical information from a system of interacting spins.[79]

Within a classical spin system every participating spin is described by a classical vector $\vec{s}$. The scaling $|\vec{s}| = \sqrt{s(s+1)}$ leads to a direct relation to the quantum mechanical counterpart of a spin $\underset{\sim}{\mathbf{s}}$. Therefore, the Heisenberg Hamiltonian of a classical spin system takes the well-known form

$$H^{\mathrm{cl}}_{\mathrm{Heisenberg}} = -J \sum_{<i,j>} \vec{s}_i \cdot \vec{s}_j \ , \tag{51}$$

where the interaction, that is restricted to neighboring spins in this case, is simply taken to be a scalar product of classical vectors and $J < 0$ refers to an antiferromagnetic coupling.

From Eq. (51) the physical meaning of classically defined spin frustration can easily be derived. Obviously, the energy of the presented classical Heisenberg system is minimized if the energies of all pairwise interactions are simultaneously minimized. Assuming an antiferromagnetic coupling, the energy of an interacting spin pair is minimized if the vectors representing the spins are aligned in an antiparallel manner. Thus, *a classical system in which an alignment that minimizes each interaction simultaneously cannot be found is called frustrated.*

Figure 5 shows the classical picture of the ground state of simple planar Heisenberg systems with antiferromagnetic nearest-neighbor interactions, i.e. a square and a triangle. The Hamiltonian is taken to be of the kind shown in Eq. (51). For the square each spin-spin interaction is energetically minimized by an antiparallel alignment of the spin vectors. In contrast to that, for the triangular system the energy is minimized by an arrangement of the spins in which neighboring spin vectors enclose an angle of 120°. Therefore, the triangle is called a frustrated system whereas the square is an example for a non-frustrated system.

So far only classical Heisenberg systems have been considered. In an attempt to extend the classical definition to quantum systems one could find a definition of spin frustration by claiming that *a quantum spin system is frustrated, if the corresponding classical spin system is frustrated.*

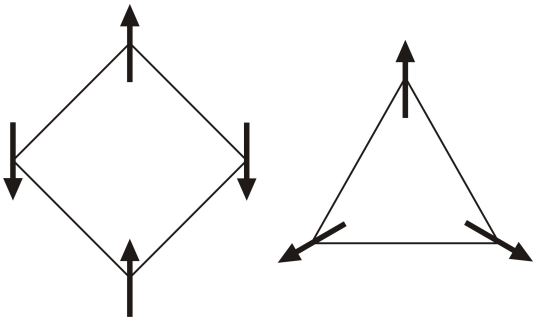

FIG. 5: Sketches of the classical ground state of a Heisenberg square (l.h.s) and a Heisenberg triangle (r.h.s) with antiferromagnetic interactions. For the square all spin vectors are simultaneously aligned in an antiparallel manner whereas this alignment is not possible for the triangle leading to geometrically caused spin frustration.

From a theoretical point of view the characterization of quantum systems by properties of the corresponding classical system is – at least – questionable since quantum and classical nature of physics are not directly comparable. Often, classical considerations regarding spin systems, e.g. magnetic molecules, only give an effective description while the quantum mechanical background remains concealed.[80]

Lieb and Mattis defined *bipartite* systems on the basis of a Heisenberg Hamiltonian without explicitly referring to classical spin systems.[81,82] Stating that *every non-bipartite system is frustrated* one can easily derive a more general definition of frustration. A bipartite system can be decomposed into two sublattices A and B such that for all exchange couplings between spins at sites x and y the inequalities

$$\begin{aligned} J(x_A, y_B) &\leq g^2 \ , \\ J(x_A, y_A) \geq g^2 \ &, \ J(x_B, y_B) \geq g^2 \ . \end{aligned} \tag{52}$$

hold. The subscripts therein indicate the sublattice the spins belong to.

From a practical point of view the system under consideration therefore has to be decomposed into two sublattices by labelling the spin sites with A and B. In order to classify the system as being bipartite a number g has to be found for which the above inequalities hold. To this end, g can be any number so that the square of it separates the inter-sublattice interactions from the intra-sublattice interactions. For the antiferromagnetic square ($J < 0$) of Fig. 6 a proper decomposition with $g = 0$, satisfying Eq. (52), can easily be found since all intra-sublattice interactions are equal to zero. As a result, this simple system can be classified as bipartite both from a classical and a quantum mechanical point of view. In the case of an antiferromagnetic triangle a decomposition together with a suitable value of g cannot be found such that the inequalities of Eq. (52) hold. It serves as a paradigm of a frustrated system according to the above definition.

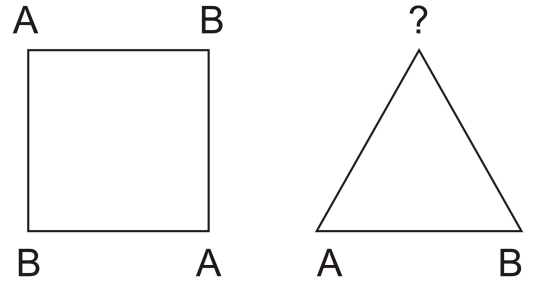

FIG. 6: Decompositions of an antiferromagnetic square (l.h.s) and a triangle (r.h.s) as required in order to classify the system as being bipartite. For the triangle a proper decomposition cannot be found.

As one can see from a comparison of Figs. 5 and 6, the latter definition of frustration extends the range of applicability of the classical definition without restricting its validity.

To be more precise, the term spin frustration introduced so far must be extended to *geometrically caused spin frustration*. By considering the definition deduced from the considerations of Lieb and Mattis this distinction becomes clear. Systems have been classified to be bipartite or frustrated only with respect to whether a proper decomposition into two sublattices can be found. The spin quantum number of the single spins, for instance, does not play any role although it is known that geometrically identical systems behave differently in dependence of it (see App. B 3).[83] In this respect, the term geometry refers to the coupling graph of the system that can be obtained by drawing the exchange pathways between the spin centers (cf. previous sections).

However, spin systems have also been called frustrated because of certain unusual physical properties. Hence, this signatures of spin frustration, i.e. the physical phenomena that are apparent if the system is frustrated, shall be given here. Whenever a spin system exhibits at least one of these signatures it is clearly frustrated. Whether systems that are non-bipartite, but do not show any of these signatures, are still – with respect to their geometry – called frustrated, is a purely semantical question and will not be touched here.

The signatures of frustration in antiferromagnetic systems are (for further reading and citations see Sec. B 2 and references therein):

1. orbital degeneracy of the ground state of the system that appears, for instance, in an equilateral triangle with half-integer spins.[84,85]

2. low-lying singlets below the first triplet as shown for half-integer archimedean-type spin systems like the cuboctahedron or the icosidodecahedron.[86,87]

3. plateaus and jumps in the magnetization curves (M vs. B) that are also apparent in the differential susceptibility (χ vs. B).[46,88]

III. GUIDE TO PUBLICATIONS

In this section the work which has been done and published in the papers listed in App. B is summarized and results are briefly discussed. From a conceptional point of view, two aspects have to be considered. A computational method in order to exactly calculate the complete energy spectra of huge magnetic molecules with the help of irreducible tensor operators and full spin-rotational symmetry as well as point-group symmetries has been developed. In addition, the computational effort which is necessarily present when calculating the energy spectra of huge magnetic molecules has been further reduced by the application of an approximate diagonalization.

Continuative references can be found in App. B and an overview of the underlying theoretical basics is given in Sec. II.

A. Numerical exact diagonalization of archimedean-type molecules

1. *Symmetry assisted complete evaluation of energy spectra using irreducible tensor operators*

In Sec. III of Ref. 1 the complete energy spectra of two spin systems described within an isotropic Heisenberg model are calculated by a numerical exact diagonalization. Since magnetic molecules that can be represented by archimedean-type spin systems like the cuboctahedron and the truncated tetrahedron have been synthesized several years ago, the choice of the investigated systems is not purely academic. These molecules are supposed to be well described within an isotropic Heisenberg model, giving reason to a labelling of resulting eigenstates and corresponding eigenvalues by the total-spin quantum number S and the total magnetic quantum number M. The geometries of the systems exhibit high symmetries, i.e. O_h and T_d point-group symmetries for the cuboctahedron and the truncated tetrahedron, respectively. They seem to be perfectly suited in order to demonstrate the combined use of spin-rotational and point-group symmetries. Moreover, results can also be used as a starting point for prospective experimental investigations comprising magnetization and susceptibility measurements.

The systems which are investigated both consist of twelve spins $s = 3/2$. The dimension of the full Hilbert space is thus $16,777,216$ being reduced in a first step by using full spin-rotational symmetry. In order to balance the computational effort which is required for calculating the energy spectra and the dimensions of the resulting matrices which have to be diagonalized additionally a D_2 point-group symmetry is used. Regarding this, the matrices in the subspaces $\mathcal{H}(S, M = S)$ are block-factorized with respect to the number of irreducible representations of D_2. However, the form of the resulting symmetrized basis states, which directly affects the computation time that is needed to set up the matrices, is rather simple. This is because a coupling scheme can be found that is invariant under all point-group operations of D_2 (cf. App. A 4). As a result, the dimensions of the matrices reduce to a maximum of $64,724$, which is a tractable matrix size for available high performance computers, while computation time is only slightly increased.

Apart from this purely technical reason for reducing the dimensions of the Hamilton matrices, O_h point-group symmetry is used for a decomposition of the $S = 0$ and $S = 1$ subspaces of the cuboctahedron into corresponding Hilbert spaces $\mathcal{H}(S, M = S, \Gamma)$. Thus, an additional quantum number Γ is given that refers to the irreducible representations of O_h. With this labelling additional geometrical information about the energy levels is obtained.

2. *Frustration effects in antiferromagnetic molecules*

The work of Ref. 3 is focused on the calculation and interpretation of thermodynamic properties of the cuboctahedron, such as the magnetization and differential susceptibility.

To this end, the energy spectra of a regular cuboctahedral spin system modeled by an isotropic Heisenberg Hamiltonian with only one coupling constant J are calculated and compared for various single-spin quantum numbers s. In Ref. 3 the cuboctahedron mainly serves as a zero-dimensional realization of extended two- and three-dimensional antiferromagnetic lattices like the Kagomé and the pyrochlore lattice. Geometrical frustration arising from corner-sharing triangles of the cuboctahedron leads to unusual magnetic properties shared with these extended antiferromagnets.

Only due to the combined use of spin-rotational symmetry and point-group symmetries the complete energy spectrum of the cuboctahedron with $s = 3/2$ could be calculated. The energy spectrum and the derived thermodynamic observables show the expected behavior in dependence of the single-spin quantum number s (see Sec. II). For half-integer spins low-lying singlets below the first triplet, a jump in the magnetization curve due to independent magnons, and a dip in the differential susceptibility exist. These features are independent of the particularly chosen s.

Motivated by recent classical investigations of the magnetic properties of the icosidodecahedron, in a second part of Ref. 3 the irregular cuboctahedron with $s = 1/2$ is investigated. Here, the term irregular refers to a random choice (within a given interval) of the constant J_{ij} which couples two spins i and j along the edges of the cuboctahedron. The stability of thermodynamic observables against random fluctuations of the coupling constant shows that a microscopic, quantum mechanically based explanation of the magnetization and susceptibility measurements performed on the molecule $\{Mo_{72}Fe_{30}\}$ is still missing.

B. Approximate diagonalization of bipartite and frustrated magnetic molecules

In Ref. 1 the development of an approximate diagonalization method for antiferromagnetically coupled molecular quantum spin systems is described. Although magnetic molecules are often modeled by an isotropic Heisenberg Hamiltonian that allows the use of full spin-rotational symmetry, one quickly reaches computational limitations when investigating thermodynamic observables over a wide temperature range by numerical exact diagonalization. This is due to the enormous demand for rapidly accessible memory which is used in the diagonalization routines in order to calculate the energy spectra. Existing numerical methods suffer from at least one of two main problems: either only investigations for very low temperatures are possible, because in each subspace of $\mathcal{H}$ only a few low-lying energy levels can be calculated with high numerical accuracy (e.g. Lanczos and DMRG), or the method is limited in its application to unfrustrated – or only slightly frustrated – systems when investigating the low-temperature behavior of thermodynamic observables (e.g. Quantum Monte Carlo).

As a first step, in Ref. 1 the theoretical background (cf. Sec. II) of the developed approximation is given, which is mainly applied to one-dimensional unfrustrated, i.e. bipartite, ring-like systems of various length and single-spin quantum number s. The idea is to diagonalize the Hamiltonian within a reduced, but carefully chosen basis subset given by low-lying energy levels of the so-called rotational-band model. As a toy model an eight-site spin ring is discussed. It is shown that the approximate diagonalization of bipartite systems constitutes a further method to reduce the memory requirements. Moreover, by using point-group symmetries an additional labelling of the energy levels is possible, and thus additional information about the physics of the system can be obtained.

In a second step, slightly frustrated systems are investigated which are obtained by introducing next-nearest-neighbor interactions with various coupling constants J_{nnn} to the toy system. A complete decomposition into irreducible representations in dependence of the introduced coupling parameter J_{nnn} demonstrates the possibility of observing so-called quantum phase transitions.

By comparing the obtained results for a twelve-site spin ring with $s = 5/2$ to experimental data of magnetization steps, it is shown that the approximate diagonalization can be a valuable complement to existing approximate methods for bipartite systems. So far such a spin ring has only been accessible by means of Quantum Monte Carlo. The approximate diagonalization is able to provide additional information regarding the temperature dependence over a wide temperature range, the energy spectrum, and the respective eigenstates. For this reason, it can be a starting point for a spectroscopic analysis with the help of nuclear magnetic resonance, electron paramagnetic resonance or inelastic neutron scattering.

Along these lines the approximate diagonalization is extended in Ref. 2 and applied to a highly frustrated system, i.e. systems with a three-sublattice structure with respect to the classical ground state. Systems of this kind are of special interest (see Sec. III A), but the energy spectra can only be completely determined for very small single-spin quantum numbers s. In order to find an approximation, which is applicable and yields useful results in cases where the full spectrum is not accessible, the convergence behavior of the approximation is discussed for a cuboctahedron with $s = 1$ and $s = 3/2$. To this end, additional non-trivial classical reference states are incorporated in order to improve the convergence. An incorporation of these non-trivial reference states clearly results in an improved convergence behavior. Especially the convergence for those states is improved which other groups have found to dominate the low-energy spectrum of the cuboctahedron and the icosidodecahedron with half-integer spins. These states are supposed to condense in an infinite number on the ground state of related extended systems.

IV. SUMMARY AND CONCLUSION

In this work the range of applicability of numerical exact diagonalization has been extended. To this end, a general scheme for the combined use of spin-rotational and point-group (spin-permutational) symmetries in Heisenberg spin systems has been developed. From a technical point of view, the Hamilton matrices have been set up with the help of the irreducible tensor operator approach using a basis that is composed of vector-coupling states. Contrary to the use of a basis composed of product states, the matrices take block-diagonal form with respect to the total-spin quantum number S without further calculations. The incorporation of point-group symmetries has been the most challenging part of this work - both theoretically and technically. The action of a general point-group operation has been traced back to a permutation of spins within the Hamiltonian inducing transitions from one coupling scheme to another one. Graph theoretical considerations that were developed in a different context have been adapted in order to calculate general recoupling coefficients describing transitions between two arbitrary coupling schemes. In parallel, the presented theoretical framework has been implemented in a computer program that was specifically adjusted to the use within a high performance computing environment.

Additionally, an approximate diagonalization method has been developed. The key idea is the numerical diagonalization within a reduced, but carefully chosen set of basis states. In order to reduce the set of basis states, a rotational-band Hamiltonian was used as a guide to select those basis states that mainly contribute to the low-lying part of the spectrum. It has been shown that the approximate diagonalization method can provide insight into systems even larger than those that can be

investigated by a numerical exact diagonalization. With respect to the approximate diagonalization, the role of frustration has been discussed. In order to reasonably approximate the spectrum, frustrated systems must be treated differently from bipartite ones. In this respect, the central task has been the incorporation of all present classical ground state families of the system.

The application of both diagonalization schemes to spin systems exhibiting ring-like and archimedean-type structures has continued investigations of antiferromagnetic molecular compounds. In this context, frustration effects in a cuboctahedral system have been investigated and related to former results that were obtained for spins of a smaller size. In archimedean-type systems the contributions from co-existing rotational-bands to the low-lying part of the spectrum have been discussed. These contributions result from different configurations of the classical ground state and lead to special features in antiferromagnetic systems that consist of corner-sharing triangles, for example low-lying singlets below the first triplet excitation in the case of half-integer spins.

In conclusion, the presented results show that with the help of symmetries numerical diagonalization techniques can provide insight into large spin systems. Up to now, the need for a huge amount of rapidly accessible memory has been the major technical drawback of numerical diagonalization techniques as used in the fields of molecular magnetism or highly frustrated magnets. By using symmetries as shown in this work this computational limitation is partially shifted towards the need for more processing units (cpus) in a parallelized environment. Since there has clearly been a tendency to further develop the use of multi-core cpus in large-scale supercomputers in the last years, the presented methods might help to investigate even larger spin systems.

V. OUTLOOK

Since the work at hand has been to a large extent focused on numerical diagonalization techniques, future investigations should certainly aim at further technical improvements. Restrictions of the presented methods are mainly due to the computational effort that results from the generation of symmetrized basis states and the calculations of the Hamilton matrices. The symmetrized basis states are – in the given form – linear combinations of many vector-coupling states. Hence, calculating single matrix elements is a rather cumbersome and time-consuming task because one has to sum over all vector-coupling states within these linear combinations. While setting up the matrices can be parallelized very well, the parallelization of the construction of the symmetrized basis turns out to be more difficult (see App. A 6). An improvement would be the implementation of more sophisticated routines for the generation of recoupling formulas (cf. App. A 5 b). This would speed up the construction of symmetrized basis states if coupling schemes have to be considered that are not invariant under the operations of the assumed point group.

Acknowledgments

This work would not have been possible without the advice and support of several persons. It is my pleasure to thank these persons who inspired and motivated me troughout the years.

First of all I would like to thank my supervisor Prof. Dr. J. Schnack (University of Bielefeld) for his remarkably great mentoring. His motivation and unmatched enthusiasm always stimulated the progress of this work. In many fruitful discussions I have intensively been influenced by his deep knowledge.

I am thankful to Prof. Dr. B. Tsukerblat (Ben Gurion University of the Negev, Israel) for sharing his knowledge about the irreducible tensor operator approach during several discussions and seminars.

I would also like to thank apl. Prof. Dr. M. Neumann for writing the second report on this thesis.

This work has been performed within the framework of the PhD program "Synthesis and Characterisation of Surfaces and Interfaces assembled from Clusters and Molecules". For leading and coordinating this program I would like thank apl. Prof. Dr. M. Neumann, Prof. Dr. L. Walder, Prof. Dr. J. Schnack, Dr. H. Elfering, and Dipl.-Phys. C. Derks. I would also like to thank all students of the PhD program for the kind atmosphere during the seminars and social events. The financial support by the Federal State of Lower Saxony is also gratefully acknowledged.

In addition, this work has been provided with computing time of the HLRB-project h1351 "Evaluation of magnetic spectra using the irreducible tensor operator approach" funded by the Leibniz Computing Center of the Bavarian Academy of Sciences.

I am thankful to my former and present colleagues at the Physics Department of the University of Osnabrück Dr. M. Brüger, Dipl.-Phys. P. Hage, and Dr. R. Steinigeweg who accompanied me during the years.

For their hospitality and for creating a very pleasant and stimulating environment for research I am very thankful to the members of the "magnetic sublattice" of the Condensed Matter Theory Group within the Physics Department of the University of Bielefeld: Dipl.-Phys. M. Höck, Dipl.-Chem. S. Leiding, Dipl.-Phys. J. Ummethum, and H. Litschewsky. I further like to thank Dipl.-Phys. M. Höck and Dipl.-Phys. J. Ummethum for carefully reading the manuscript.

Finally, I am indebted to my whole family. They always supported me and kept faith in me.

Most of all, I am deeply grateful to my wife Kathrin. Without her support and unlimited patience this work would never have been finished. At all times, her love and trust encouraged me to proceed.

* Electronic address: rschnall@uos.de

[1] R. Schnalle and J. Schnack, Phys. Rev. B **79**, 104419 (2009).
[2] R. Schnalle, A. M. Läuchli, and J. Schnack, Cond. Mat. Phys. **12**, 331 (2009).
[3] J. Schnack and R. Schnalle, Polyhedron **28**, 1620 (2009).
[4] T. Lis, Acta Chrystallogr. B **36**, 2042 (1980).
[5] R. Sessoli, D. Gatteschi, A. Caneschi, and M. A. Novak, Nature **365**, 141 (1993).
[6] D. Gatteschi, A. Caneschi, L. Pardi, and R. Sessoli, Science **265**, 1054 (1994).
[7] Z. H. Jang, A. Lascialfari, F. Borsa, and D. Gatteschi, Phys. Rev. Lett. **84**, 2977 (2000).
[8] Y. Furukawa, K. Watanabe, K. Kumagai, F. Borsa, and D. Gatteschi, Phys. Rev. B **64**, 104401 (2001).
[9] M. T. Pope and A. Müller, Angew. Chem. **103**, 56 (1991).
[10] A. Müller, F. Peters, M. Pope, and D. Gatteschi, Chem. Rev. **98**, 239 (1998).
[11] A. Müller, P. Kögerler, and A. W. M. Dress, Coord. Chem. Rev. **222**, 193 (2001).
[12] T. Glaser, M. Heidemeier, E. Krickemeyer, H. Bögge, A. Stammler, R. Fröhlich, E. Bill, and J. Schnack, Inorg. Chem. **48**, 607 (2009).
[13] C. A. Christmas, H. L. Tsai, L. Pardi, J. M. Kesselman, P. K. Gantzel, R. K. Chadha, D. Gatteschi, D. F. Harvey, and D. N. Hendrickson, J. Am. Chem. Soc. **115**, 12483 (1993).
[14] K. L. Taft, C. D. Delfs, G. C. Papaefthymiou, S. Foner, D. Gatteschi, and S. J. Lippard, J. Am. Chem. Soc. **116**, 823 (1994).
[15] A. Lascialfari, D. Gatteschi, F. Borsa, and A. Cornia, Phys. Rev. B **55**, 14341 (1997).
[16] A. Lascialfari, D. Gatteschi, F. Borsa, and A. Cornia, Phys. Rev. B **56**, 8434 (1997).
[17] G. L. Abbati, A. Caneschi, A. Cornia, A. C. Fabretti, and D. Gatteschi, Inorg. Chim. Acta **297**, 291 (2000).
[18] C. P. Pradeep, D.-L. Long, P. Kögerler, and L. Cronin, Chem. Comm. pp. 4254–4256 (2007).
[19] A. J. Blake, R. O. Gould, C. M. Grant, P. E. Y. Milne, S. Parsons, and R. E. P. Winpenny, J. Chem. Soc.-Dalton Trans. pp. 485–495 (1997).
[20] A. Müller, S. Sarkar, N. Shah, H. Bögge, M. Schmidtmann, S. Sarkar, P. Kögerler, B. Hauptfleisch, A. X. Trautwein, and V. Schünemann, Angew. Chem., Int. Ed. **38**, 3238 (1999).
[21] F. Torres, J. M. Hernandez, X. Bohigas, and J. Tejada, Appl. Phys. Lett. **77**, 3248 (2000).
[22] O. Derzhko and J. Richter, Phys. Rev. B **70**, 104415 (2004).
[23] J. Richter, J. Schulenburg, A. Honecker, J. Schnack, and H.-J. Schmidt, J. Phys.: Condens. Matter **16**, 779 (2004).
[24] D. Gatteschi, Adv. Mater. **6**, 635 (1994).
[25] P. Clark and T. St. Pierre, Magnetic Resonance Imaging **18**, 431 (2000).
[26] B. Cage, S. Russek, R. Shoemaker, and A. Barker, Polyhedron **26**, 2413 (2007).
[27] M. N. Leuenberger and D. Loss, Nature **410**, 789 (2001).
[28] J. Tejada, E. Chudnovsky, E. del Barco, and J. Hernandez, Nanotechnology **186**, 181 (2001).
[29] X. Wang and P. Zanardi, Phys. Lett. A **301**, 1 (2002).
[30] X. Wang, Phys. Rev. A **66**, 034302 (2002).
[31] G. A. Timco, S. Carretta, F. Troiani, F. Tuna, R. J. Pritchard, C. A. Muryn, E. J. L. McInnes, A. Ghirri, A. Candini, P. Santini, et al., Nature Nanotechnology **4**, 173 (2008).
[32] L. Bogani and W. Wernsdorfer, Nature Materials **7**, 179 (2008).
[33] W. Heisenberg, Z. f. Phys. **49**, 619 (1928).
[34] A. Bencini and D. Gatteschi, *EPR of exchange coupled systems* (Springer Verlag, 1990).
[35] C. Delfs, D. Gatteschi, L. Pardi, R. Sessoli, K. Wieghardt, and D. Hanke, Inorg. Chem. **32**, 3099 (1993).
[36] S. Sachdev, Phys. Rev. B **45**, 12377 (1992).
[37] A. P. Ramirez, Annu. Rev. Mater. Sci. **24**, 453 (1994).
[38] P. Lecheminant, B. Bernu, C. Lhuillier, L. Pierre, and P. Sindzingre, Phys. Rev. B **56**, 2521 (1997).
[39] C. Waldtmann, H. U. Everts, B. Bernu, C. Lhuillier, P. Sindzingre, P. Lecheminant, and L. Pierre, Eur. Phys. J. B **2**, 501 (1998).
[40] J. Greedan, J. Mater. Chem. **11**, 37 (2001).
[41] D. Kouzoudis, J. Magn. Magn. Mater. **173**, 259 (1997).
[42] D. Kouzoudis, J. Magn. Magn. Mater. **189**, 366 (1998).
[43] K. Bärwinkel, H.-J. Schmidt, and J. Schnack, J. Magn. Magn. Mater. **212**, 240 (2000).
[44] R. Moessner and J. T. Chalker, Phys. Rev. B **58**, 12049 (1998).
[45] C. Schröder, H. Nojiri, J. Schnack, P. Hage, M. Luban, and P. Kögerler, Phys. Rev. Lett. **94**, 017205 (2005).
[46] C. Schröder, H.-J. Schmidt, J. Schnack, and M. Luban, Phys. Rev. Lett. **94**, 207203 (2005).
[47] E. Manousakis, Rev. Mod. Phys. **63**, 1 (1991).
[48] J. N. Reimers and A. J. Berlinsky, Phys. Rev. B **48**, 9539 (1993).
[49] M. E. Zhitomirsky, A. Honecker, and O. A. Petrenko, Phys. Rev. Lett. **85**, 3269 (2000).
[50] M. E. Zhitomirsky, Phys. Rev. B **67**, 104421 (2003).
[51] A. M. Läuchli, in *Highly Frustrated Magnetism*, edited by C. Lacroix, P. Mendels, and F. Mila (Springer Verlag, 2009), chap. Numerical Simulations of Frustrated Systems, to appear.
[52] A. W. Sandvik and J. Kurkijärvi, Phys. Rev. B **43**, 5950 (1991).
[53] A. W. Sandvik, Phys. Rev. B **59**, R14157 (1999).
[54] M. Suzuki, Prog. Theor. Phys. **56**, 1454 (1976).
[55] M. Troyer and U.-J. Wiese, Phys. Rev. Lett. **94**, 170201 (2005).
[56] S. R. White, Phys. Rev. B **48**, 10345 (1993).
[57] U. Schollwöck, Rev. Mod. Phys. **77**, 259 (2005).
[58] O. Legeza and G. Fath, Phys. Rev. B **53**, 14349 (1994).
[59] S. Liang and H. Pang, Phys. Rev. B **49**, 9214 (1994).
[60] I. Peschel, X. Wang, M. Kaulke, and K. Hallberg, eds., *Density-Matrix Renormalization* (Springer, Berlin, 1999).
[61] C. Lanczos, J. Res. Nat. Bur. Stand. **45**, 255 (1950).
[62] E. Davidson, J. Comp. Phys. **17**, 87 (1975).
[63] P. W. Anderson, Phys. Rev. **115** (1959).
[64] G. Chaboussant, A. Sieber, S. Ochsenbein, H.-U. Güdel, M. Murrie, A. Honecker, N. Fukushima, and B. Normand, Phys. Rev. B **70**, 104422 (2004).
[65] B. L. Silver, *Irreducible Tensor Methods* (Academic Press Inc., New York, 1976).
[66] T. Moriya, Phys. Rev. **120**, 91 (1960).
[67] R. Bŏca, Coord. Chem. Rev. **248**, 757 (2004).

[68] E. P. Wigner, *Group Theory and Its Application to the Quantum Mechanics of Atomic Spectra* (Academic Press Inc., New York, 1959).
[69] U. Fano and G. Racah, *Irreducible Tensor Sets* (Academic Press Inc., New York, 1959).
[70] A. R. Edmonds, *Angular Momentum in Quantum Mechanics* (Princeton University Press, Princeton, 1957).
[71] E. U. Condon and G. H. Shortley, *The Theory of Atomic Spectra* (Cambridge University Press, New York, 1951).
[72] M. Tinkham, *Group theory and quantum mechanics* (Dover Publications, New York, 2003).
[73] A. P. Yutsis, I. B. Levinson, and V. V. Vanagas, *The mathematical aparatus of the theory of angular momentum* (Israel Program for Scientific Translation, Jerusalem, 1962).
[74] D. A. Varshalovich, A. N. Moskalev, and V. K. Khersonskii, *Quantum theory of angular momentum* (World Scientific Publishing, 1988).
[75] H. Lueken, *Magnetochemie*, Teubner Studienbücher Chemie (B.G. Teubner Stuttgart, Leipzig, 1999).
[76] A. Müller, Science **300**, 749 (2003).
[77] G. S. Griffith, Structure and Bonding **10**, 87 (1972).
[78] F. A. Cotton, *Chemical Applications of Group Theory* (Wiley, New York, 1990), 3rd ed.
[79] L. Engelhardt, M. Luban, and C. Schröder, Phys. Rev. B **74**, 054413 (2006).
[80] C. Schröder, R. Prozorov, P. Kögerler, M. D. Vannette, X. Fang, and M. Luban, Phys. Rev. B **77**, 224409 (2008).
[81] E. H. Lieb, T. Schultz, and D. C. Mattis, Ann. Phys. (N.Y.) **16**, 407 (1961).
[82] E. H. Lieb and D. C. Mattis, J. Math. Phys. **3**, 749 (1962).
[83] A. Honecker and M. E. Zhitomirsky, J. Phys.: Conf. Ser. **145**, 012082 (2009).
[84] O. Kahn, Chem. Phys. Lett. **265**, 109 (1997).
[85] D. Dai and M. H. Whangbo, J. Chem. Phys. **121**, 672 (2004).
[86] R. Schmidt, J. Schnack, and J. Richter, J. Magn. Magn. Mater. **295**, 164 (2005).
[87] J. Schnack, R. Schmidt, and J. Richter, Phys. Rev. B **76**, 054413 (2007).
[88] J. Schulenburg, A. Honecker, J. Schnack, J. Richter, and H.-J. Schmidt, Phys. Rev. Lett. **88**, 167207 (2002).
[89] B. S. Tsukerblat, M. I. Belinskii, and V. E. Fainzil'berg, Sov. Sci. Rev. B Chem. **9**, 337 (1987).
[90] J. J. Borras-Almenar, J. M. Clemente-Juan, E. Coronado, and B. S. Tsukerblat, Inorg. Chem. **38**, 6081 (1999).
[91] B. S. Tsukerblat and M. I. Belinskii, *Magnetochemistry and Radiospectroscopy of Exchange Clusters* (Acad. Sci. Moldova, Kishinev (Russ.), 1983).
[92] O. Kahn, *Molecular Magnetism* (VCH, New York, 1993).
[93] O. Waldmann, Phys. Rev. B **61**, 6138 (2000).
[94] V. E. Sinitsyn, I. G. Bostrem, and A. S. Ovchinnikov, J. Phys. A-Math. Theor. **40**, 645 (2007).
[95] V. Fack, S. N. Pitre, and J. van der Jeugt, Comp. Phys. Comm. **86**, 105 (1995).
[96] G. Racah, Phys. Rev. **62**, 438 (1942).
[97] P. G. Burke, Comp. Phys. Comm. **1**, 241 (1970).
[98] V. Fack, S. N. Pitre, and J. van der Jeugt, Comp. Phys. Comm. **83**, 275 (1994).
[99] A. Bar-Shalom and M. Klapisch, Comp. Phys. Comm. **50**, 375 (1988).
[100] P. M. Lima, Comp. Phys. Comm. **66**, 89 (1991).
[101] V. Fack, S. N. Pitre, and J. van der Jeugt, Comp. Phys. Comm. **101**, 155 (1997).
[102] D. Van Dyck and V. Fack, Comp. Phys. Comm. **154**, 219 (2003).
[103] L. C. Biedenharn and J. D. Louck, *The Racah-Wigner Algebra in Quantum Theory* (Addison-Wesley, 1981), vol. 9 of *Encyclopedia of Mathematics and its Applications*, chap. Coupling of n angular momenta: recoupling theory, pp. 435–481.
[104] URL http://www.openmp.org/wp.
[105] URL http://www.netlib.org/lapack.

APPENDIX A: REALIZATION OF THE IRREDUCIBLE TENSOR OPERATOR TECHNIQUE

In this section the theoretical foundations presented in Sec. II shall be specified. To this end, a spin square deals as a small example system. It is demonstrated how an appropriate basis can be constructed and how the Heisenberg Hamiltonian and additional non-Heisenberg terms look like when expressed as irreducible tensor operators. Furtheron, it is shown how the matrix elements can be evaluated by decoupling the irreducible tensor operator that describes the system. A central aspect is the use of point-group symmetries in combination with irreducible tensor operators. Graph-theoretical considerations are presented that allow to determine the action of point-group operations on vector-coupling states. Finally, some remarks on performing calculations with the help of high performance computing are given.

1. The construction of basis states

The reduction of the dimensionalities of the Hilbert spaces in which the Hamilton matrices are set up in order to solve the eigenvalue problem is always a desirable, but also numerically involved task. Especially if the basis a priori reflects symmetry properties of the system, an appropriate choice can be of great help. As mentioned in Sec. II, a basis that consists of vector-coupling states and incorporates full spin-rotational ($SU(2)$) symmetry would be the first choice. In isotropic spin systems as described by a Heisenberg Hamiltonian the Hamilton matrix is then block-diagonalized with respect to S and M without further calculations since there are no transition elements between states of a different total magnetic quantum number M and different total-spin quantum number S.

The vector-coupling states used in the present work appear in the form $|\alpha\, S\, M\rangle$. α denotes a set of intermediate quantum numbers resulting from the chosen coupling scheme according to which the spins are coupled. The choice of the coupling scheme is somewhat arbitrary since it only reflects the bracketing in the expression for the total spin operator of the system $\underset{\sim}{\mathbf{S}} = \sum_i \underset{\sim}{\mathbf{s}}_i$.

The simplest choice of a coupling scheme would probably be a successive coupling of the single-spin vector operators $\underset{\sim}{\mathbf{s}}_i$. In the case of a spin square the set of intermediate quantum numbers, if coupled according to a successive coupling scheme, looks like

$$\alpha = \{s_{12} = \overline{S}_1, s_{123} = \overline{S}_2\}$$

leading to a vector-coupling state of the form $|s_1 s_2 \overline{S}_1 s_3 \overline{S}_2 s_4 S M\rangle$. Here, the notation of the intermediate spin quantum numbers, i.e. s_{12} and s_{123}, is changed in comparison to Sec. II B 1. Intermediate spins are now numbered with respect to their order of appearance in the coupling scheme and additionally overlined. This notation has a clear advantages if larger spin systems are investigated and is used in the following. In order to clarify which spins are coupled, the single-spin quantum numbers s_i can also be found in the ket. It would not be necessary to include them since they appear as fixed numbers, but it turns out to be more convenient.

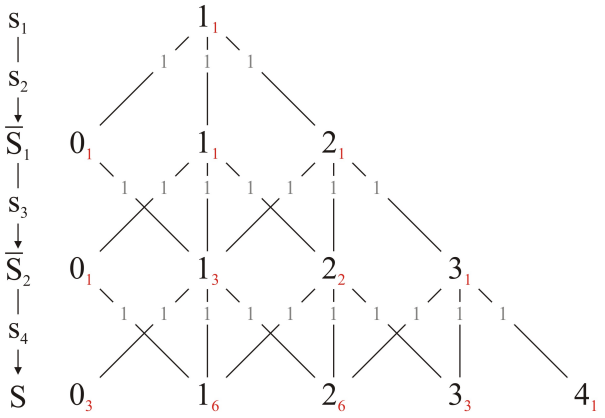

FIG. 7: Successive coupling of four spins $s = 1$. The (red) subscripts denote the multiplicity, i.e. the number of paths leading to the spin quantum number. The gray numbers refer to the spin quantum numbers of the coupled single spins. On the left the coupling scheme is indicated.

Now, if the coupling scheme is chosen and the framework of the resulting basis states is fixed, one has to construct the basis states by finding those values of the intermediate spins that are valid according to Eq. (19). This procedure can be visualized by constructing a coupling pyramid as it is shown in Fig. 7. In Fig. 7 four spins with $s = 1$ are successively coupled in order to yield the values of the total-spin quantum number S. The red subscripts denote the number of different paths leading to the same value for an intermediate spin quantum number, i.e. the multiplicity. The small gray numbers indicate that the quantum numbers of the coupled single spins are given by $s_i = 1$. For the sake of clarity, on the left of Fig. 7 the underlying coupling scheme is given once more.

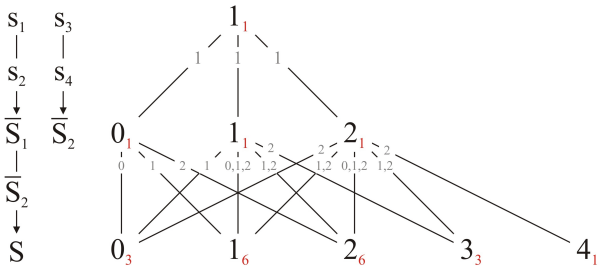

FIG. 8: Pairwise coupling of four spins $s = 1$. The (red) subscripts denote the multiplicity, i.e. the number of paths leading to the spin quantum number. The gray numbers refer to the spin quantum numbers of the coupled single or intermediate spins. On the left the coupling scheme is indicated.

Of course, a successive coupling scheme is not the only way to couple the single spins $\underset{\sim}{\mathbf{s}}_i$ to a total spin $\underset{\sim}{\mathbf{S}}$. For example, the construction of quasi-classical states as described in Refs. 1 and 3 requires a different coupling scheme. There, a coupling scheme is chosen in which spins belonging to a certain sublattice are coupled in order to get the total sublattice spin that is afterwards coupled to the total spin of the system. In Fig. 8 a coupling pyramid for a different coupling scheme of a spin square is shown. The spins $\underset{\sim}{\mathbf{s}}_1$, $\underset{\sim}{\mathbf{s}}_2$ and $\underset{\sim}{\mathbf{s}}_3$, $\underset{\sim}{\mathbf{s}}_4$ are coupled to yield intermediate spins $\underset{\sim}{\overline{\mathbf{S}}}_1$ and $\underset{\sim}{\overline{\mathbf{S}}}_2$, respectively. The intermediate spins are then coupled to the total spin $\underset{\sim}{\mathbf{S}}$.

The resulting multiplicity of states with the same quantum number S is obviously independent of the chosen coupling scheme. At this point it is important to realize once again that these states, although resulting from different coupling schemes, form basis sets of the same Hilbert space $\mathcal{H}$. In the case of a square the coupling of four single spins $s = 1$ discussed above results in basis states that span the subspaces $\mathcal{H}(S)$ with $S = 0, 1, \ldots, 4$. Writing this result in a different way using Eq. (47), one obtains for the direct product of the irreducible representations $D^{(1)}$ of the single spins the following expression:

$$D^{(1)} \otimes D^{(1)} \otimes D^{(1)} \otimes D^{(1)} = \\ 3 \cdot D^{(0)} + 6 \cdot D^{(1)} + 6 \cdot D^{(2)} + 3 \cdot D^{(3)} + 1 \cdot D^{(4)} \ .$$

The knowledge of the dimensions of the resulting irreducible representations, i.e. subspaces $\mathcal{H}(S)$, is a central task whenever performing numerical exact diagonalization. Deduced from a successive coupling of the spins, the dimensions $\dim \mathcal{H}(S)$ can be calculated by a simple recurrence formula.

The number of paths leading to a certain combination (S, n) is denoted by d_S. n refers to the number of participating spins in each step and runs from 1 to N. n can also be seen as labelling the rows of the coupling pyramid for a successive coupling (see Fig. 7). In the case of a homonuclear system with N spins s, the multiplicity $d_S(S, n+1)$ is given by

$$d_S(S, n+1) = \sum_{S'=|S-s|}^{\min(S+s, n\cdot s)} d_S(S', n) \ , \qquad \text{(A1)}$$

where S lies in the interval that is bounded by

$$(n+1)s \geq S \geq \begin{cases} 0 & \text{if } 2s(n+1) \text{ even} \\ \frac{1}{2} & \text{if } 2s(n+1) \text{ odd} \end{cases} \qquad \text{(A2)}$$

according to a vector coupling rule (cf. Eq. (19)). The number of paths leading to a certain quantum number S for one spin is just

$$d_S(S, 1) = \begin{cases} 1 & \text{if } S = s \\ 0 & \text{else} \end{cases} \ . \qquad \text{(A3)}$$

The dimension of the Hilbert space $\mathcal{H}(S)$ is then given by $\dim \mathcal{H}(S) = d_S(S, N) \cdot (2S + 1)$.

The dimensions within a heteronuclear spin system, i.e. a system with different values of single-spin quantum numbers, are obtained along the same route. However, the range of valid values for S has to be calculated for each step of recurrence separately, in contrast to the use of Eq. (A2). Furthermore, the sum in Eq. (A1) would run from $S' = |S - s_i|$ to $\min(S + s_i, \sum_{i=1}^{n} s_i)$ where the spin quantum number of every single spin s_i is individually labelled by the index i.

2. The Heisenberg Hamiltonian expressed as irreducible tensor operator

In order to determine the spectra of magnetic molecules as it is done throughout this work, the Heisenberg Hamiltonian of Eq. (12) has to be expressed as irreducible tensor operator. In this section a general expression for the Heisenberg Hamiltonian is presented which can be used as a starting point for the calculation of the energy spectrum using the irreducible tensor operator approach.

spin dimer - The first step in finding an expression for the Heisenberg Hamiltonian in the form of an irreducible tensor operator is done by considering a spin dimer. The Hamiltonian of the dimer takes the simple form

$$\underset{\sim}{H}_{\text{dimer}} = -J \, \underset{\sim}{\mathbf{s}}(1) \cdot \underset{\sim}{\mathbf{s}}(2) \ . \qquad \text{(A4)}$$

Now, using Eq. (38) the above Eq. (A4) can easily be reproduced. Since the Heisenberg term is given by a scalar product, the corresponding compound irreducible tensor operator is of rank $k = 0$. Using Eqs. (37) – (40) one finds the expression

$$\begin{aligned} &\left\{ \underset{\sim}{\mathbf{s}}^{(1)}(1) \otimes \underset{\sim}{\mathbf{s}}^{(1)}(2) \right\}^{(0)} \\ &= \sum_{q_1, q_2} C^{1\,1\,0}_{q_1\,q_2\,0} \cdot \underset{\sim}{s}^{(1)}_{q_1}(1) \underset{\sim}{s}^{(1)}_{q_2}(2) \\ &= \frac{1}{\sqrt{3}} \Big(\underset{\sim}{s}^{(1)}_{-1}(1) \cdot \underset{\sim}{s}^{(1)}_{1}(2) + \underset{\sim}{s}^{(1)}_{1}(1) \cdot \underset{\sim}{s}^{(1)}_{-1}(2) \\ &\quad - \underset{\sim}{s}^{(1)}_{0}(1) \cdot \underset{\sim}{s}^{(1)}_{0}(2) \Big) \\ &= -\frac{1}{\sqrt{3}} \, \underset{\sim}{\mathbf{s}}(1) \cdot \underset{\sim}{\mathbf{s}}(2) \ . \end{aligned}$$

Thus, the tensorial form of the Heisenberg Hamiltonian of a spin dimer is

$$\underset{\sim}{H}_{\text{dimer}} = \sqrt{3} J \left\{ \underset{\sim}{\mathbf{s}}^{(1)}(1) \otimes \underset{\sim}{\mathbf{s}}^{(1)}(2) \right\}^{(0)} \ . \qquad \text{(A5)}$$

spin triangle - Since the tensorial form of $\underset{\sim}{H}_{\text{dimer}}$ in Eq. (A5) describes a simple bilinear spin-spin interaction, an expression for a general Heisenberg Hamiltonian can now be developed. As a first extension a spin triangle is considered. The Hamiltonian that has to be converted

to an irreducible tensor operator is

$$\begin{aligned} \underset{\sim}{H}_{\triangle} = &- J \left(\underset{\sim}{\mathbf{s}}(1) \cdot \underset{\sim}{\mathbf{s}}(2) + \underset{\sim}{\mathbf{s}}(2) \cdot \underset{\sim}{\mathbf{s}}(3) \right. \\ &\left. + \underset{\sim}{\mathbf{s}}(3) \cdot \underset{\sim}{\mathbf{s}}(1) \right) . \end{aligned} \tag{A6}$$

In a very general form the successive coupling of three single-spin irreducible tensor operators of ranks k_1, k_2 and k_3 leads to

$$\begin{aligned} &\underset{\sim}{\mathbf{T}}^{(k)}_{\cdot\cdot\cdot}(k_1, k_2, k_3, \overline{k}_1) = \\ &\quad \left\{ \left\{ \underset{\sim}{\mathbf{s}}^{(k_1)}(1) \otimes \underset{\sim}{\mathbf{s}}^{(k_2)}(2) \right\}^{(\overline{k}_1)} \otimes \underset{\sim}{\mathbf{s}}^{(k_3)}(3) \right\}^{(k)} . \end{aligned} \tag{A7}$$

Here k denotes the rank of the resulting irreducible tensor operator and $\overline{k}_1$ the rank of the intermediate (coupled) one. The ranks of the many-particle tensor operators are given by the coupling rules for spin quantum numbers known from the spin vector coupling. For example, the rank $\overline{k}_1$ is given by $\overline{k}_1 = |k_1 - k_2|, |k_1 - k_2| + 1, \ldots, k_1 + k_2$ with k being determined accordingly. It must be emphasized that $\underset{\sim}{\mathbf{T}}^{(k)}_{\cdot\cdot\cdot}$ includes all spin-spin interactions of a trimeric spin system, and thus it has to be specified in order to give the desired tensorial formulation of $\underset{\sim}{H}_{\triangle}$.

With $\underset{\sim}{\mathbf{s}}^{(0)} = \underset{\sim}{\mathbb{1}}$ and the tensorial expression found for a bilinear coupling in Eq. (A5) one arrives at

$$\begin{aligned} \underset{\sim}{H}_{\triangle} &= \sqrt{3} J \left(\underset{\sim}{T}^{(0)}_{\cdot\cdot\cdot}(1,1,0,0) + \underset{\sim}{T}^{(0)}_{\cdot\cdot\cdot}(1,0,1,1) \right. \\ &\quad \left. + \underset{\sim}{T}^{(0)}_{\cdot\cdot\cdot}(0,1,1,1) \right) \\ &= \sqrt{3} J \sum_{<i,j>} \underset{\sim}{T}^{(0)}_{\cdot\cdot\cdot}(\{k_i\}, \{\overline{k}_i\} | k_i = k_j = 1) . \end{aligned} \tag{A8}$$

The notation of $\underset{\sim}{T}^{(0)}_{\cdot\cdot\cdot}(\{k_i\}, \{\overline{k}_i\} | k_i = k_j = 1)$ indicates that only the ranks of single-spin tensor operators i and j are chosen to equal 1 whereas the other tensor operators are of zero rank. The rank of the intermediate tensor operator $\overline{k}_1$ is fixed by the contributions of k_1 and k_2 to the zero-rank tensor operator $\underset{\sim}{\mathbf{T}}^{(k=0)}_{\cdot\cdot\cdot}$.

Following Eqs. (A5) and (A8), the Heisenberg Hamiltonian of a general spin system is given by

$$\begin{aligned} &\underset{\sim}{H}_{\text{Heisenberg}} = \\ &\quad \sqrt{3} \sum_{<i,j>} J_{ij} \, \underset{\sim}{T}^{(0)}(\{k_i\}, \{\overline{k}_i\} | k_i = k_j = 1) , \end{aligned} \tag{A9}$$

where the irreducible tensor operator $\underset{\sim}{\mathbf{T}}^{(k)}(\{k_i\}, \{\overline{k}_i\})$ directly depends on the investigated system and the chosen coupling scheme for the coupling of the single-spin tensor operators $\underset{\sim}{\mathbf{s}}^{(k_i)}(i)$.

As an example, the resulting expression for the general, tetrameric tensor operator $\underset{\sim}{\mathbf{T}}^{(k)}_{\cdot\cdot\cdot\cdot}$ in the case of a spin square shall be presented. The underlying coupling scheme of the single-spin tensor operators is chosen to be pairwise because it is often advantageous to couple this way when additionally point-group symmetries are used (see App. A 4). Then, the general irreducible tensor operator of a tetrameric system takes the form

$$\begin{aligned} &\underset{\sim}{\mathbf{T}}^{(k)}_{\cdot\cdot\cdot\cdot}(k_1, k_2, k_3, k_4, \overline{k}_1, \overline{k}_2) = \\ &\quad \left\{ \left\{ \underset{\sim}{\mathbf{s}}^{(k_1)}(1) \otimes \underset{\sim}{\mathbf{s}}^{(k_2)}(2) \right\}^{(\overline{k}_1)} \right. \\ &\quad \left. \otimes \left\{ \underset{\sim}{\mathbf{s}}^{(k_3)}(3) \otimes \underset{\sim}{\mathbf{s}}^{(k_4)}(4) \right\}^{(\overline{k}_2)} \right\}^{(k)} . \end{aligned} \tag{A10}$$

The values of the ranks appearing in Eq. (A10) for the spin square modeled by a Heisenberg Hamiltonian are shown in Tab. I. The ranks of the single-spin tensor operators are fixed by the particular spin-spin interaction. Then, the ranks of the intermediate tensor operators $\overline{k}_1$ and $\overline{k}_2$ can be constructed from the known coupling rules with the given ranks k_i, $i = 1, \ldots, 4$, so as to yield an irreducible tensor operator with $k = 0$.

	k_1	k_2	k_3	k_4	$\overline{k}_1$	$\overline{k}_2$	k
$<1,2>$	1	1	0	0	0	0	0
$<2,3>$	0	1	1	0	1	1	0
$<3,4>$	0	0	1	1	0	0	0
$<4,1>$	1	0	0	1	1	1	0

TABLE I: Values of the ranks for a spin square described by a Heisenberg Hamiltonian. The rows refer to the nearest-neighbor interaction $< i, j >$ between single spins i and j.

a. *Non-Heisenberg contributions to the Hamiltonian*

Although not considered in the work at hand, the irreducible tensor operator approach also serves as a powerful tool for the evaluation of the spectra of non-isotropic many-body spin systems. As already mentioned in Sec. II A, many magnetic molecules can only be well described by including non-Heisenberg interactions. These additional terms within the Hamiltonian model those physical effects that cannot be treated by only considering a Heisenberg exchange between localized many-electron systems. In general, including non-Heisenberg terms like a single-ion anisotropy or an antisymmetric exchange results in a mixing of states with different values of the total-spin quantum number S. Thus, the matrix representation of the Hamiltonian is no longer block-factorized with respect to the irreducible representations of $SU(2)$, i.e. S will not serve as a good quantum number anymore. However, the calculation of the matrix elements within a basis of vector-coupling states is not affected and can still be performed with the help of the Wigner-Eckart theorem.

In this section non-Heisenberg contributions to the Hamiltonian shall be expressed in terms of irreducible tensor operators. This was already done in App. A 2 for

$\underset{\sim}{T}^{(2)}_2(\underset{\sim}{\mathbf{s}}\cdot\underset{\sim}{\mathbf{s}}') = \underset{\sim}{s}^{(1)}_{+1}\cdot\underset{\sim}{s}'^{(1)}_{+1}$
$\underset{\sim}{T}^{(2)}_1(\underset{\sim}{\mathbf{s}}\cdot\underset{\sim}{\mathbf{s}}') = \underset{\sim}{s}^{(1)}_{+1}\underset{\sim}{s}'^{(1)}_{0} - \underset{\sim}{s}^{(1)}_{0}\underset{\sim}{s}'^{(1)}_{+1}$
$\underset{\sim}{T}^{(2)}_0(\underset{\sim}{\mathbf{s}}\cdot\underset{\sim}{\mathbf{s}}') = \sqrt{\frac{3}{2}}\left(\underset{\sim}{s}^{(1)}_{0}\underset{\sim}{s}'^{(1)}_{0} - \frac{1}{3}\underset{\sim}{\mathbf{s}}\cdot\underset{\sim}{\mathbf{s}}'\right)$
$\underset{\sim}{T}^{(2)}_{-1}(\underset{\sim}{\mathbf{s}}\cdot\underset{\sim}{\mathbf{s}}') = \underset{\sim}{s}^{(1)}_{-1}\underset{\sim}{s}'^{(1)}_{0} + \underset{\sim}{s}^{(1)}_{0}\underset{\sim}{s}'^{(1)}_{-1}$
$\underset{\sim}{T}^{(2)}_{-2}(\underset{\sim}{\mathbf{s}}\cdot\underset{\sim}{\mathbf{s}}') = \frac{1}{2}\underset{\sim}{s}^{(1)}_{-1}\cdot\underset{\sim}{s}'^{(1)}_{-1}$

TABLE II: Components of a second rank irreducible tensor operator, composed of single-spin tensor operators, resulting from a decomposition according to Eq. (38).

the pure bilinear Heisenberg interaction. In Eq. (A9) the Heisenberg interaction was formulated in terms of a zero-rank irreducible tensor operator $\underset{\sim}{\mathbf{T}}^{(0)}(\{k_i\},\{\overline{k}_i\})$. The resulting expression can be seen as one contribution to a generalized Hamiltonian[89,90] that contains all possible interactions and operates on the whole spin space, i.e.

$$\underset{\sim}{H}_{\text{general}} = \sum_{\{k_i\}}\sum_{\{\overline{k}_i\}}\sum_{k,q} C^{(k)}_q(\{k_i\},\{\overline{k}_i\})\,\underset{\sim}{T}^{(k)}_q(\{k_i\},\{\overline{k}_i\})\ . \tag{A11}$$

$\underset{\sim}{T}^{(k)}_q$ is the q-th component of the irreducible tensor operator $\underset{\sim}{\mathbf{T}}^{(k)}$ that is a tensorial product of single-spin tensor operators with respect to a certain coupling scheme in analogy to the tensor operator of Eq. (A10). As indicated by the summation indices, the multiple sum contains all possible ranks of $\underset{\sim}{\mathbf{T}}^{(k)}$ that can be constructed from the sets $\{k_i\}$ and $\{\overline{k}_i\}$. $C^{(k)}_q(\{k_i\},\{\overline{k}_i\})$ describes semi-empirical parameters of different contributions. In the case of a Heisenberg interaction as it is shown in Eq. (A9) these parameter are $C^{(0)}(\{k_i\},\{\overline{k}_i\}) = -\sqrt{3}J_{ij}$.

From the generalized Hamiltonian of Eq. (A11) one can deduce the form of the non-Heisenberg terms.[91] These contributions are given in Sec. II A in terms of single-spin operators. In the case of an antisymmetric exchange (Eq. (7)) a proper reformulation with the help of Eq. (37) and Tab. II leads to

$$\underset{\sim}{H}_{\text{antisymmetric}} = -i\sqrt{2}\sum_{i,j}\sum_{q}(-1)^q G^{(1)}_{q,ij}\underset{\sim}{T}^{(1)}_{-q}(k_i=k_j=1)\ , \tag{A12}$$

where the dependence of $\underset{\sim}{\mathbf{T}}^{(k)}$ on the sets $\{k_i\}$ and $\{\overline{k}_i\}$ is although existing not written explicitly. Here, the vector $\vec{G}_{ij}$ is expressed in a local coordinate frame (x',y',z') as an irreducible spherical tensor of first rank. Its components are defined in analogy to Eq. (37) as

$$G^{(1)}_{\pm1,ij} = \mp\sqrt{\frac{1}{2}}\left(G^{x'}_{ij} \pm iG^{y'}_{ij}\right)\ ,$$
$$G^{(1)}_{0,ij} = G^{z'}_{ij}\ .$$

Assuming that the traceless symmetric tensor $\mathbf{D}_{ij}$ takes diagonal form in a local frame, the Hamiltonian for the anisotropic exchange of Eq. (8) can be written in terms of irreducible tensor operators as

$$\underset{\sim}{H}_{\text{anisotropic}} = \sum_{i,j} e_{ij}\left(\underset{\sim}{T}^{(2)}_2(k_i=k_j=1) + \underset{\sim}{T}^{(2)}_{-2}(k_i=k_j=1)\right) + \sum_{i,j} d_{ij}\,\underset{\sim}{T}^{(2)}_0(k_i=k_j=1)\ . \tag{A13}$$

The factors d_{ij} and e_{ij} are given as a combination of the diagonal components of $\mathbf{D}_{ij}$ according to

$$d_{ij} = -\sqrt{\frac{1}{6}}\left(D^{x'x'}_{ij} + D^{y'y'}_{ij} - 2D^{z'z'}_{ij}\right)\ ,$$
$$e_{ij} = \frac{1}{2}\left(D^{x'x'}_{ij} - D^{y'y'}_{ij}\right)\ . \tag{A14}$$

It has to be mentioned that there is no term which is related to the trace of $\mathbf{D}_{ij}$ since this tensor was assumed to be traceless in Eq. (A13). This means that terms arising from $\mathrm{Tr}\,(\mathbf{D}_{ij}) = D^{x'x'}_{ij} + D^{y'y'}_{ij} + D^{z'z'}_{ij}$ have already been included in the Heisenberg Hamiltonian.

In terms of irreducible tensor operators the single-ion anisotropy of Eq. (9) takes as a special case of the anisotropic exchange the form

$$\underset{\sim}{H}_{\text{single-ion}} = \sum_i d_i\left(-\frac{1}{\sqrt{3}}\underset{\sim}{s}^{(0)}(i) + \sqrt{\frac{2}{3}}\underset{\sim}{s}^{(2)}_0(i)\right) + \sum_i e_i\left(\underset{\sim}{s}^{(2)}_2(i) + \underset{\sim}{s}^{(2)}_{-2}(i)\right)\ , \tag{A15}$$

where d_i and e_i follow from Eq. (A14) by setting $i=j$.

Taking a closer look at the matrix elements of the non-Heisenberg Hamiltonians from Eqs. (A12), (A13), and (A15), the Wigner-Eckart theorem directly reflects whether a mixing of states occurs, i.e. whether non-zero matrix elements between vector-coupling states with different values of S and M are present. By evaluating the Wigner-3J symbol from Eq. (41),

$$\begin{pmatrix} S & k & S' \\ -M & q & M' \end{pmatrix}\ ,$$

selection rules can easily be found with respect to Eq. (19). In the case of a Heisenberg Hamiltonian all matrix elements vanish unless the states belong to the same subspace $\mathcal{H}(S,M)$. In contrast, mixing is caused by antisymmetric as well as anisotropic interactions. $\underset{\sim}{H}_{\text{antisymmetric}}$ mixes states with $\Delta S = 0,1$, because k is equal to 1 for the compound tensor operator $\underset{\sim}{\mathbf{T}}^{(k)}$ in Eq. (A12). $\underset{\sim}{H}_{\text{anisotropic}}$ is composed of a sum in which the compound

tensor operator takes $k = 2$ (see Eq. (A13)). Thus, the mixing occurs between states with $\Delta S = 0, 1, 2$. $\underset{\sim}{H}_{\text{single-ion}}$ also mixes states according to the selection rule $\Delta S = 0, 1, 2$.

Concerning the above stated selection rules one must be aware of some restrictions. For instance, $\underset{\sim}{H}_{\text{antisymmetric}}$ does not allow transitions between states with $S = S' = 0$ or $S = S' = \frac{1}{2}$ due to the vector coupling rule. Similar exceptions can be found for the anisotropic exchange and the single-ion anisotropy.

In the field of molecular magnetism the rhombic component of the single-ion anisotropy is often set to zero, i.e. when describing single-molecule magnets $e_i = 0 \,\forall\, i$.[92] In the local frames of the spin sites the Hamiltonian then only contains the $q = 0$-component of $\underset{\sim}{\mathbf{T}}^{(2)}$ leading to a non-vanishing Wigner symbol only if $M = M'$. Thus, the total magnetic quantum number M remains a good quantum number if the anisotropy is uniaxial with the axes pointing into the global z-direction. In this case, M can still be used in order to classify the eigenstates of the system.

3. Matrix elements - decoupling

The calculations of the matrix elements of the Hamiltonian in Eq. (A9) are performed with the help of the Wigner-Eckart theorem (Eq. (41)). For this reason, the coupling scheme of the basis states $|\alpha\, S\, M\rangle$ cannot be chosen independently from $\underset{\sim}{\mathbf{T}}^{(k)}$. Those quantum numbers which appear within the set α should also appear in the sets $\{k_i\}$ and $\{\overline{k}_i\}$, i.e. the couplings for the generation of the basis states and the general irreducible tensor operator of the system should be chosen to be equal. Otherwise, transformations between states of different coupling schemes would be necessary.

In order to show how matrix elements can be calculated, the application of the *decoupling* procedure is discussed for a square system. The Heisenberg Hamiltonian in the tensorial form can be derived from Eq. (A9) and is given by

$$\underset{\sim}{H}_{\square} = \sqrt{3} J \sum_{<i,j>} \underset{\sim}{T}^{(0)}_{::}(\{k_i\}, \{\overline{k}_i\} | k_i = k_j = 1) \; . \tag{A16}$$

The general irreducible tensor operator of the tetrameric system $\underset{\sim}{\mathbf{T}}^{(k)}_{::}$ based on a pairwise coupling scheme was already presented in Eq. (A10). The values of the ranks appearing in $\underset{\sim}{T}^{(k=0)}_{::}(\{k_i\}, \{\overline{k}_i\})$ are tabulated in Tab. I. The pairwise coupling scheme in the used construction of $\underset{\sim}{\mathbf{T}}^{(k)}_{::}$ corresponds to basis states of the form

$$|\alpha\, S\, M\rangle = |s_1 s_2 \overline{S}_1 s_3 s_4 \overline{S}_2 S M\rangle \; .$$

By the application of the Wigner-Eckart theorem, Eq. (41), the calculation of the matrix elements of $\underset{\sim}{H}_{\square}$ is now – apart from the prefactor and the summation over the nearest-neighbor interactions according to Eq. (A16) – reduced to the evaluation of terms like

$$\begin{aligned} &\langle \alpha\, S\, M | \underset{\sim}{T}^{(0)}_{::}(\{k_i\}, \{\overline{k}_i\}) | \alpha'\, S'\, M' \rangle = \\ &\quad (-1)^{S-M} \begin{pmatrix} S & 0 & S' \\ -M & 0 & M' \end{pmatrix} \\ &\quad \times \langle s_1 s_2 \overline{S}_1 s_3 s_4 \overline{S}_2 S || \underset{\sim}{\mathbf{T}}^{(0)}_{::} || s_1 s_2 \overline{S}'_1 s_3 s_4 \overline{S}'_2 S' \rangle \; . \end{aligned} \tag{A17}$$

In the case of a square four such terms appear in $\underset{\sim}{H}_{\square}$ differing from each other by the values of $\{k_i\}$ and $\{\overline{k}_i\}$.

Since the Wigner-3J symbol in Eq. (A17) is reduced to

$$\begin{pmatrix} S & 0 & S' \\ -M & 0 & M' \end{pmatrix} = \frac{(-1)^{S-M}}{\sqrt{2S+1}} \cdot \delta_{S,S'} \delta_{M,M'}$$

because of its special form, the Eq. (A17) itself is reduced to

$$\begin{aligned} &\langle \alpha\, S\, M | \underset{\sim}{T}^{(0)}_{::}(\{k_i\}, \{\overline{k}_i\}) | \alpha'\, S\, M \rangle = \\ &\frac{(-1)^{2(S-M)}}{\sqrt{2S+1}} \cdot \langle s_1 s_2 \overline{S}_1 s_3 s_4 \overline{S}_2 S || \underset{\sim}{\mathbf{T}}^{(0)}_{::} || s_1 s_2 \overline{S}'_1 s_3 s_4 \overline{S}'_2 S \rangle \; . \end{aligned} \tag{A18}$$

Since all matrix elements between states of different S and M vanish, it becomes obvious that all calculations can be performed in subspaces $\mathcal{H}(S, M)$. Furthermore, because $\underset{\sim}{H}_{\square}$ is independent of an external magnetic field and thus no M-dependence of the energies is given, the spectrum can be evaluated in subspaces $\mathcal{H}(S, M = S)$.

Following Eq. (A18) the matrix elements can directly be obtained by determining the reduced matrix elements of $\underset{\sim}{\mathbf{T}}^{(0)}_{::}$. By a successive application of Eq. (44), i.e. a successive decoupling of $\underset{\sim}{\mathbf{T}}^{(0)}_{::}$, the reduced matrix elements are traced back to the reduced matrix elements of single-spin tensor operators that are given in Eqs. (42) and (43) for $k = 0, 1$.

For the reduced matrix element of $\underset{\sim}{\mathbf{T}}^{(k)}_{::}$ the decoupling yields

$$\langle s_1 s_2 \overline{S}_1 s_3 s_4 \overline{S}_2 S || \underset{\sim}{\mathbf{T}}^{(k)}_{::} || s_1 s_2 \overline{S}'_1 s_3 s_4 \overline{S}'_2 S' \rangle =$$
$$\left[(2S+1)(2S'+1)(2k+1)\right]^{\frac{1}{2}} \left[(2\overline{S}_2+1)(2\overline{S}'_2+1)(2\overline{k}_2+1)\right]^{\frac{1}{2}} \left[(2\overline{S}_1+1)(2\overline{S}'_1+1)(2\overline{k}_1+1)\right]^{\frac{1}{2}}$$
$$\times \begin{pmatrix} \overline{S}_1 & \overline{S}'_1 & \overline{k}_1 \\ \overline{S}_2 & \overline{S}'_2 & \overline{k}_2 \\ S & S' & k \end{pmatrix} \begin{pmatrix} s_3 & s_3 & k_3 \\ s_4 & s_4 & k_4 \\ \overline{S}_2 & \overline{S}'_2 & \overline{k}_2 \end{pmatrix} \begin{pmatrix} s_1 & s_1 & k_1 \\ s_2 & s_2 & k_2 \\ \overline{S}_1 & \overline{S}'_1 & \overline{k}_1 \end{pmatrix} \langle s_1 || \underset{\sim}{\mathbf{s}}^{(k_1)} || s_1 \rangle \langle s_2 || \underset{\sim}{\mathbf{s}}^{(k_2)} || s_2 \rangle \langle s_3 || \underset{\sim}{\mathbf{s}}^{(k_3)} || s_3 \rangle \langle s_4 || \underset{\sim}{\mathbf{s}}^{(k_4)} || s_4 \rangle \quad . \tag{A19}$$

In the case of $\underset{\sim}{H}_{\square}$, the appearing ranks of the tensor operators can be found in Tab. I and S' is forced to be $S' = S$ by the Wigner-3J symbol in Eq. (A17).

The clear structure of the resulting expression for a reduced matrix element in Eq. (A19) now allows one to write a highly flexible and structured computer program that takes over the calculation and diagonalization of the Hamilton matrix. Regarding the calculation of the matrix elements, a recurrence formula can be implemented which decouples the irreducible tensor operator of the system step-by-step.

4. Using point-group symmetries

In Sec. II C some general remarks about the use of point-group symmetries have already been made. In order to transform the Hamilton matrix to a block-diagonal form with respect to irreducible representations $\Gamma^{(n)}$ of a point group $\mathcal{G}$, one has to construct symmetrized basis functions $|\alpha\, S\, M\, \Gamma^{(n)}\rangle$. Equation (50) provides the projection operator that projects out that part of a state which belongs to the n-th irreducible representation of $\mathcal{G}$. However, the main challenge when constructing symmetrized basis states is to find an expression for the action of the operators $\underset{\sim}{G}(R_i)$ on states of the form $|\alpha\, S\, M\rangle$.

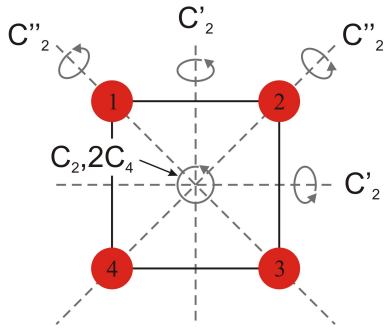

FIG. 9: Sketch of a spin square with D_4-symmetry operations.

Figure 9 shows the coupling graph of a square with D_4-symmetry operations. The operations are labelled with respect to n-fold rotations around the given axes. Operations belonging to the same class are marked with identical labels while identical operations belonging to different classes can be distinguished by the number of primes. The above mentioned operators $\underset{\sim}{G}(R_i)$ which correspond to the displayed operations on the coupling graph can be defined by their action on the product basis composed of the single-spin eigenstates of $\underset{\sim}{s}^z(i)$. The states of the product basis of N identical spins can be denoted by

$$|s_1 m_1\rangle \otimes |s_2 m_2\rangle \otimes \cdots \otimes |s_N m_N\rangle \equiv |m_1\, m_2\, \ldots\, m_N\rangle$$

and fulfill the eigenvalue equation

$$\underset{\sim}{s}^z(i)\ |m_1\, \ldots\, m_i\, \ldots\, m_N\rangle = m_i\ |m_1\, \ldots\, m_i\, \ldots\, m_N\rangle.$$

according to their definition.

Now, in a spin system consisting of N spins an operator $\underset{\sim}{G}(R)$ is considered that is given in the form $\underset{\sim}{G}(\pi(1)\,\pi(2)\,\ldots\,\pi(N))$ and describes a point-group operation. The notation $\underset{\sim}{G}(\pi)$ indicates for all $i = 1, \ldots, N$ that the point-group operation interchanges the spin at site i with the spin at site $\pi(i)$. The action of the operator $\underset{\sim}{G}(R)$ on the product basis is given by

$$\underset{\sim}{G}(R)\ |m_1\, m_2\, \ldots\, m_N\rangle = |m_{\pi(1)}\, m_{\pi(2)}\, \ldots\, m_{\pi(N)}\rangle. \tag{A20}$$

In Eq. (A20) the following happens: by the action of $\underset{\sim}{G}(R)$ the single-spin system at site i takes the z-component which the system at site $\pi(i)$ has taken previously. The result is a different state of the product basis with permuted m-values.

In Tab. III the operators corresponding to the D_4-symmetry operations on a square are given. The operators are classified with respect to the classes they belong to.

D_4	**Classes**				
	E	C_2	$2C_4$	$2C'_2$	$2C''_2$
op's	$\underset{\sim}{G}(1\,2\,3\,4)$	$\underset{\sim}{G}(3\,4\,1\,2)$	$\underset{\sim}{G}(4\,1\,2\,3)$ $\underset{\sim}{G}(2\,3\,4\,1)$	$\underset{\sim}{G}(2\,1\,4\,3)$ $\underset{\sim}{G}(4\,3\,2\,1)$	$\underset{\sim}{G}(1\,4\,3\,2)$ $\underset{\sim}{G}(3\,2\,1\,4)$

TABLE III: Classes of the D_4 point group with corresponding operators for the spin square.

The operators $\underset{\sim}{G}(R)$ are only defined by their action on product states whereas the details of constructing symmetrized basis states that are linear combinations of vector-coupling states of the form $|\alpha\, S\, M\rangle$ are still unknown. How to find an expression for the action of $\underset{\sim}{G}(R)$ on these vector-coupling states is – to some extent – shown in Refs. 93 and 94.

In this section a different perspective concerned with the application of general symmetry operations to a vector-coupling basis is presented. As an example, a π-rotation around the central C_2-axis of a spin square is considered (cf. Fig. 9). The corresponding operator acting in spin space can be found in Tab. III and takes the form $\underset{\sim}{G}(3\,4\,1\,2)$. According to a successive coupling scheme, the vector-coupling basis states are given in the form $|s_1 s_2 \overline{S}_1 s_3 \overline{S}_2 s_4 S M\rangle$. It must be emphasized here that the underlying coupling scheme, that determines the way how basis states are constructed, can be chosen independently from any symmetry considerations, although a suitable choice will reduce the calculations as it is discussed below.

According to the generalized Clebsch-Gordan coefficients for the coupling of four spins and Eq. (32), unfolding the state $|s_1 s_2 \overline{S}_1 s_3 \overline{S}_2 s_4 S M\rangle$ into a linear combination of product states results in the expression

$$\begin{aligned} &|s_1 s_2 \overline{S}_1 s_3 \overline{S}_2 s_4\, S\, M\rangle = \\ &\sum_{\sum_i m_i = M} C^{s_1\, s_2\, \overline{S}_1}_{m_1\, m_2\, \overline{M}_1} \cdot C^{\overline{S}_1\, s_3\, \overline{S}_2}_{\overline{M}_1\, m_3\, \overline{M}_2} \cdot C^{\overline{S}_2\, s_4\, S}_{\overline{M}_2\, m_4\, M} \\ &\quad \times |m_1\, m_2\, m_3\, m_4\rangle\ . \end{aligned} \tag{A21}$$

The summation indices are entirely determined by the constraint $\sum_i m_i = M$. The values of the intermediate magnetic quantum numbers $\overline{M}_i$ can be deduced from the magnetic quantum numbers of the involved single spins, i.e. $\overline{M}_1 = m_1 + m_2$ and $\overline{M}_2 = \overline{M}_1 + m_3$.

Following Eqs. (A20) and (A21), performing the π-rotation described by the operator $\underset{\sim}{G}(3\,4\,1\,2)$ results in the expression

$$\begin{aligned} &\underset{\sim}{G}(3\,4\,1\,2)\ |s_1 s_2 \overline{S}_1 s_3 \overline{S}_2 s_4\, S\, M\rangle = \\ &\sum_{\sum_i m_i = M} C^{s_1\, s_2\, \overline{S}_1}_{m_1\, m_2\, \overline{M}_1} \cdot C^{\overline{S}_1\, s_3\, \overline{S}_2}_{\overline{M}_1\, m_3\, \overline{M}_2} \cdot C^{\overline{S}_2\, s_4\, S}_{\overline{M}_2\, m_4\, M} \\ &\quad \times |m_3\, m_4\, m_1\, m_2\rangle\ . \end{aligned} \tag{A22}$$

Due to the performed permutation on the product states the resulting state cannot easily be represented as a vector-coupling state belonging to the former coupling scheme given by the successive addition of spin operators: $\underset{\sim}{\mathbf{s}}(1) + \underset{\sim}{\mathbf{s}}(2) = \underset{\sim}{\overline{\mathbf{S}}}(1)$, $\underset{\sim}{\overline{\mathbf{S}}}(1) + \underset{\sim}{\mathbf{s}}(3) = \underset{\sim}{\overline{\mathbf{S}}}(2)$, and $\underset{\sim}{\overline{\mathbf{S}}}(2) + \underset{\sim}{\mathbf{s}}(4) = \underset{\sim}{\mathbf{S}}$.

At this point, it becomes obvious that the operator $\underset{\sim}{G}$ is inducing a transition from the coupling scheme, according to which the basis states have initially been constructed, to another one. A proper re-labelling of the summation indices in the sum of Eq. (A22) with respect to a point-group operation R^{-1}, i.e. a $(-\pi)$-rotation around the central C_2-axis, reveals the resulting coupling scheme in which $\underset{\sim}{G}(3\,4\,1\,2)|s_1 s_2 \overline{S}_1 s_3 \overline{S}_2 s_4\, S\, M\rangle$ can be represented as a vector-coupling state.[93] In this special case one finds that $\underset{\sim}{G}(3\,4\,1\,2)$ is inducing a transition to a coupling scheme given by $\underset{\sim}{\mathbf{s}}(3) + \underset{\sim}{\mathbf{s}}(4) = \underset{\sim}{\overline{\mathbf{S}}}(1')$, $\underset{\sim}{\overline{\mathbf{S}}}(1') + \underset{\sim}{\mathbf{s}}(1) = \underset{\sim}{\overline{\mathbf{S}}}(2')$, and $\underset{\sim}{\overline{\mathbf{S}}}(2') + \underset{\sim}{\mathbf{s}}(2) = \underset{\sim}{\mathbf{S}}$. As a shorthand notation one can write

$$|s_1 s_2 \overline{S}_1 s_3 \overline{S}_2 s_4 S M\rangle \xrightarrow{\underset{\sim}{G}(3\,4\,1\,2)} |s_3 s_4 \overline{S}_{1'} s_1 \overline{S}_{2'} s_2 S M\rangle\ ,$$

with the limitation that this expression does not give the concrete values of the appearing quantum numbers of the states. Nevertheless, it illustrates the transition between vector-coupling states of different and thus independent coupling schemes.

In order to clarify the action of an operator representing a point-group operation on a vector-coupling state, the states are now additionally labelled according to the coupling scheme they are belonging to. Additionally, the set of quantum numbers referring to the coupling scheme is abbreviated by Greek letters. Primes indicate different basis states within the same coupling scheme. With these conventions one obtains the following general result for a transition between two coupling schemes a and b which is induced by an operator $\underset{\sim}{G}$ representing a point-group operation:

$$\underset{\sim}{G}\ |\alpha\, S\, M\rangle_a = \delta_{\alpha,\beta}\ |\beta\, S\, M\rangle_b\ . \tag{A23}$$

The Kronecker symbol $\delta_{\alpha,\beta}$ on the right hand side indicates that the values of the spin quantum numbers of the different sets α and β are the same. Re-expressing the right hand side of Eq. (A23) within states belonging to the coupling scheme a, i.e. inserting a suitable form of the identity operator $\underset{\sim}{\mathbb{1}}$, directly leads to the very important final result

$$\begin{aligned} &\underset{\sim}{G}\ |\alpha\, S\, M\rangle_a = \\ &\qquad \sum_{\alpha'} \delta_{\alpha,\beta}\ {}_a\langle \alpha'\, S\, M|\beta\, S\, M\rangle_b\ |\alpha'\, S\, M\rangle_a, \end{aligned} \tag{A24}$$

which contains so-called *general recoupling coefficients* ${}_a\langle \alpha\, S\, M|\beta\, S\, M\rangle_b$. A general recoupling coefficient can be seen as a scalar product between vector-coupling states belonging to different coupling schemes a and b.

Coming back to the π-rotation in the square described above and neglecting the additional labelling of the states with respect to the coupling schemes a and b, Eq. (A24) turns into

$$\begin{aligned} &\underset{\sim}{G}(3\,4\,1\,2)\ |s_1 s_2 \overline{S}_1 s_3 \overline{S}_2 s_4 S M\rangle = \\ &\quad \sum_{\overline{S}'_1, \overline{S}'_2} \delta_{\overline{S}_1, \overline{S}_{1'}} \delta_{\overline{S}_2, \overline{S}_{2'}} |s_1 s_2 \overline{S}'_1 s_3 \overline{S}'_2 s_4 S M\rangle \\ &\quad \times\ \langle s_1 s_2 \overline{S}'_1 s_3 \overline{S}'_2 s_4 S M| s_3 s_4 \overline{S}_{1'} s_1 \overline{S}_{2'} s_2 S M\rangle\ . \end{aligned} \tag{A25}$$

As can be seen from Eq. (A25), the main task when calculating the action of a point-group operation on a

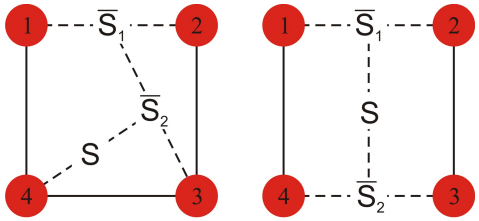

FIG. 10: Visualization of two possible couplings for the square: successive coupling scheme (l.h.s.) and pairwise coupling scheme (r.h.s.).

vector-coupling state is the determination of the general recoupling coefficients connecting states of the initial and the resulting coupling scheme. Generating a formula for general recoupling coefficients can only be performed in a rather advanced procedure. In Sec. A 5 a scheme based on graph-theoretical considerations is presented that allows such calculations.

Regarding the recoupling coefficients that appear when performing point-group operations, a very helpful simplification shall be mentioned here. From Eq. (A22) it can be seen that the action of the operator $\underset{\sim}{G}(3\,4\,1\,2)$ on the product states prevents the re-expression of the resulting linear combination of product states as a simple vector-coupling state belonging to the initial coupling scheme. However, the choice of the coupling scheme according to which the initial basis was constructed is somewhat arbitrary. In order to minimize the computational effort, which is directly related to the number of states with non-zero recoupling coefficient in Eq. (A25), one has to choose a non-successive coupling scheme. A favorable coupling scheme of this kind is shown in Fig. 10. This scheme is referred to as pairwise coupling scheme and the basis states look like $|s_1 s_2 \overline{S}_1 s_3 s_4 \overline{S}_2 SM\rangle$. The π-rotation around the central C_2-axis of the square now induces a transition that can be symbolized by

$$|s_1 s_2 \overline{S}_1 s_3 s_4 \overline{S}_2 SM\rangle \xrightarrow{\underset{\sim}{G}(3\,4\,1\,2)} |s_3 s_4 \overline{S}_{1'} s_1 s_2 \overline{S}_{2'} SM\rangle$$

and leads according to Eq. (A23) to a recoupling coefficient of the form

$$\langle s_1 s_2 \overline{S}_1 s_3 s_4 \overline{S}_2 SM | s_3 s_4 \overline{S}_{1'} s_1 s_2 \overline{S}_{2'} SM\rangle \ .$$

Now, the calculation of a formula for this recoupling coefficient is trivial since the intermediate spin operators of the initial and the resulting coupling scheme are mutually the same, i.e. $\underset{\sim}{\overline{\mathbf{S}}}(1') = \underset{\sim}{\overline{\mathbf{S}}}(2)$ and $\underset{\sim}{\overline{\mathbf{S}}}(2') = \underset{\sim}{\overline{\mathbf{S}}}(1)$. Unfolding $|s_3 s_4 (\overline{S}_{1'} = \overline{S}_2) s_1 s_2 (\overline{S}_{2'} = \overline{S}_1) SM\rangle$ into a linear combination of product states in analogy to Eq. (A21) leads to

$$|s_3 s_4 \overline{S}_2 s_1 s_2 \overline{S}_1 SM\rangle = \sum_{\sum_i m_i = M} C^{s_3\, s_4\, \overline{S}_2}_{m_3\, m_4\, \overline{M}_2} \cdot C^{s_1\, s_2\, \overline{S}_1}_{m_1\, m_2\, \overline{M}_1} \cdot C^{\overline{S}_2\, \overline{S}_1\, S}_{\overline{M}_2\, \overline{M}_1\, M} \times |m_1\, m_2\, m_3\, m_4\rangle \ .$$

In order to convert the Clebsch-Gordan coefficients to a form that appears when unfolding states of the form $|s_1 s_2 \overline{S}_1 s_3 s_4 \overline{S}_2 SM\rangle$ one simply has to use the symmetry property of the Clebsch-Gordan coefficients from Eq. (23). This leads to

$$C^{\overline{S}_2\, \overline{S}_1\, S}_{\overline{M}_2\, \overline{M}_1\, M} = (-1)^{\overline{S}_1 + \overline{S}_2 - S} C^{\overline{S}_1\, \overline{S}_2\, S}_{\overline{M}_1\, \overline{M}_2\, M} \ ,$$

and thus an expression for the recoupling coefficient is obtained which only contains one simple phase factor:

$$\langle s_1 s_2 \overline{S}_1 s_3 s_4 \overline{S}_2 SM | s_3 s_4 \overline{S}_{1'} s_1 s_2 \overline{S}_{2'} SM\rangle = (-1)^{\overline{S}_1 + \overline{S}_2 - S} \ .$$

The action of the operator performing a π-rotation on a state belonging to the pairwise coupling scheme mentioned above therefore directly results in a state belonging to the same coupling scheme with an attached phase factor. Thus, it has been shown that with a cleverly chosen coupling scheme the computational effort, that is required for the calculation of symmetrized basis states according to Eq. (50), can be minimized. The graphical visualization of possible coupling schemes in a square shown in Fig. 10 makes it obvious that one will find a simple recoupling formula depending only on phase factors whenever one can find a coupling scheme that is invariant under the performed symmetry operation.[93] Since one has to sum over all symmetry operations of the group in order to construct symmetrized basis states of a given irreducible representation (see Eq. (50)), the underlying coupling scheme should be chosen in such a way as to simplify all or at least most of the resulting recoupling coefficients. This means that the coupling scheme should be invariant under all or at least most of the symmetry operations.

However, one will not always be able to find a coupling scheme that simplifies the calculation of the recoupling coefficients as shown above. Especially if the system under consideration is exhibiting three-fold symmetry axes, such a procedure turns out to be impossible by means of a pairwise coupling scheme. In this case a generalization of finding a recoupling formula independent of the choice of the coupling scheme becomes necessary.

5. The calculation of general recoupling coefficients

The problem of calculating general recoupling coefficients has to be divided into two parts. The first part is the generation of a formula that describes the transition between two different coupling schemes. The second – and much easier – part is the evaluation of a given formula using a specific set of quantum numbers.[95] This section is exclusively focused on the first part, i.e. the generation of a recoupling formula that links different coupling schemes in systems with an arbitrary number of participating spins which turns out to be more difficult.

By definition the expressions for the transition elements between two different coupling schemes result in

Wigner-nJ symbols (cf. Sec. II B 1). While for three interacting spins Wigner-6J symbols occur, the size n of these Wigner coefficients increases with every additional spin taken into account. For four interacting spins the recoupling coefficient is expressed by a Wigner-9J symbol and for five interacting spins the recoupling is described by Wigner-12J symbols. From a computational point of view it turns out to be unfavorable to use algebraic expressions for higher symbols than Wigner-9J symbols although there exist expressions for 12J symbols and 15J symbols.[74] In order to find an effective way to describe general recoupling coefficients, one should use expressions in which only Wigner-6J symbols appear. These 6J symbols can be calculated using the formula[96]

$$\begin{Bmatrix} j_1 & j_2 & j_3 \\ J_1 & J_2 & J_3 \end{Bmatrix} = \Delta(j_1,j_2,j_3)\Delta(j_1,J_2,J_3) \times \Delta(J_1,j_2,J_3)\Delta(J_1,J_2,j_3)\sum_t \frac{(-1)^t(t+1)!}{f(t)} \ , \tag{A26}$$

where the *triangle coefficient* $\Delta(a,b,c)$ reads

$$\Delta(a,b,c) = \left(\frac{(a+b-c)!\,(a-b+c)!\,(-a+b+c)!)}{(a+b+c+1)!}\right)^{\frac{1}{2}} .$$

The function $f(t)$ in Eq. (A26) is given by

$$\begin{aligned} f(t) = {} & (t-j_1-j_2-j_3)!\,(t-j_1-J_2-J_3)! \\ & \times (t-J_1-j_2-J_3)!\,(t-J_1-J_2-j_3)! \\ & \times (j_1+j_2+J_1+J_2-t)!\,(j_2+j_3+J_2+J_3-t)! \\ & \times (j_3+j_1+J_3+J_1-t)! \ . \end{aligned}$$

The sum in Eq. (A26) is running over nonnegative integer values of t for which no factorial in $f(t)$ has a negative argument. Since the evaluation of Wigner-6J symbols is a rather involved task as can be seen from Eq. (A26), it is helpful to analyze the symmetry properties of the appearing symbols (cf. Fig. II B 1) in order to reduce the computational effort when constructing symmetrized basis states. In this regard, when expressing the action of a point-group operation on a basis state according to Eq. (A24), only those recoupling coefficients have to be calculated which are non-zero.

a. *Binary trees*

In the literature one can find successful implementations that deal with the generation of formulas for general recoupling coefficients which only involve a series of phase factors and Wigner-6J symbols. The most intuitive way of generating a recoupling formula is to operate on so-called binary trees.[97,98] The correspondence between a binary tree and a given coupling scheme is rather obvious. Each coupling of two spins s_a and s_b to a compound spin s_c forms a triad that corresponds to an elementary binary tree shown in Fig. 11. This tree is composed of only three angular momenta and can simultaneously be seen as representing a Clebsch-Gordan coefficient. From such elementary trees a binary tree can be built up step-by-step that represents the chosen coupling scheme. The tree constructed this way then contains all Clebsch-Gordan coefficients that result from the decomposition of a vector-coupling state belonging to the particular coupling scheme into product states (cf. Eqs. (31) and (32)).

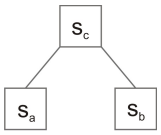

FIG. 11: Binary tree that corresponds to a single coupling of two spins s_a and s_b to a compound spin s_c.

Operating on binary trees in order to generate a formula for a general recoupling coefficient directly leads to the procedure that limits the resulting expressions to 6J symbols. Here, the generation of a formula for the recoupling coefficient $\langle s_1 s_2 \overline{S}_1 s_3 \overline{S}_2 s_4 SM | s_3 s_4 \overline{S}_{1'} s_1 \overline{S}_{2'} s_2 SM\rangle$, that appears in Eq. (A25), shall be presented. In this case, generating a recoupling formula corresponds to finding a transition between the binary trees that are shown in Fig. 12. In other words, one transforms the set of Clebsch-Gordan coefficients that is represented by the initial tree (l.h.s. of Fig. 12) to the set that is represented by the targeted tree (r.h.s. of Fig. 12).

Following the usual graph-theoretical name convention the single-spin quantum numbers are referred to as *leave nodes* while the intermediate spin quantum numbers are called *coupled nodes*. The total-spin quantum number appears as a coupled node of a special kind and is called *root*.

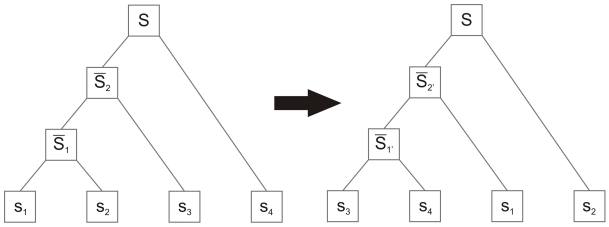

FIG. 12: Transition between two binary trees that has to be performed in order to calculate the recoupling coefficient $\langle s_1 s_2 \overline{S}_1 s_3 \overline{S}_2 s_4 SM | s_3 s_4 \overline{S}_{1'} s_1 \overline{S}_{2'} s_2 SM\rangle$.

There are in general two types of operations that have to be performed in a certain manner in order to yield the desired form of the recoupling coefficient. These operations are shown in Fig. 13 and are called an *exchange* operation and a *flop* operation. Both operations are only performed on subtrees of the initial tree, thus only leading to changes in the particular subtree while leaving the

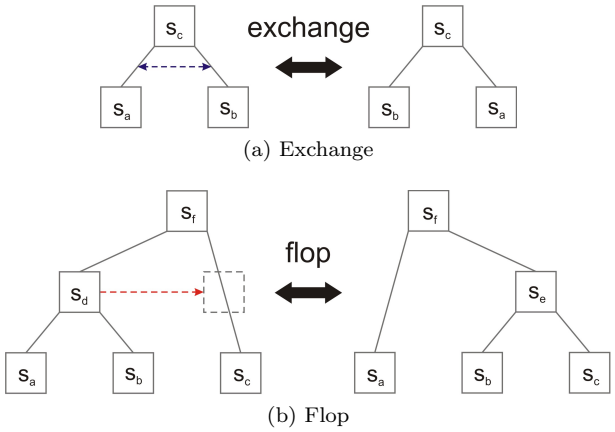

(a) Exchange

(b) Flop

FIG. 13: Operations on a binary tree that lead to a formula for a general recoupling coefficient.

rest of the tree unchanged. With every operation a certain contribution to the recoupling formula is obtained.

An exchange operation refers to a recoupling coefficient that appears when considering the recoupling of two spins s_a and s_b within a single triad. Obviously, the only way of recoupling these spins is to perform an exchange between them. The effect of this operation can easily be derived from unfolding the vector-coupling states $|s_a s_b s_c\rangle$ and $|s_b s_a s_c\rangle$ in terms of product states according to Eq. (22). A state of the form $|s_a s_b s_c\rangle$ can be written as a state of the form $|s_b s_a s_c\rangle$ by using the symmetry property of the Clebsch-Gordan coefficients from Eq. (23), leading to a recoupling coefficient

$$\langle s_a s_b s_c | s_b s_a s_c \rangle = (-1)^{\pm(s_a+s_b-s_c)} \ . \tag{A27}$$

In analogy, a flop operation refers to the recoupling of three spins s_a, s_b, and s_c. Denoting the intermediate spin by s_d and the total spin by s_f, a successive coupling scheme would lead to states that can be written as $|s_a s_b s_d s_c s_f\rangle$. However, a second coupling scheme can be designed that results in states of the form $|s_a s_b s_c s_e s_f\rangle$. By definition a transition between these coupling schemes is described by a Wigner-6J symbol resulting in

$$\begin{aligned}\langle s_a s_b s_d s_c s_f | s_a s_b s_c s_e s_f \rangle = \\ (-1)^{\pm(s_a+s_b+s_c+s_f)} \sqrt{(2s_d+1)(2s_e+1)} \\ \times \begin{Bmatrix} s_a & s_b & s_d \\ s_c & s_f & s_e \end{Bmatrix} \ .\end{aligned} \tag{A28}$$

It has to be mentioned that the flop operation shown in Fig. 13(b) was assumed to create a node, i.e. a spin quantum number that already exists in the targeted coupling scheme, namely s_e. Whenever a flop operation is performed that creates a node which is unknown in the targeted coupling scheme, a summation variable has to be introduced within the resulting contribution to the recoupling formula. This summation variable is completely determined by the symmetry of the appearing Wigner-6J coefficient. The contribution resulting from a flop operation that creates an unknown node $s_{e'}$ within the binary tree would look like

$$\begin{aligned}(-1)^{\pm(s_a+s_b+s_c+s_f)} \sum_{s_{e'}} \sqrt{(2s_d+1)(2s_{e'}+1)} \\ \times \begin{Bmatrix} s_a & s_b & s_d \\ s_c & s_f & s_{e'} \end{Bmatrix} \ .\end{aligned}$$

The desired formula for the recoupling coefficient from Eq. (A25) is now obtained by performing a proper sequence of exchange and flop operations. This sequence is in detail displayed in Fig. 14. It is not the only possible sequence of operations on the binary tree that leads to a recoupling formula for the discussed transition. However, in this simple case the displayed sequence leads to an optimal formula minimizing the number of resulting Wigner-6J symbols.

The result of the operations then reads

$$\begin{aligned}\langle s_1 s_2 \overline{S}_1 s_3 \overline{S}_2 s_4 S M | s_3 s_4 \overline{S}_{1'} s_1 \overline{S}_{2'} s_2 S M \rangle = \\ \sqrt{(2\overline{S}_{1'}+1)(2\overline{S}_2+1)(2\overline{S}_1+1)(2\overline{S}_{2'}+1)} \\ \times (-1)^{s_1+s_2+s_3+s_4+3S} \begin{Bmatrix} \overline{S}_1 & s_3 & \overline{S}_2 \\ s_4 & S & \overline{S}_{1'} \end{Bmatrix} \begin{Bmatrix} s_2 & s_1 & \overline{S}_1 \\ \overline{S}_{1'} & S & \overline{S}_{2'} \end{Bmatrix} \ .\end{aligned} \tag{A29}$$

This simple form was only reached because the flop operations shown in Figs. 14(a) and 14(c) create nodes that already exist in the final coupling scheme, i.e. $\overline{S}_{1'}$ and $\overline{S}_{2'}$.

As long as such simple recoupling coefficients are considered, the process of determining a proper sequence leading from the initial coupling scheme to the targeted one can be easily done by hand and does not need any automatization. Nevertheless, more sophisticated problems result in transitions between binary trees that cannot easily be treated. Then, it becomes necessary to set up an algorithm that automatically creates a proper – ideally optimal – sequence. Regarding binary trees, known implementations[97,98] of such algorithms can be seen as trial-and-error procedures.

By performing a subsequence of operations, initially containing only one exchange or flop operation, one tries to find a tree containing a node that is known in the targeted coupling scheme. Whenever it is impossible to find such a tree with the given number of operations in the subsequence, the number of considered operations is increased, i.e. the subsequence is extended. A successful implementation of this procedure leads to a stepwise creation of the targeted tree in which each step is guaranteed to be performed with the smallest (overall) number of exchange and flop operations. However, the minimization of the number of operations within the performed subsequences does not assure that the resulting recoupling

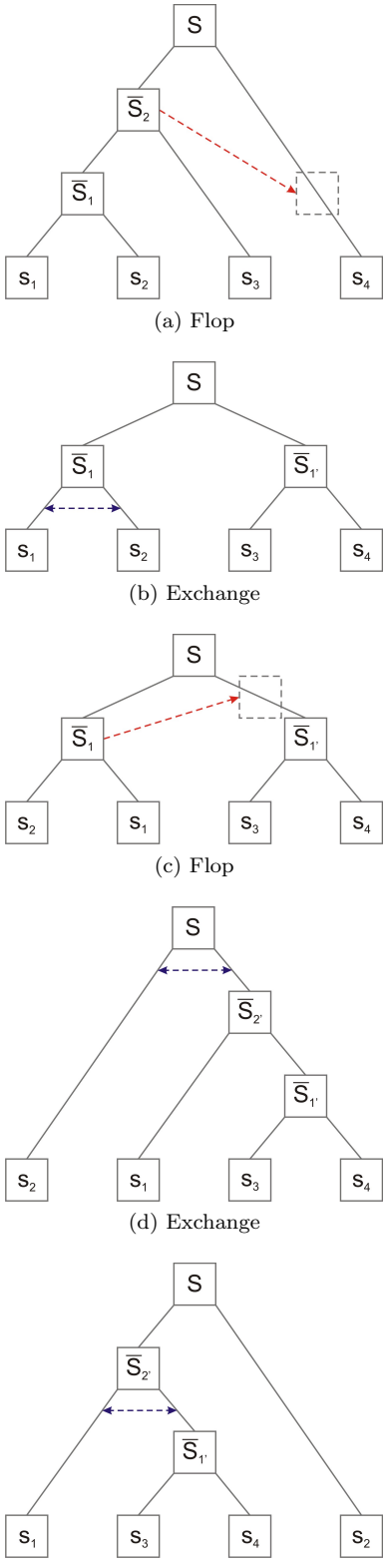

FIG. 14: Sequence of operations leading to the recoupling coefficient $\langle s_1 s_2 \overline{S}_1 s_3 \overline{S}_2 s_4 S M | s_3 s_4 \overline{S}_{1'} s_1 \overline{S}_{2'} s_2 S M \rangle$.

formula is optimal. In general, a recoupling formula is optimal if the number of occurring summation variables and Wigner-6J coefficients is minimal. Since summation variables and 6J symbols are only introduced by flop operations, generating an improved recoupling formula directly corresponds to reducing the number of performed flops.

b. *Graph theoretical solution - Yutsis graphs*

As it was shown in the last section, operating on binary trees in order to generate a recoupling formula involving only phase factors, square roots, and Wigner-6J symbols already leads to a simple and successful procedure. However, the process of determining an optimized sequence of operations remains concealed. In order to improve this process and thus improving the recoupling formula, ideas resulting from more advanced graph-theoretical considerations can be applied. In Refs. 99,100,101,102 the problem of generating a recoupling formula was solved with the help of *Yutsis graphs*. This procedure, providing a technically more difficult, but at the same time theoretically more transparent way of generating an improved recoupling formula, shall be reviewed in this section.

The creation of Yutsis graphs is a straightforward task starting from the background given in App. A 5 a. In order to understand how these graphs evolve, an explanation of how to construct a Yutsis graph shall be given here. Additionally, the reduction of such a graph leading to an improved recoupling formula will be discussed briefly. The interested reader will find a deeper and more theoretical investigation of general features of Yutsis graphs in the literature.[73,103]

As already discussed in Sec. II B 1 an expression for a recoupling coefficient in terms of Clebsch-Gordan coefficients or Wigner-3J symbols can be found by decomposing the bra and the ket states into sums of product states. In order to clarify this procedure, the recoupling coefficient $\langle s_1 s_2 \overline{S}_1 s_3 \overline{S}_2 s_4 S M | s_3 s_4 \overline{S}_{1'} s_1 \overline{S}_{2'} s_2 S M \rangle$ shall be discussed in detail as an example. The decomposition of the bra state was already done in App. A 4 and is given in terms of Clebsch-Gordan coefficients in Eq. (A21). Replacing the Clebsch-Gordan coefficients by Wigner-3J symbols yields

$$
\begin{aligned}
&|s_1 s_2 \overline{S}_1 s_3 \overline{S}_2 s_4 \, S \, M\rangle = \\
&\sum_{\{m_i\}} \left\{ \sum_{\{\overline{M}_i\}} C(\alpha) \begin{pmatrix} s_1 & s_2 & \overline{S}_1 \\ m_1 & m_2 & -\overline{M}_1 \end{pmatrix} \begin{pmatrix} \overline{S}_1 & s_3 & \overline{S}_2 \\ \overline{M}_1 & m_3 & -\overline{M}_2 \end{pmatrix} \right. \\
&\left. \times \begin{pmatrix} \overline{S}_2 & s_4 & S \\ \overline{M}_2 & m_4 & -M \end{pmatrix} \right\} |m_1 \, m_2 \, m_3 \, m_4\rangle \, ,
\end{aligned}
\tag{A30}
$$

where $C(\alpha)$ contains the square roots as well as the phase factors that appear when transforming Clebsch-Gordan coefficients into Wigner symbols. The multiple sums run

over all single-spin magnetic quantum numbers m_i and the magnetic quantum numbers $\overline{M}_i$ of the intermediate spins. The curly brackets are reminiscent of a generalized Wigner coefficient. The same decomposition yields for the ket state

$$|s_3 s_4 \overline{S}_{1'} s_1 \overline{S}_{2'} s_2\, S\, M\rangle = \sum_{\{m_i\}} \left\{ \sum_{\{\overline{M}_{i'}\}} C(\beta) \begin{pmatrix} s_3 & s_4 & \overline{S}_{1'} \\ m_3 & m_4 & -\overline{M}_{1'} \end{pmatrix} \begin{pmatrix} \overline{S}_{1'} & s_1 & \overline{S}_{2'} \\ \overline{M}_{1'} & m_1 & -\overline{M}_{2'} \end{pmatrix} \times \begin{pmatrix} \overline{S}_{2'} & s_2 & S \\ \overline{M}_{2'} & m_2 & -M \end{pmatrix} \right\} |m_1\, m_2\, m_3\, m_4\rangle \ . \tag{A31}$$

From Eqs. (A30) and (A31) one immediately finds the following expression for the recoupling coefficient:

$$\begin{aligned} &\langle s_1 s_2 \overline{S}_1 s_3 \overline{S}_2 s_4\, S\, M | s_3 s_4 \overline{S}_{1'} s_1 \overline{S}_{2'} s_2\, S\, M\rangle \\ &= \sum_{\{m_i\},\{m_i'\}} P^\alpha(\{m_i\}) \cdot P^\beta(\{m_i'\}) \\ &\quad \times \langle m_1\, m_2\, m_3\, m_4 | m_1'\, m_2'\, m_3'\, m_4'\rangle \\ &= \sum_{\{m_i\},\{m_i'\}} \delta_{\{m_i\},\{m_i'\}}\ P^\alpha(\{m_i\}) \cdot P^\beta(\{m_i'\}) \ . \end{aligned} \tag{A32}$$

The abbreviations P^α and P^β stand for the generalized Wigner coefficients that depend on the quantum numbers of the underlying coupling schemes which the sets α and β refer to. The derived expression for the recoupling coefficient in Eq. (A32) is still involving magnetic quantum numbers. Since a recoupling coefficient is in general independent of any magnetic quantum number, a simplification can be found that only involves spin quantum numbers. Such a simplification was already found in the former section with the help of binary trees and will now be discussed on the basis of Yutsis graphs.

The main idea of generating a recoupling formula with the help of Yutsis graphs is – in a first step – to set up a graphical representation of generalized Wigner coefficients as they appear in Eqs. (A30) and (A31). Afterwards, these graphs are joined in order to build up a Yutsis graph that represents the recoupling coefficient. A simplification of the constructed Yutsis graph according to special operations then leads to the desired formula that is independent of magnetic quantum numbers.

FIG. 15: Two diagrams of the same Wigner-3J symbol with different sign of the nodes. The sign is related to the cyclic ordering of the lines.

The building blocks of Yutsis graphs are diagrammatic representations of Wigner-3J symbols which generalized Wigner coefficients are composed of. Figure 15 shows two diagrammatic representations of the same Wigner-3J symbol

$$\begin{pmatrix} s_a & s_b & s_c \\ m_a & m_b & m_c \end{pmatrix} \ .$$

Such a representation consists of three lines and one node. With every spin quantum number in the Wigner symbol a line is identified. The three lines are connected by the node. The node is labelled with a (+) or (−) sign while the lines are characterized by the direction they are pointing in. The (−) sign denotes a clockwise orientation of the spin quantum numbers within the corresponding Wigner-3J symbol (cf. Fig. 15(b)) whereas the (+) sign indicates an anticlockwise ordering (cf. Fig. 15(a)). The free ends of the lines represent the projections of the spin quantum numbers, i.e. the magnetic quantum numbers m_a, m_b, and m_c. If a line leads away from the node, the corresponding magnetic quantum number appears with a positive sign in the Wigner symbol, whereas it appears with a negative sign if the line is directed towards the node.

It is obvious that any operation that changes the diagrams of the Wigner symbol in Fig. 15 will lead to a Wigner symbol that differs from the original one. Changing the sign of the node or simultaneously changing the directions of all lines results in a factor that can be obtained from the symmetry properties of the Wigner-3J symbols described in Sec. II B 1. The change of the sign corresponds to an uneven permutation of spins within the Wigner-3J symbol (cf. Eq. (25)) while the change of all directions of the lines corresponds to multiplying the lower row of the original Wigner-3J symbol by −1 (cf. Eq. (26)). Both operations result in a phase factor of $(-1)^{s_a+s_b+s_c}$ whereas any rotation of the diagram has no effect on the Wigner-3J symbol since the ordering remains unchanged.

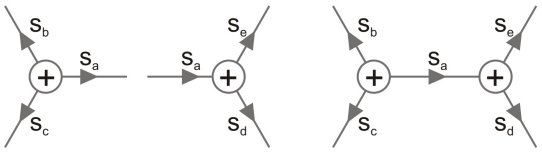

FIG. 16: Contracting the open ends of two lines labelled by s_a that leads to a summation over the magnetic quantum number m_a of the joined lines.

In order to construct a graph that represents a generalized Wigner coefficient, another operation has to be introduced. As shown in Fig. 16, the diagrams of two Wigner symbols can be contracted if two lines exist that are labelled by the same quantum number and point into the same direction. The resulting graph then represents a summation over the corresponding magnetic quantum

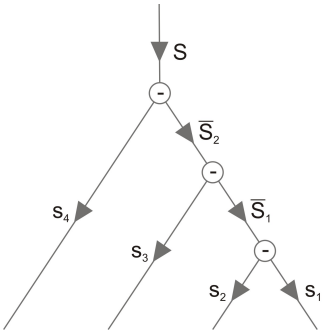

(a) Initial coupling scheme

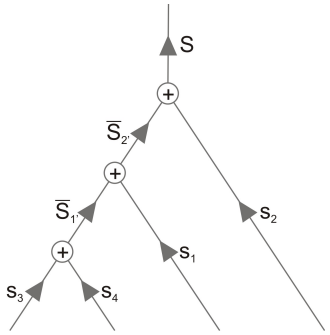

(b) Targeted coupling scheme

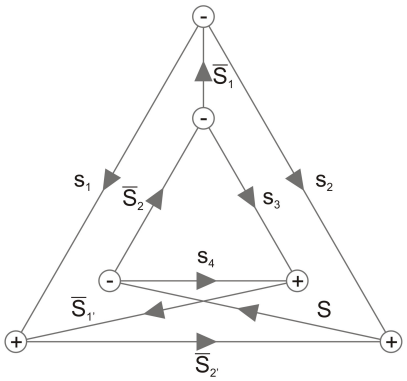

(c) Yutsis graph

FIG. 17: Graphical representation of the generalized Wigner coefficients for the coupling schemes contained in the recoupling coefficient $\langle s_1 s_2 \overline{S}_1 s_3 \overline{S}_2 s_4 SM | s_3 s_4 \overline{S}_{1'} s_1 \overline{S}_{2'} s_2 SM \rangle$ as well as the resulting Yutsis graph.

number given by

$$\sum_{m_a} \begin{pmatrix} s_a & s_b & s_c \\ m_a & m_b & m_c \end{pmatrix} \begin{pmatrix} s_a & s_d & s_e \\ -m_a & m_d & m_e \end{pmatrix} . \qquad \text{(A33)}$$

Figures 17(a) and 17(b) show graphical representations of the generalized Wigner coefficients as found in Eqs. (A30) and (A31). They are easily constructed following the conventions introduced above.

The arrangement of the diagrams representing generalized Wigner coefficients is chosen in such a way as to ease the contraction of both graphs and was proposed in

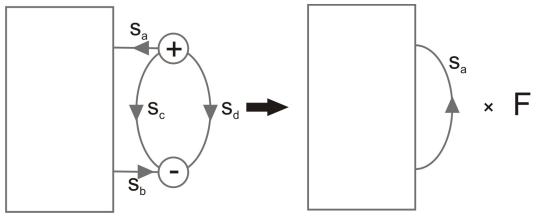

(a) Reduction of a 2-cycle

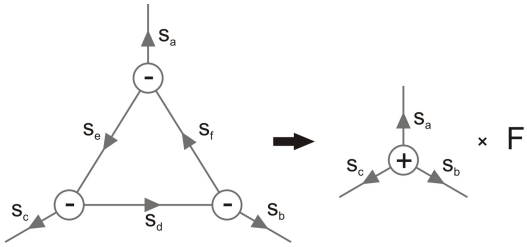

(b) Reduction of a 3-cycle

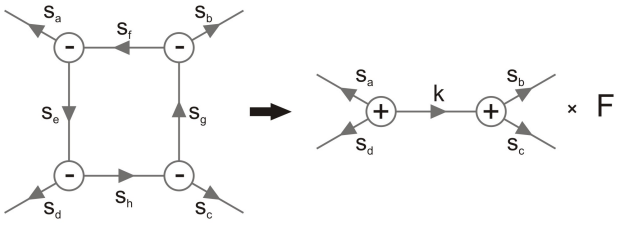

(c) Reduction of a 4-cycle

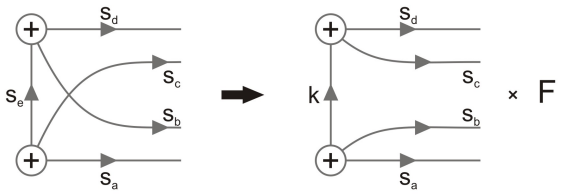

(d) Interchange

FIG. 18: Operations on a Yutsis graph and resulting contributions to the recoupling formula.

Ref. 73. The graph representing the left hand side of the recoupling coefficient contains only negative nodes with the spins being ordered clockwise around these nodes. In the graph belonging to the right hand side of the recoupling coefficient the spins are ordered anticlockwise around the nodes that exclusively have a positive sign. The directions of the lines are chosen in Fig. 17(a) as to match the conventional form of Wigner-3J symbols in generalized Wigner coefficients. In Fig. 17(b) they are chosen in the opposite direction in order to compensate the phase factors that result from the positive signs of the nodes.

In Fig. 17(c) both diagrams of the Wigner coefficients are contracted. The contraction corresponds to a summation over the magnetic quantum numbers m_i, $i = 1, \ldots, 4$, as well as over M. The summations over the magnetic quantum numbers of the intermediate spins

N	F
2	$(2s_a+1)^{-1}\delta_{s_a,s_b}$
3	$\begin{Bmatrix} s_a & s_b & s_c \\ s_d & s_e & s_f \end{Bmatrix}$
4	$\sum_k (-1)^{k+s_f-s_h}(2k+1) \begin{Bmatrix} s_a & s_d & k \\ s_h & s_f & s_e \end{Bmatrix} \begin{Bmatrix} s_b & s_c & k \\ s_h & s_f & s_g \end{Bmatrix}$
>4	$\sum_k (-1)^{s_b+s_c+s_e+k}(2k+1) \begin{Bmatrix} s_a & s_b & k \\ s_d & s_c & s_e \end{Bmatrix}$

TABLE IV: Contributions F to the recoupling formula resulting from the reduction of a N-cycle (cf. Fig. 18). The case $N > 4$ refers to an interchange operation which is used in order to express larger cycles in terms of 2-, 3-, and 4-cycles.

$\{\overline{M}_i\}$ and $\{\overline{M}_{i'}\}$ has already been included in the representations of the coupling schemes in Figs. 17(a) and 17(b), respectively. The resulting Yutsis graph then represents – apart from square roots and phase factors – the recoupling coefficient that is given in Eq. (A32).

In general, a recoupling coefficient is equal to a Yutsis graph, which is constructed according to the above rules, times an additional factor.[73] This factor contains phase factors and square roots that emerge from expressing Clebsch-Gordan coefficients in terms of Wigner-3J symbols and can be written as

$$(-1)^{2\left(S+\sum_{i=1}^{N-2}\overline{S}_{i'}+\mathcal{S}\right)}\left[\prod_{i=1}^{N-2}\left(2\overline{S}_i+1\right)\left(2\overline{S}_{i'}+1\right)\right]^{1/2}. \tag{A34}$$

Here N is the number of single spins in the system under consideration and the sum in the exponent is running over all intermediate spin quantum numbers $\overline{S}_{i'}$ of the targeted coupling scheme. $\mathcal{S}$ represents the sum of the so-called *first coupled angular momenta*, i.e. the sum of those spins that appear in the bra-ket notation of the recoupling coefficient in the first position of each coupling triad. In the case of the recoupling coefficient $\langle s_1 s_2 \overline{S}_1 s_3 \overline{S}_2 s_4 SM | s_3 s_4 \overline{S}_{1'} s_1 \overline{S}_{2'} s_2 SM\rangle$, the sum of the first coupled angular momenta is given by

$$\mathcal{S} = s_1 + \overline{S}_1 + \overline{S}_2 + s_3 + \overline{S}_{1'} + \overline{S}_{2'} \ .$$

The formula for the recoupling coefficient is now obtained by a successive reduction of *cycles* that appear in the graph. A cycle refers to a loop that connects a certain number of nodes. Depending on the number of connected nodes, different operations exist that reduce the graph. Figure 18 shows the operations leading to a reduction of 2-, 3-, and 4-cycles. Additionally, an interchange operation is shown that can be used in order to express cycles which cannot be reduced immediately, i.e. cycles with more than four nodes, in terms of 2-, 3-, and 4-cycles.[101] The contributions F to the recoupling formula resulting from the shown operations are listed in Tab. IV. The values for the quantum numbers k related to the re-labelled edges in Figs. 18(c) and 18(d) are determined by the symmetry properties of the Wigner-6J symbols within these contributions. Whenever performing reductions on a Yutsis graph, the directions of the edges as well as the signs of the nodes have to be considered carefully. Within the Yutsis graph that is supposed to be reduced these directions and signs eventually have to be changed in order to match the constellation of the edges and the nodes shown in Fig. 18. In this process the change of the direction of an edge s, i.e. a contracted line, contributes with $(-1)^{2s}$ to the phase of the recoupling coefficient.

The contributions to the recoupling formula arising from reducing the Yutsis graph according to the above mentioned operations are discussed in detail in Ref. 73 and shall not be further explained here for the sake of brevity.

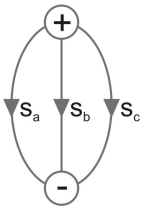

FIG. 19: Graphical representation of a triangular delta.

A Yutsis graph is said to be reduced whenever a graphical representation is obtained that corresponds to the one in Fig. 19. This representation is called a *triangular delta* and gives a factor 1, if s_a, s_b, and s_c satisfy the triangular condition (Eq. (19)), and a factor 0 otherwise.[73]

Coming back to the example of calculating the recoupling coefficient $\langle s_1 s_2 \overline{S}_1 s_3 \overline{S}_2 s_4 SM | s_3 s_4 \overline{S}_{1'} s_1 \overline{S}_{2'} s_2 SM\rangle$ that is displayed in Fig. 17(c), one immediately finds two 3-cycles which can be reduced in order to generate a recoupling formula: s_1-s_2-$\overline{S}_{2'}$ and s_3-s_4-$\overline{S}_2$. As a result of this reduction, the recoupling formula contains apart from phase factors and square roots two Wigner-6J symbols as in Eq. (A29).

However, as already mentioned in App. A 5 a there is in general more than one possibility of reducing a graph. Figure 20 shows a possible first step that reduces the outer triangle spanned by the edges s_1, s_2, and $\overline{S}_{2'}$. For the sake of clarity the signs of the nodes as well as the directions of the edges are omitted since they only contribute to the phase of the recoupling coefficient. As one can see after reducing the outer triangle, four different triangles appear. The reduction of each triangle would then lead to a triangular delta and therefore to a completed recoupling formula. These formulas look slightly different but, can of course be transformed into each other. One possible expression for the recoupling

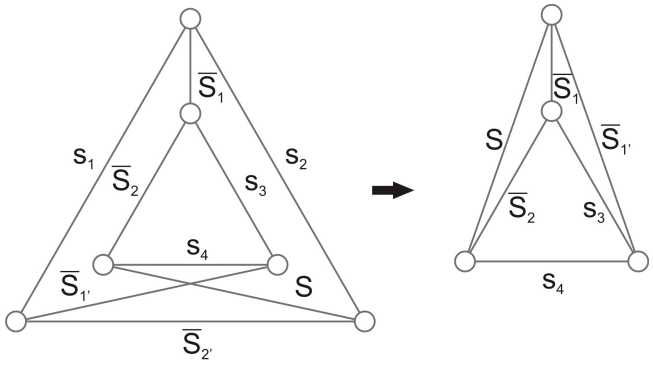

FIG. 20: Reduction of the outer triangle of the Yutsis graph from Fig. 17(c).

coefficient is given by

$$\begin{aligned}\langle s_1 s_2 \overline{S}_1 s_3 \overline{S}_2 s_4 SM | s_3 s_4 \overline{S}_{1'} s_1 \overline{S}_{2'} s_2 SM\rangle = \\ (-1)^{-s_1-s_2-s_3-s_4+\overline{S}_1-\overline{S}_{1'}+2\overline{S}_{2'}} \\ \times \sqrt{(2\overline{S}_{1'}+1)(2\overline{S}_{2'}+1)(2\overline{S}_1+1)(2\overline{S}_2+1)} \\ \times \begin{Bmatrix} S & \overline{S}_1 & \overline{S}_{1'} \\ s_1 & \overline{S}_{2'} & s_2 \end{Bmatrix} \begin{Bmatrix} s_4 & S & \overline{S}_2 \\ \overline{S}_1 & s_3 & \overline{S}_{1'} \end{Bmatrix} .\end{aligned} \tag{A35}$$

So far, this section has dealt with the construction of a Yutsis graph and those operations that reduce this graph to a triangular delta. In principle, one could generate recoupling formulas and calculate general recoupling coefficients with this information. In the discussed example of Fig. 17(c) only triangles appear leading to an easy reduction contributing two Wigner-6J symbols to the recoupling formula. However, in larger systems with high symmetry often more complicated recoupling coefficients have to be calculated (cf. App. B). In order to minimize the computational effort it is desirable that to generate a formula that contains as few Wigner-6J symbols and summation indices as possible. Again, these result from triangles, squares, and cycles of higher order.

The most intuitive way of generating an improved recoupling formula is to reduce the smallest cycles first. This idea was implemented in Refs. 99,100,101 and already yields considerably improved formulas in comparison to the use of a trial-and-error technique. However, these formulas can be further improved by using a more sophisticated strategy of reducing cycles.[102]

Summarizing this section, one can say that with the help of graph-theoretical methods the effect of general point-group operations on vector-coupling states can be determined. Once this effect is known, the eigenstates of the system under consideration can be labelled with respect to irreducible representations of the point group. This characterization not only reduces the dimensions of the Hamilton matrices saving hardware resources, but it also provides deeper insight into the physics of the system arising from the geometry.

6. Irreducible tensor operator technique and high performance computing

The computational realization of the theoretical background presented in this work has been a central task. The performed calculations would not have been possible without developing a highly parallelized computer program that is well adapted to the use in a high performance computing environment. With respect to this, some general remarks on the implementation of the developed concepts shall be given in this section.

Since several terms appear in this section which might be unknown to the reader, their particular meaning as well as related aspects shall be discussed first. The term *computation time* refers to the cumulative time that is needed in order to perform a certain number of floating point operations (FLOP's). The *execution time* refers to the runtime of the considered part of the program. Assuming a parallel execution of the program with optimal performance, the computation time remains unchanged although the operations are performed in parallel. A reduction of the computation time can be achieved by reducing the number of FLOP's that have to be performed. In contrast to this, the execution time usually decreases with increasing number of processing units. The change of the execution time as a function of the used processing units is called *scaling behavior*. It is referred to as optimal if the execution time is divided by two whenever the number of used processing units is doubled. The *speed up* S_p using p processing units is defined as

$$S_p = \frac{T_1}{T_p} , \tag{A36}$$

where T_1 and T_p refer to the execution times of the sequential and the parallelized algorithm, respectively. As can be seen, an optimal speed up corresponds to $S_p = p$. The optimal speed up can be achieved if the whole source code can be parallelized without dependencies between the operations which are executed in parallel. Practically, sequential regions and communication between the processing units often limit the speed up to a value that is lower than the number of used processing units.

In general, the computational realization of the presented framework can be divided into two completely independent parts. On the one hand a matrix representation of the Hamiltonian is set up with the help of the irreducible tensor operator approach. On the other hand this matrix or independent blocks of it are diagonalized, i.e. the eigenvalues and eigenvectors are determined numerically.

In the irreducible tensor operator approach the matrix elements are calculated using the Wigner-Eckart theorem and the decoupling procedure presented in App. A 3. Since the decoupling procedure splits up reduced matrix elements of compound tensor operators, calculations are most easily performed by a recursive implementation of this particular step. As can be seen from Eq. (A19), in

every single decoupling process a Wigner-9J symbol appears. Due to calculational reasons the Wigner-9J symbols are expressed in terms of Wigner-6J symbols. As a result, a large amount of Wigner symbols has to be calculated in order to set up the Hamilton matrix. In general, Wigner-6J symbols are calculated using Eq. (A26), and calculations can be sped up if the values of the Wigner symbols, once calculated, are stored and read out from the memory whenever needed. However, only those values of the Wigner symbols should be stored that are non-zero. Otherwise one would use too much memory that is required afterwards in order to store the Hamilton matrix. Regarding this point, by analyzing their symmetry properties it can be checked whether the Wigner symbols are non-zero and have to be looked up.

If point-group symmetries are used, a very decisive role concerning the computation time is played by the construction of symmetrized basis states. These functions appear as linear combinations of the initial basis states. The weight of the states that are included in these linear combinations is determined by general recoupling coefficients. If a coupling scheme can be found that is invariant under all point-group operations, the number of states that contribute to a linear combination representing a symmetrized basis state is minimized. As already mentioned, a reduction of computation time is achieved by choosing a coupling scheme that minimizes the number of appearing summation indices and Wigner-6J symbols.

A second part is concerned with the diagonalization of the Hamilton matrix. Since all appearing matrices are hermitian, only the upper triangle of the matrix has to be determined. This way computation time is drastically lowered.

As long as a proper scaling is achieved the most intuitive way to speed up calculations using high performance computers is to distribute calculations among many processing units. Next, some remarks on the performance of the program code that has been written in order to determine the energy spectra of magnetic molecules shall be given.

The program has been parallelized by using OpenMP[104] directives. There are three regions that are executed in parallel: the construction of symmetrized basis states, calculation of the Hamilton matrix, and its diagonalization. The diagonalization has been performed using routines based on the `LAPACK`[105] package. Often, these routines are already parallelized and cannot be further optimized that way. It turned out that on the architectures the calculations have been performed on the diagonalization routines only scale well up to the use of four cores. For this reason, the matrix diagonalization always contributes as a constant to the execution times in the following considerations since it has always been performed using four processing units, i.e. cores. The remaining part of the source code has shown a different behavior if parallelized. Mostly, a considerable speed up has been achieved by calculating single matrix elements in parallel, because the matrix elements only depend on the quantum numbers of the involved states and are completely independent from each other. In addition to the parallel set up of the matrices several steps within the construction of symmetrized basis states have also been parallelized.

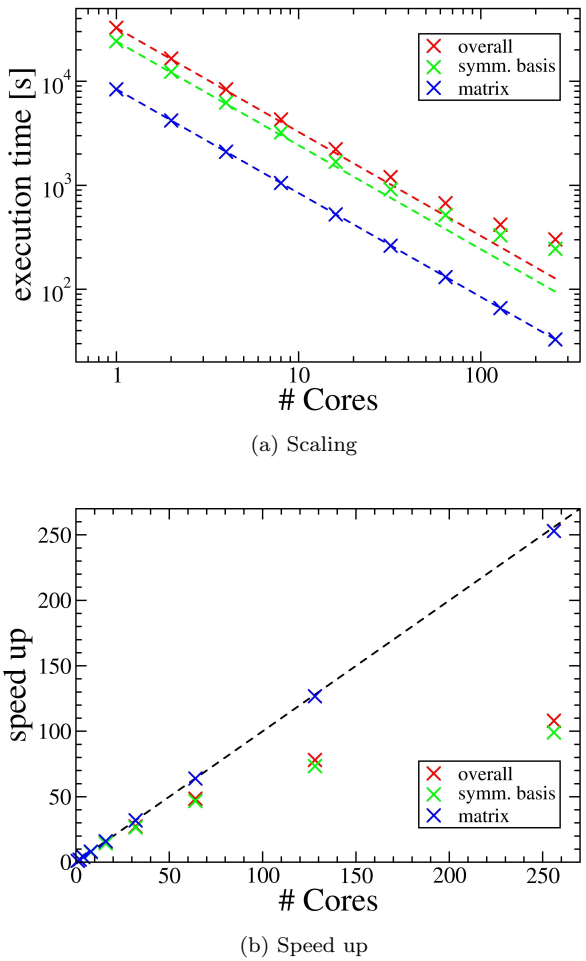

(a) Scaling

(b) Speed up

FIG. 21: Overall scaling (red crosses) and scaling of openMP parallelized regions (green and blue crosses) of exemplary calculations on the SGI altix 4700 platform of HLRB II (top). Speed up of the calculations (bottom). The dashed lines refer to optimal scaling behavior.

Figure 21 shows the performance of the parallelized program for the determination of the energy eigenvalues of a cuboctahedral system with $s = 3/2$ and applied O_h point-group symmetry in the subspace $\mathcal{H}(S = 0, M = 0, E_g)$. Calculations have been performed on the SGI altix 4700 platform of HLRB II at the Leibniz Computing Center in Garching.

One clearly sees that the overall performance is dominated by contributions from the construction of symmetrized basis states. Using an increasing number of cores, the speed up of the construction of symmetrized basis states already starts deviating from the optimal behavior if more than 16 cores are used. This deviation is not surprising since the construction of the symmetrized

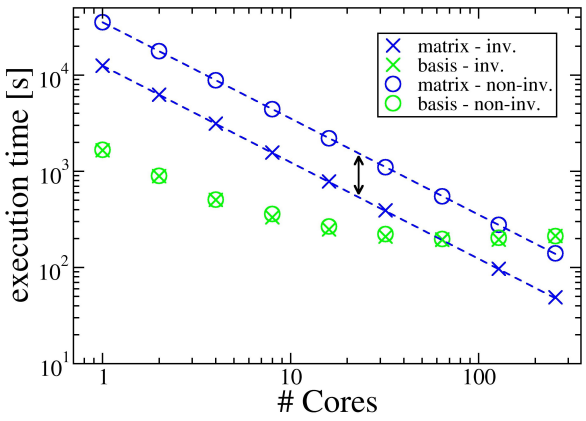

FIG. 22: Scaling of OpenMP parallelized regions. Exemplary calculations have been performed using different coupling schemes (cuboctahedron $s = 3/2$, D_2, $\mathcal{H}(S = 0, M = 0, A_1)$). The crosses refer to an invariant coupling scheme while the circles refer to a non-invariant coupling scheme. The black arrow indicates the different execution times for the set up of the matrices and the dashed lines show the optimal scaling behavior.

basis states can only be partially parallelized. In contrast, the scaling behavior within the region that is concerned with the calculation of the matrix elements is optimal up to the use of 256 cores. Resulting from the contributions of the parallelized and the remaining sequential regions, the overall speed up seems to be limited to a value of about 120.

The above considerations show that the construction of symmetrized basis states plays an important role for extending the limits of numerical exact diagonalization with the help of the concepts presented in this work. Whenever the dimensions of the appearing matrices are to be reduced by the incorporation of point-group symmetries, a certain amount of additional computation time has to be spent on the construction of symmetrized basis states. Since the construction procedure cannot easily be parallelized, the use of more processing units within this particular region does not always lead to the desired reduction of execution time. In any case, one has to ensure that the recoupling formulas, which determine the number of performed FLOP's, are the simplest in order to reduce computation time. As already mentioned, this can be achieved by choosing a coupling scheme that is invariant under the operations of the assumed point-group. The resulting recoupling formulas do then not contain Wigner symbols and are optimal.

In Fig. 22 the execution times for the determination of the energy eigenvalues of a cuboctahedron with $s = 3/2$ in the subspace $\mathcal{H}(S = 0, M = 0, A_1)$ are shown in dependence on the chosen coupling scheme. The used point-group symmetry has been D_2 and execution times are given for the the choice of a completely invariant and a non-invariant coupling scheme, respectively. Comparing the scaling behavior, one can see that the performance of both calculations is limited by the construction of the symmetrized basis states. Furthermore, it becomes obvious that the set up of the matrices is heavily influenced by the particular form of the symmetrized basis states. In the case of the non-invariant coupling scheme the set up of the matrix has been much slower than in the case of the invariant coupling scheme because the symmetrized basis states involve more states of the initial (vector-coupling) basis.

APPENDIX B: PRE-PRINTS OF PUBLICATIONS

1. Phys. Rev. B 79, 104419 (2009)

Numerically exact and approximate determination of energy eigenvalues for antiferromagnetic molecules using irreducible tensor operators and general point-group symmetries

Roman Schnalle*
Universität Osnabrück, Fachbereich Physik, D-49069 Osnabrück, Germany

Jürgen Schnack†
Universität Bielefeld, Fakultät für Physik, Postfach 100131, D-33501 Bielefeld, Germany
(Dated: September 1, 2009)

For small enough quantum systems numerical exact and complete diagonalization of the Hamiltonian enables one to evaluate and discuss all static, dynamic, and thermodynamic properties. In this article we consider Heisenberg spin-systems and extend the range of applicability of the exact diagonalization method by showing how the irreducible tensor operator technique can be combined with an unrestricted use of general point-group symmetries. We also present ideas how to use spin-rotational and point-group symmetries in order to obtain approximate spectra.

PACS numbers: 75.10.Jm,75.50.Xx,75.40.Mg,75.50.Ee
Keywords: Heisenberg model, Numerically exact energy spectrum

I. INTRODUCTION

The knowledge of energy spectra of small magnetic systems such as magnetic molecules is indispensable for the (complete) understanding of their spectroscopic, dynamic, and thermodynamic properties. In this respect numerical exact diagonalization of the appropriate quantum Hamiltonian is a highly desired method. Nevertheless, such an attempt is very often severely restricted due to the huge dimension of the underlying Hilbert space. For a magnetic system of N spins of spin quantum number s the dimension is $(2s+1)^N$ which grows exponentially with N. Group theoretical methods can help to ease this numerical problem. A further benefit is given by the characterization of the obtained energy levels by quantum numbers and classification according to irreducible representations.

Along these lines much effort has been put into the development of an efficient numerical diagonalization technique of the Heisenberg model using irreducible tensor operators, i.e. employing the full rotational symmetry of angular momenta.[1–6] A combination of this meanwhile well established technique with point-group symmetries is not very common since a rearrangement of spins due to point-group operations easily leads to complicated basis transformations between different coupling schemes. A possible compromise is to use only part of the spin-rotational symmetry (namely rotations about the z–axis) together with point-group symmetries[7] or to expand all basis states in terms of simpler product states.[8–10] To the best of our knowledge only a few attempts have been undertaken to combine the full spin-rotational symmetry with point-group symmetries. O. Waldmann combines the full spin-rotational symmetry with those point-group symmetries that are compatible with the spin coupling scheme, i.e. avoid complicated basis transforms between different coupling schemes.[11] Especially low-symmetry groups such as D_2 are often applicable since the coupling scheme can be organized accordingly, compare Ref. 12 for an early investigation. Sinitsyn, Bostrem, and Ovchinnikov follow a similar route for the square lattice antiferromagnet by employing D_4 point-group symmetry.[13,14] This already establishes a very powerful numerical method.

In this article we show how the irreducible tensor operator technique can be combined with an unrestricted use of general point-group symmetries. The problem, that the application of point-group operations leads to states belonging to a basis characterized by a different coupling scheme whose representation in the original basis is not (easily) known, can be solved by means of graph theoretical methods that have been developed in another context.[15,16] We discuss how this methods can be implemented and present results for numerical exact diagonalizations of Heisenberg spin systems of unprecedented size.

Having these methods developed we also discuss ideas of approximately obtaining energy spectra of so-called bipartite, i.e. non-frustrated, antiferromagnetic spin systems. The idea is to perform numerical diagonalizations in the orthogonal Hilbert subspaces characterized by spin and point-group quantum numbers using only a restricted but carefully chosen basis subset. We demonstrate how this idea works for archetypical spin systems such as bipartite or slightly frustrated spin rings. The advantage compared to alternative approximate methods such as Density Matrix Renormalization Group[17–19] (DMRG), Lanczos,[20] or Quantum Monte Carlo[21–23] (QMC) techniques is, that one obtains many energy levels together with their spectroscopic classification which can be of great use for the discussion of Electron Paramagnetic Resonance (EPR), Nuclear Magnetic Resonance (NMR), or Inelastic Neutron Scattering (INS) spectra. In this respect our idea can provide a valuable complement to the already established approximate

methods.

The article is organized as follows. In Sec. II we explain the idea of a combined usage of spin-rotational and point-group symmetry. Section III provides examples for full diagonalization studies. Our approximate diagonalization scheme is introduced in Sec. IV, whereas Sec. V provides example calculations on bipartite systems. The paper closes with a summary.

II. THEORETICAL METHOD

A. Irreducible tensor operator approach

The physics of many magnetic molecules can be well understood with the help of the isotropic Heisenberg model with nearest-neighbor coupling. The action of an external magnetic field is accounted for by an additional Zeeman term. The resulting Hamiltonian then looks like

$$\underset{\sim}{H} = -\sum_{i,j} J_{ij} \underset{\sim}{\mathbf{s}}(i) \cdot \underset{\sim}{\mathbf{s}}(j) + g\mu_B \underset{\sim}{\mathbf{S}} \cdot \vec{B} \ . \tag{1}$$

The sum reflects the exchange interaction between single spins given by spin operators $\underset{\sim}{\mathbf{s}}$ at sites i and j. For the sake of simplicity we assume a common isotropic g–tensor. Then the Zeeman term couples the total spin operator $\underset{\sim}{\mathbf{S}} = \sum_{i=1}^{N} \underset{\sim}{\mathbf{s}}(i)$ to the external magnetic field $\vec{B}$. A negative value of J_{ij} refers to an antiferromagnetic coupling.

For the following discussion an antiferromagnetic nearest-neighbor exchange coupling of constant value $J < 0$ is assumed (which can easily be generalized), then the Heisenberg part can be written as

$$\underset{\sim}{H}_{\mathrm{Heisenberg}} = -J \sum_{<i,j>} \underset{\sim}{\mathbf{s}}(i) \cdot \underset{\sim}{\mathbf{s}}(j) \ , \tag{2}$$

where the summation parameter $< i, j >$ indicates the summation running over nearest-neighbor spins counting each pair only once. Since the commutation relations

$$\left[\underset{\sim}{H}_{\mathrm{Heisenberg}}, \underset{\sim}{\mathbf{S}} \right] = 0 \tag{3}$$

hold it is possible to find a common eigenbasis $\{|\nu\rangle\}$ of $\underset{\sim}{H}_{\mathrm{Heisenberg}}$, $\underset{\sim}{\mathbf{S}}^2$ and $\underset{\sim}{S}_z$. We denote the corresponding eigenvalues as E_ν, S_ν and M_ν. Due to spin-rotational symmetry, Eq. (3), the eigenvalues of the Hamiltonian (1) can be evaluated (later) according to

$$E_\nu(B) = E_\nu + g\mu_B B M_\nu \ , \tag{4}$$

where the direction of the external field $\vec{B}$ defines the z-axis.

Calculating the eigenvalues here corresponds to finding a matrix representation of the Hamiltonian and diagonalizing it numerically. A very efficient and elegant way of finding the matrix elements of Eq. (2) is based on the use of irreducible tensor operators. Apart from its elegance it drastically reduces the dimensionality of the problem because it becomes possible to work directly within the subspace $\mathcal{H}(S, M = S)$ of the total Hilbert space $\mathcal{H}$ characterized by quantum numbers S and $M = S$; for typical dimensions compare for instance Ref. 24.

The calculation of matrix elements of the given Hamiltonian using irreducible tensor operators is compulsorily related to the application of the Wigner-Eckart-theorem. The Wigner-Eckart-theorem

$$\langle \alpha\, S\, M | \underset{\sim}{T}^{(k)}_q | \alpha'\, S'\, M' \rangle = (-1)^{S-M} \langle \alpha\, S || \underset{\sim}{\mathbf{T}}^{(k)} || \alpha'\, S' \rangle \begin{pmatrix} S & k & S' \\ -M & q & M' \end{pmatrix} \tag{5}$$

states that a matrix element of the q-th component of an irreducible tensor operator $\underset{\sim}{\mathbf{T}}^{(k)}$ of rank k is given by the reduced matrix element $\langle \alpha\, S || \underset{\sim}{\mathbf{T}}^{(k)} || \alpha'\, S' \rangle$ and a factor containing a Wigner-3J symbol.[25]

It should be emphasized that the reduced matrix element is completely independent of any magnetic quantum number M. The basis in Eq. (5) is given following the well-known vector-coupling-scheme. The quantum number α within the ket $|\alpha\, S\, M\rangle$ refers to a set of intermediate spin quantum numbers resulting from the coupling of single spins s to the total spin quantum number S. In order to apply the Wigner-Eckart-theorem it is necessary to express the Heisenberg Hamiltonian in Eq. (2) with the help of irreducible tensor operators. Therefore the single-spin vector operators $\underset{\sim}{\mathbf{s}}(i)$ can be seen as irreducible tensor operators of rank $k = 1$ with components $q = -1, 0, 1$. The relation to the components of the vector operators is given by

$$\underset{\sim}{s}^{(1)}_0 = \underset{\sim}{s}^{z}, \quad \underset{\sim}{s}^{(1)}_{\pm 1} = \mp \sqrt{\frac{1}{2}} \left(\underset{\sim}{s}^{x} \pm i \underset{\sim}{s}^{y} \right) \ . \tag{6}$$

Writing the Heisenberg exchange term as a tensor product of the single-spin irreducible tensor operators results in[2]

$$\underset{\sim}{H}_{\mathrm{Heisenberg}} = \sqrt{3} J \sum_{<i,j>} \underset{\sim}{T}^{(0)}(\{k_l\}, \{\overline{k}_m\} | k_i = k_j = 1) \ . \tag{7}$$

$\underset{\sim}{T}^{(0)}$ is a zero-rank irreducible tensor operator depending on the set $\{k_l\}$, $l = 1, \ldots, N$, which gives the ranks of single-spin irreducible tensor operators and the set $\{\overline{k}_m\}$, $m = 1, \ldots, N-1$, which refers to the ranks of intermediate irreducible tensor operators. In a successive coupling scheme within a system of N spins an irreducible tensor operator of this kind would look like

$$\underset{\sim}{T}^{(0)}(\{k_l\}, \{\overline{k}_m\}) = \{ \ldots \{ \{ \underset{\sim}{\mathbf{s}}^{(k_1)}(1) \otimes \underset{\sim}{\mathbf{s}}^{(k_2)}(2) \}^{(\overline{k}_1)} \otimes \underset{\sim}{\mathbf{s}}^{(k_3)}(3) \}^{(\overline{k}_2)} \ldots \}^{(\overline{k}_{N-2})} \otimes \underset{\sim}{\mathbf{s}}^{(k_N)}(N) \}^{(0)} \ . \tag{8}$$

The notation $\underset{\sim}{T}^{(0)}(\{k_l\}, \{\overline{k}_m\} | k_i = k_j = 1)$ corresponds to the situation in which the ranks of all single-spin tensor

operators are zero except those at sites i and j which are tensor operators of rank 1.

The set $\{\overline{k}_m\}$ results from the chosen coupling scheme, for example of the form of Eq. (8), with known ranks of single-spin tensor operators taking into account addition rules for spin quantum numbers of the vector coupling scheme like $\overline{k}_1 = |k_1 - k_2|, \ldots, k_1 + k_2$.

After writing the Heisenberg Hamiltonian as a sum of irreducible tensor operators the matrix elements within a basis of the form $|\alpha\, S\, M\rangle$ can be calculated by the application of the Wigner-Eckart-theorem. The reduced matrix elements are determined using the so-called *decoupling* procedure.[3,4] Since the irreducible tensor operator $\underset{\sim}{\mathbf{T}}^{(k)}$ is given as a tensor product of irreducible tensor operators with regard to a certain coupling scheme (comp. Eq. (8)), the reduced matrix element $\langle \alpha\, S||\underset{\sim}{\mathbf{T}}^{(k)}||\alpha'\, S'\rangle$ can successively be decomposed into a product of single-spin irreducible tensor operators and Wigner-9J symbols.

B. General point-group symmetries

The use of irreducible tensor operators for the calculation of the matrix elements of the Hamiltonian and as a result also of the energy spectrum is essential for the treatment of magnetic molecules containing many interacting paramagnetic ions. Nevertheless, it is sometimes necessary to further reduce the dimensionality of the problem, either because computational resources are limited or a labeling of certain energy levels becomes advantageous, e.g. for spectroscopic classification.[26,27] Such a reduction can be done if the Hamiltonian remains invariant under certain permutations of spin centers. Often the spin-permutational symmetry of the Hamiltonian coincides with spatial symmetries of the molecule, i.e. point-group symmetries, therefore the term point-group symmetry is used while one refers to the invariance of the Hamiltonian under permutations of spins.

Using point-group symmetries of the system results in a decomposition of the Hamilton matrix $\langle \alpha\, S\, M|\underset{\sim}{H}|\alpha'\, S\, M\rangle$ into irreducible representations $\Gamma^{(n)}(\mathcal{G})$ of a group $\mathcal{G}$ whose elements $\underset{\sim}{G}(R)$, i.e. the operators corresponding to the symmetry operations R, do commute with $\underset{\sim}{H}$.

The symmetrized basis functions which span the irreducible representations n are found by the application of the projection operator $\mathcal{P}^{(n)}$ to the full set of basis vectors $|\alpha\, S\, M\rangle$ and subsequent orthonormalization. The over-complete set of basis states $\{|\alpha\, S\, M\, \Gamma^{(n)}\rangle\}$ spanning the n-th irreducible representation $\Gamma^{(n)}(\mathcal{G})$ is generated by[28]

$$\mathcal{P}^{(n)}|\alpha\, S\, M\rangle = \left(\frac{l_n}{h}\sum_R \left(\chi^{(n)}(R)\right)^* \underset{\sim}{G}(R)\right)|\alpha\, S\, M\rangle\ , \tag{9}$$

where l_n is the dimension of the irreducible representation $\Gamma^{(n)}$, h denotes the order of $\mathcal{G}$ and $\chi^{(n)}(R)$ is the character of the n-th irreducible representation of the symmetry operation R.

Equation (9) contains the main challenge while creating symmetrized basis states. The action of the operators $\underset{\sim}{G}(R)$ on basis states of the form $|\alpha\, S\, M\rangle$ has to be known. Of course, one could expand $|\alpha\, S\, M\rangle$ into a linear combination of product states $|m_1\, m_2 \ldots m_N\rangle$. Then the action of $\underset{\sim}{G}(R)$ leads to a permutation of magnetic quantum numbers m_i within the ket $|m_1\, m_2 \ldots m_N\rangle$. But, the recombination of the symmetry-transformed product states into basis states $|\alpha\, S\, M\rangle$ will then be much too time consuming for larger systems.

Following Ref. 11 the action of $\underset{\sim}{G}(R)$ on states $|\alpha\, S\, M\rangle$ can directly be evaluated without expanding it into product states. Suppose there is a certain coupling scheme a in which spin operators $\underset{\sim}{\mathbf{s}}(i)$ are coupled to yield the total spin operator $\underset{\sim}{\mathbf{S}}$. Generally the action of operators $\underset{\sim}{G}(R)$ on states $|\alpha\, S\, M\rangle$ leads to a different coupling scheme b. Now those states which belong to the coupling scheme b have to be reconverted into a linear combination of states belonging to a. This is technically a rather involved calculation, and one would not like to do it by hand and for every coupling scheme separately. To the best of our knowledge it has never been noted or even used that the conversion from any arbitrary (!) coupling scheme b into the desired coupling scheme a can be well automatized. Suppose there is a state $|\alpha\, S\, M\rangle_a$ belonging to the coupling scheme a. The action of a arbitrary group element $\underset{\sim}{G}(R)$ results in a state $|\alpha\, S\, M\rangle_b$ belonging to a different coupling scheme b. Then the re-expression takes the following form

$$\underset{\sim}{G}(R)|\alpha\, S\, M\rangle_a = \sum_{\alpha'} |\alpha'\, S\, M\rangle_a\ {}_a\langle \alpha'\, S\, M|\alpha\, S\, M\rangle_b\ , \tag{10}$$

where a term like ${}_a\langle \alpha'\, S\, M|\beta\, S\, M\rangle_b$ is known as *general re-coupling coefficient*. The calculation of general re-coupling coefficients and the evaluation of Eq. (10) can be performed with the help of graph theoretical methods.[15,16]

An implementation of these methods within a computer program is a straightforward task (follow directions given in Refs. 15,16). Nevertheless, we would like to provide some practical comments. Since such a program should be as general as possible, it does not employ analytical solutions (as done for the D_4 symmetry in Refs. 13,14) but numerical solutions. This concerns the reorthogonalization of the over-complete set of basis states $\{|\alpha\, S\, M\, \Gamma^{(n)}\rangle\}$ spanning the n-th irreducible representation $\Gamma^{(n)}(\mathcal{G})$, which is performed with a Gram-Schmidt orthogonalization procedure, as well as the evaluation of the generalized recoupling coefficients which is numerically done as described in Refs. 15,16. A considerable computational speedup can be achieved by tabulating Wigner-9J symbols beforehand, since they are heavily used during the calculations.

III. NUMERICAL EXACT DIAGONALIZATION

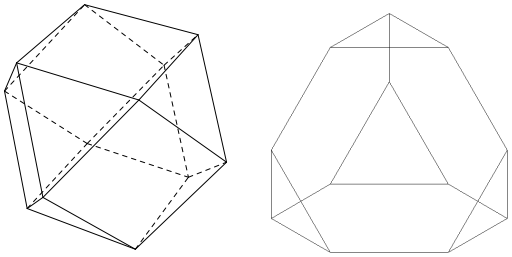

FIG. 1: Structure of the cuboctahedron (l.h.s.) and the truncated tetrahedron (r.h.s.).[29]

In this section we like to present two applications for realistic spin systems that can be treated using irreducible tensor operator techniques and point-group symmetries, but not otherwise. Both systems – cuboctahedron and truncated tetrahedron – consist of $N = 12$ spins of spin quantum number $s = 3/2$ (Hilbert space dimension 16,777,216). The two spin systems, which are realized as antiferromagnetic molecules – cuboctahedron[30] and truncated tetrahedron[31], see Fig. 1 for the structure – belong to the class of geometrically frustrated spin systems[32–34] and are thus hardly accessible by means of Quantum Monte Carlo.

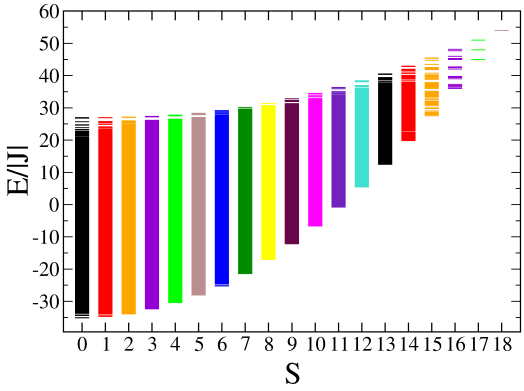

FIG. 2: (Color online) Complete energy spectrum of the antiferromagnetic cuboctahedron with $s = 3/2$.

Figure 2 shows the energy spectrum of the antiferromagnetic cuboctahedron with $s = 3/2$. This spectrum was obtained using only D_2 point-group symmetry which is already sufficient in order to obtain sufficiently small Hamilton matrices. In addition Fig. 3 demonstrates for the subspaces of total spin $S = 0$ and $S = 1$ that a representation in the full O_h group can be achieved which yields level assignments according to the irreducible representations of this group.

A complete energy spectrum allows to calculate thermodynamic properties as functions of both temperature T and magnetic field B. For the cuboctahedron this was

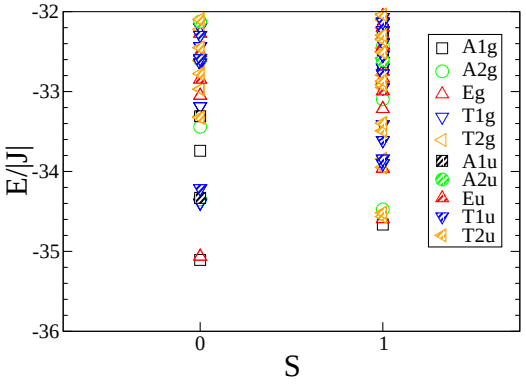

FIG. 3: (Color online) Low-lying energy spectrum of the antiferromagnetic cuboctahedron with $s = 3/2$ in subspaces of $S = 0$ and $S = 1$. The symbols denote the irreducible representations of the O_h group.

already done elsewhere.[34] Therefore, we like to discuss another frustrated structure, the truncated tetrahedron which was synthesized quite recently.[31] In principle this geometry permits two different exchange constants, one inside the triangles (J_1) and the other between the triangles (J_2), compare Fig. 1. A practical symmetry for this molecule is for instance C_{2v}, whereas the full symmetry is T_d. Figure 4 displays the complete energy spectrum for the case $J_1 = J_2 = J$. The inset of Fig. 4 magnifies the low-energy sector. As in the case of many other frustrated antiferromagnetic systems the spectrum exhibits more than one singlet below the first triplet.[32]

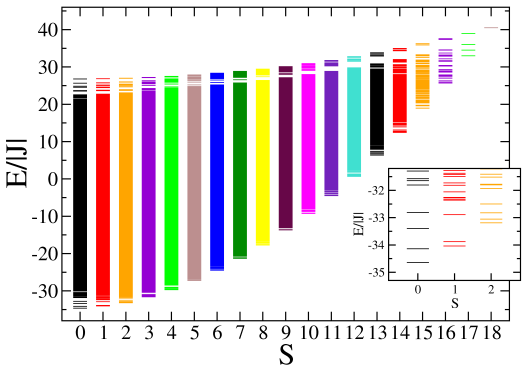

FIG. 4: (Color online) Complete energy spectrum of the antiferromagnetic truncated tetrahedron with $J_1 = J_2 = J$. The inset shows low-lying levels in subspaces with $S = 0, 1, 2$.

In Fig. 5 we show the zero-field specific heat (top) as well as the zero-field differential magnetic susceptibility (bottom). The fine structure of the specific heat, which is especially pronounced for $s = 3/2$, results from the low-energy gap structure. The sharp peak is an outcome of the gap between the lowest singlet and the group of levels around the second singlet and the first two triplets, the latter being highly degenerate (both nine-fold including M-degeneracy). This unusual degeneracy of the lowest

triplets is also the origin of the quick rise and subsequent flat behavior of the susceptibility in the case of $s = 3/2$.

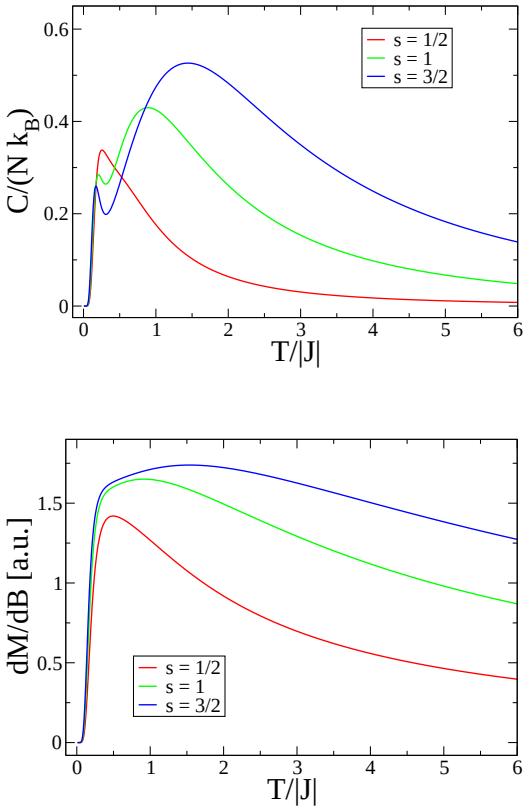

FIG. 5: (Color online) Specific heat $c(T, B = 0)$ (top) and differential magnetic susceptibility $\chi(T, B = 0)$ (bottom) of the truncated tetrahedron with $J_1 = J_2 = J$.

In connection with the truncated tetrahedron it might be interesting to realize the technical progess. The truncated tetrahedron with $s = 1/2$ was investigated in 1992.[35] The dimension of its Hilbert space is 4096, whereas the dimension for $s = 3/2$ is 16,777,216.

IV. APPROXIMATE DIAGONALIZATION

The previous sections demonstrate that numerical exact diagonalization in connection with irreducible tensor operators is a powerful tool to investigate thermodynamical properties of large magnetic molecules. Nevertheless, sometimes the use of total-spin and point-group symmetries is not sufficient to obtain small enough matrices. For such cases we suggest an approximate diagonalization in this section. The approximation is partially based on perturbation theory arguments. First ideas along this line were already suggested in Ref. 36. We will generalize and largely extend this idea.

Let's assume that the spin system is described by a Hamiltonian $\underset{\sim}{H}$ which acts in the Hilbert space $\mathcal{H}$. Suppose there is a zeroth-order Hamiltonian $\underset{\sim}{H}_0$ and a decomposition according to

$$\underset{\sim}{H} = \underset{\sim}{H}_0 + \lambda \underset{\sim}{H}' \ . \tag{11}$$

In the case of non-degenerate eigenstates $|\phi_i^{(0)}\rangle$ of $\underset{\sim}{H}_0$ the series expansion

$$|\phi_i\rangle = |\phi_i^{(0)}\rangle + \lambda|\phi_i^{(1)}\rangle + \lambda^2|\phi_i^{(2)}\rangle + \ldots, \tag{12}$$

$$E_i = E_i^{(0)} + \lambda E_i^{(1)} + \lambda^2 E_i^{(2)} + \ldots \ , \tag{13}$$

holds for the exact eigenstates $|\phi_i\rangle$ and corresponding eigenvalues E_i. The index $i = 1, \ldots, n$ denotes the states of the system. The energy eigenvalues and eigenstates in zeroth-order result from a (typically simple or even analytical) diagonalization of $\underset{\sim}{H}_0$ within an arbitrary basis of $\mathcal{H}$.

We label the eigenvalues $E_i^{(0)}$ and eigenstates $|\phi_i^{(0)}\rangle$ in such a manner that

$$E_i^{(0)} < E_{i+1}^{(0)}, \quad \forall\, i = 1, \ldots, n-1 \tag{14}$$

holds. Now we do not follow conventional perturbation theory as it would lead to a successive introduction of additional terms within the series expansion in Eq. (12), i.e. terms with increasing order of λ. Instead, we diagonalize the full Hamiltonian $\underset{\sim}{H}$ within a reduced set $\{|\phi_i^{(0)}\rangle\}$, $i = 1, \ldots, n_{\mathrm{red}}$, of eigenstates of $\underset{\sim}{H}_0$, where $n_{\mathrm{red}} \leq n$ is referred to as *cut-off parameter*. The resulting eigenvalues and eigenstates of this approximation are denoted as E_i^{approx} and $|\phi_i^{\mathrm{approx}}\rangle$. Such an approximate scheme is always converging since for $n_{\mathrm{red}} = n = \dim(\mathcal{H})$ all basis states are incorporated and the diagonalization corresponds to an exact treatment of the system, i. e.

$$E_i^{\mathrm{approx}} \xrightarrow{n_{\mathrm{red}} \to n} E_i \ , \quad |\phi_i^{\mathrm{approx}}\rangle \xrightarrow{n_{\mathrm{red}} \to n} |\phi_i\rangle \ \forall \ i \ . \tag{15}$$

It is clear that the speed of convergence depends on the choice of $\underset{\sim}{H}_0$.

The speed of convergence will be different for the various states. Since the approximate diagonalization is performed with the n_{red} low-lying states of $\underset{\sim}{H}_0$ according to (14) one expects that the low-lying energy levels converge quickest against their true values. As in perturbation theory this assumption relies on the hypothesis that energetically higher-lying levels do mix into the desired low-lying state with decreasing weight. In perturbation theory this expresses itself in the second order corrections

$$E_i^{(2)} = \sum_{i \neq j} \frac{|\langle \phi_i^{(0)} | \underset{\sim}{H}' | \phi_j^{(0)} \rangle|^2}{E_i^{(0)} - E_j^{(0)}} \ , \tag{16}$$

which decrease with increasing energetic distance $E_i^{(0)} - E_j^{(0)}$. In our approximate diagonalization the diagonal

$$\langle \phi_i^{(0)} | \underset{\sim}{H} | \phi_i^{(0)} \rangle = E_i^{(0)} + \lambda E_i^{(1)} \tag{17}$$

$$E_i^{(1)} = \langle \phi_i^{(0)} | \underset{\sim}{H}' | \phi_i^{(0)} \rangle \tag{18}$$

and off-diagonal terms $\langle\phi_i^{(0)}|\underset{\sim}{H}'|\phi_j^{(0)}\rangle$ of perturbation theory appear as diagonal and off-diagonal matrix elements of the reduced Hamilton matrix. Therefore, the approximate diagonalization includes zeroth and first order by definition and all higher orders partially up to the cut-off. The inclusion of eigenstates belonging to degenerate eigenvalues of $\underset{\sim}{H}_0$ poses no problem in our scheme. One should only include all eigenstates of a degenerate eigenvalue into the approximate diagonalization, otherwise the convergence is unnecessarily deteriorated.

A. Approximate diagonalization based on the rotational-band model

As a zeroth-order approximation $\underset{\sim}{H}_0$ of the isotropic Heisenberg Hamiltonian (2) the rotational-band Hamiltonian[37–39]

$$\underset{\sim}{H}_0 \equiv \underset{\sim}{H}_{\mathrm{RB}} = -\frac{DJ}{2N}\left[\underset{\sim}{\mathbf{S}}^2 - \sum_{n=1}^{N_s}\underset{\sim}{\mathbf{S}}_n^2\right] . \tag{19}$$

is chosen.[36] This choice rests on the observation that in bipartite antiferromagnetic spin systems the lowest eigenvalues within subspaces of total spin S follow the *Landé-rule*,[40,41] i.e.

$$E_{\min}(S) - E_0 \propto S(S+1) . \tag{20}$$

The prefactor $-\frac{DJ}{2N}$ in Eq. (19) can be seen as an effective exchange constant which couples the sublattice spins $\underset{\sim}{\mathbf{S}}_n$ to the total spin $\underset{\sim}{\mathbf{S}}$ of the system. The value of D

$$D = 2\cdot\frac{N_b}{N}\cdot\frac{1}{1-1/N_s} \tag{21}$$

is chosen to match the energy of the ferromagnetic state of the system described by an isotropic Heisenberg Hamiltonian.[37] N_s denotes the number of sublattices which the classical ground state of the system is composed of, N_b represents the number of bonds of the system. The eigenstates of $\underset{\sim}{H}_{\mathrm{RB}}$ are analytically given in the form $|S_1\ \ldots\ S_{N_s}\,S\,M\rangle$, which is an enormous advantage for the following calculations. The corresponding eigenvalues are

$$E_{\mathrm{RB}}(S_1,\ldots,S_{N_s},S) = -\frac{DJ}{2N}\left[S(S+1) - \sum_{n=1}^{N_s} S_n\,(S_n+1)\right] . \tag{22}$$

The spectrum of the rotational-band Hamiltonian consists of eigenvalues that form parabolas, so-called rotational-bands. In the following a rotational-band is defined as a set of eventually energetically degenerate eigenstates $|S_1\ldots S_{N_s}\,S\,M\rangle$ with fixed values of quantum numbers S_n of the sublattice spins.

Figure 6 shows the spectrum of the rotational-band Hamiltonian for a spin ring of $N = 8$ spins with $s = 5/2$.

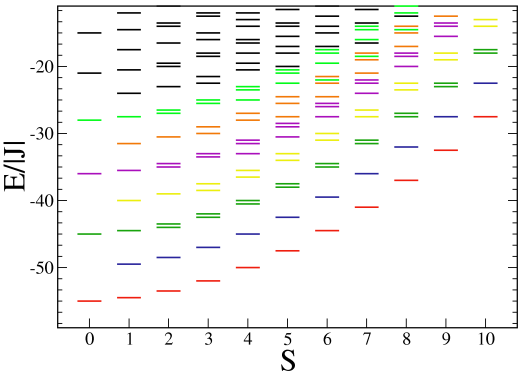

FIG. 6: (Color online) Part of the energy spectra of the rotational-band Hamiltonian for a antiferromagnetic spin ring $N = 8$, $s = 5/2$. Seven super-bands are colored.

The lowest bands refer to a sublattice spin configuration of $S_1 = S_2 = 4\cdot 5/2 = 10$. The next bands result from a deviation of one sublattice spin from its maximum value $S_{n,\max} = N/N_s\cdot s$. In such a way the whole spectrum can be constructed following Eq. (22). The eigenstates of the rotational-band Hamiltonian are highly degenerate due to the many possibilities of combining single spins $\underset{\sim}{\mathbf{s}}_i$ to the sublattice spins $\underset{\sim}{\mathbf{S}}_n$ and further on sublattice spins $\underset{\sim}{\mathbf{S}}_n$ to the total spin $\underset{\sim}{\mathbf{S}}$.

Figure 6 also shows that the rotational-band spectrum is clustered into *super-bands* (highlighted by color). A super-band contains those rotational-bands for which the sum of sublattice spin quantum numbers is the same. One clearly sees that within the rotational-band spectrum the low-lying super-bands are well separated.

Inserting $\underset{\sim}{H}_{\mathrm{RB}}$ into Eq. (11) yields

$$\underset{\sim}{H} = \underset{\sim}{H}_{\mathrm{Heisenberg}} = \underset{\sim}{H}_{\mathrm{RB}} + \underset{\sim}{H}' \tag{23}$$

as a starting point for an approximate diagonalization. With respect to computational resources and due to the fact that the eigenstates of $\underset{\sim}{H}_{\mathrm{RB}}$ are given in the form $|S_1\ \ldots\ S_{N_s}\,S\,M\rangle$ the diagonalization is performed in subspaces $\mathcal{H}(S, M = S)$ using the irreducible tensor operator technique. In addition, point-group symmetries can be used for a further reduction of the dimensionality. However, only those point-groups can be applied which do not alter the sublattice structure, i.e. do not lead to rotational-bands that are not included in the approximate basis set. Then the symmetry operations on a state belonging to a certain rotational-band will always produce states which belong to the same band.

V. BIPARTITE SYSTEMS - SPIN RING

A. Convergence

In the following we discuss the properties of the proposed approximate diagonalization for the example of an

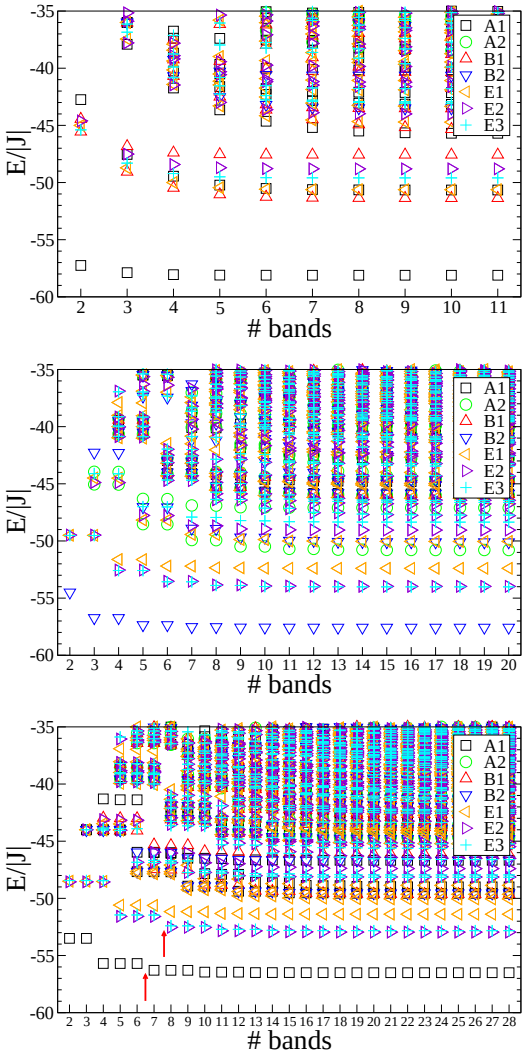

FIG. 7: (Color online) Energy levels of an a antiferromagnetic spin ring $N = 8$ with $s = 5/2$ as a function of the number of occupied rotational-bands used for diagonalization in subspaces $S = 0$ (top), $S = 1$ (center) and $S = 2$ (bottom). The arrows in the $S = 2$ subspace refer to the steps within the convergence behavior mentioned in the text. The states are labeled according to irreducible representations of D_8.

antiferromagnetic spin ring of $N = 8$ spins with $s = 5/2$. Figure 7 shows the convergence of the energy levels. In order to label the levels the full symmetry group D_8 of an octagon was used. One clearly sees that the convergence within the $S = 0$ subspace is fast and smooth (looking almost exponential).

In subspaces of $S = 1$ and $S = 2$ the convergence is also fast, but when only few bands are incorporated sharp steps can be observed. This is highlighted by two arrows in the bottom graph of Fig. 7. The stepwise convergence is continued in subspaces with $S > 2$ in a very regular way. It can be observed that with increasing energy within a certain subspace $\mathcal{H}(S, M = S)$ the steps are slightly washed out. The occurrence of the steps depends on the rotational-band the states are belonging to. For example, the energy of the lowest state (i.e. the first rotational-band) within $\mathcal{H}(S = 2, M = 2)$ is decreasing if 7 bands are incorporated into the approximate diagonalization while the energies of states belonging to the second rotational-band are lowered if 8 bands are incorporated, see also discussion in Sec. V B.

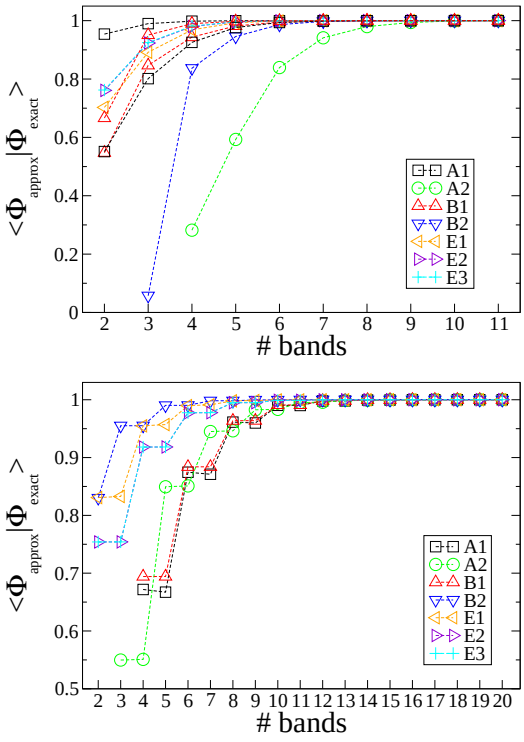

FIG. 8: (Color online) Convergence of the eigenstates of an a antiferromagnetic spin ring $N = 8$ with $s = 5/2$ as a function of the number of occupied rotational-bands used for diagonalization in subspaces $S = 0$ (top) and $S = 1$ (bottom). The states are labeled according to irreducible representations of D_8.

In Fig. 8 the convergence of some low-lying eigenstates of this spin ring are presented. The convergence behaves in analogy to the convergence of the eigenvalues. The stepwise convergence in $S = 1$ becomes obvious. Nevertheless, while using only a fraction of basis states (approximately 30% of the basis states within each subspace) the approximate low-lying eigenstates are practically converged against the exact eigenstates. In addition, it can be seen that states of higher energy converge slower than low-lying states.

We also investigate the convergence for various single spin quantum number s. In Fig. 9 the relative difference between the approximate energy values and the exact values is displayed for various s in the subspace $S = 0$. The levels which have been chosen belong to the first three occupied rotational-bands. One clearly sees that the approximate diagonalization converges more rapidly

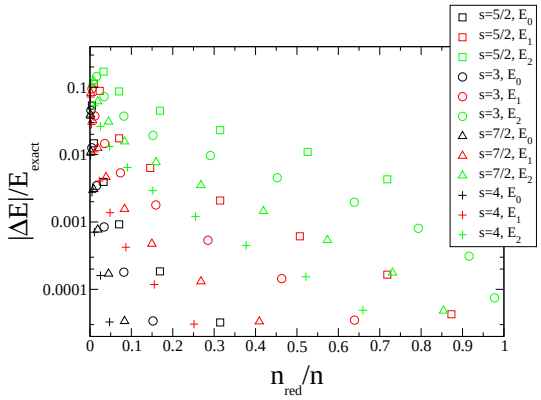

FIG. 9: (Color online) Relative difference between approximate and exact energy eigenvalues for the lowest states of the first three occupied rotational-bands for an antiferromagnetic spin ring $N = 8$ with various s and total spin $S = 0$. E_0 refers to the energy of the lowest state of the first rotational-band, E_1 to the lowest state of the second rotational-band and E_3 to the lowest state of the third rotational-band respectively.

the higher the single spin is. This is not surprising since the rotational-band model (19), which is based on classical assumptions, is itself more accurate the larger s is.

B. Approximate selection rule

It turns out that the aforementioned occurrence of steps can be understood and even be employed for a further reduction of the size of Hamilton matrices. The underlying reason is that the full Hamiltonian connects states belonging to different rotational-bands with very different strength. After having inspected the reduced Hamilton matrices of various bipartite systems we arrive at the following empirical selection rule.

The matrix elements $\langle S_{1,a}\, S_{2,a}\, S\, M|\underset{\sim}{H}|S_{1,b}\, S_{2,b}\, S\, M\rangle$ of the full Hamiltonian between rotational-band states are (several) orders of magnitude bigger than all other matrix elements if

$$|S_{1,a} - S_{2,a}| - |S_{1,b} - S_{2,b}| = 0\ . \qquad (24)$$

Here $S_{1,a}$ and $S_{2,a}$ denote the total spins of sublattices one and two in $\langle S_{1,a}\, S_{2,a}\, S\, M|$, respectively. Matrix elements that are not compatible with this rule can be neglected which (after a proper rearrangement) results in a new block-diagonal structure of the reduced Hamilton matrix. These blocks are of smaller size and can be diagonalized separately.

C. Application to $\{Fe_{12}\}$

We now apply the approximate diagonalization to an existing molecular spin ring[42] that contains 12 Fe^{3+} ions with $s = 5/2$. The system can be modeled by an isotropic Heisenberg Hamiltonian with antiferromagnetic nearest-neighbor coupling J.[42,43] It was theoretically investigated in Ref. 23 with the help of QMC methods; the exchange parameter was determined to be $J = -35.2$ K.

Our intention is to show that it is advantageous to combine a stochastic method such as QMC and an exact or approximate diagonalization. In such a combination the role of QMC would be to determine the exchange parameters from thermodynamical observables as done in Ref. 23. For large systems this is practically impossible using exact or approximate diagonalization since diagonalization requires an enormous numerical effort whereas QMC methods scale much more favorable with system size for bipartite systems or even frustrated systems above a certain temperature. The role of exact or approximate diagonalization then would be to use the exchange parameters obtained by QMC for the evaluation of the energy spectrum which then can be used e.g. to interpret INS measurements.[2,44]

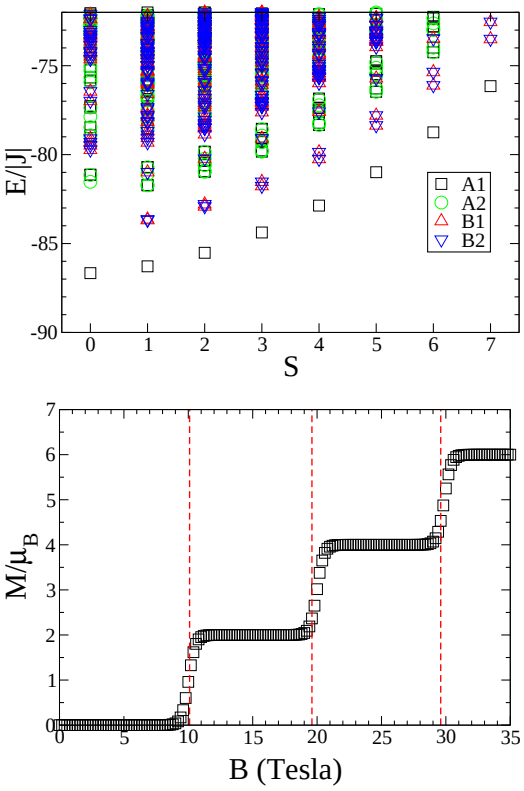

FIG. 10: (Color online) Approximate spectrum of a spin ring with $N = 12$ spins $s = 5/2$ calculated using 8 bands, D_2 point-group symmetry and the approximate selection rule in Eq. (24) (top). Corresponding magnetization of the system (bottom). The dashed red lines refer to experimental data of the first three magnetization steps from Ref. 43 with $J = -35.2$ K and $k_BT/J = 0.01$.

Figure 10 shows the low-energy part of the approximate spectrum of the $\{Fe_{12}\}$ compound modeled by an isotropic Heisenberg Hamiltonian. For the approximate

calculation of the spectrum full rotational symmetry as well as D_2 point-group symmetry are used. The calculations are performed using 8 occupied rotational-bands in the $S = 0$ subspace and the corresponding number of bands in subspaces with $S > 0$. Overall $21,570,976$ states have been taken into account, which are only about 15 % of all basis states ($\dim(\mathcal{H}) = 144,840,476$). Additionally the approximate selection rule given in Eq. (24) was used in order to reduce the dimensionality of the matrices which have to be diagonalized.

Figure 10 also displays the magnetization curve, which is derived from the partition function made of only the approximate energy levels. As one can see the experimental magnetization steps[43] can be reproduced using the approximate diagonalization. We would like to mention that this magnetization curve can be obtained by QMC as well, since the system is bipartite.

D. Next-nearest-neighbor coupling – introducing frustration

In the previous parts we demonstrate that the approximate diagonalization scheme based on the rotational-band Hamiltonian yields good results for bipartite, i.e. unfrustrated antiferromagnetic spin systems. We now want to investigate how robust the approximate diagonalization is against the introduction of frustration. To this end we study a spin ring with $N = 8$ and $s = 5/2$ with antiferromagnetic nearest-neighbor coupling $J = J_{nn}$ and an additional antiferromagnetic next-nearest-neighbor-coupling J_{nnn} which acts frustrating. In a corresponding classical system the Néel state (up-down-up-down- ...) would no longer be the ground state, instead canting can occur. One can qualitatively say that with increasing J_{nnn}/J_{nn} also the frustration increases.

Figure 11 displays the effect of J_{nnn} in the subspace $\mathcal{H}(S = 0, M = S)$ for the same system that is discussed in Fig. 7 for $J_{nnn} = 0$. The energy gap between the ground state and the first excited state decreases with increasing frustration. Moreover, the convergence of the ground state as well as of excited states becomes slower. With $J_{nnn}/J_{nn} = 0.4$ the convergence is rather poor and the quantum mechanical ground state now belongs to the irreducible representation B_1 of the symmetry group D_8. This means that the true ground state is not the result of an adiabatic continuation ($\lambda : 0 \to 1$ in Eq. (11)) from the ground state of the rotational-band model, which belongs to A_1. We just like to mention for the interested reader, that this change of the character of the ground state constitutes a so-called Quantum Phase Transition; in this case for the antiferromagnetic chain with next-nearest-neighbor exchange.

Summarizing, if frustration is only small the approximate diagonalization still yields good results. Moreover, the approximate selection rule (24) is also applicable which is very helpful in calculating the full spectrum of the system.

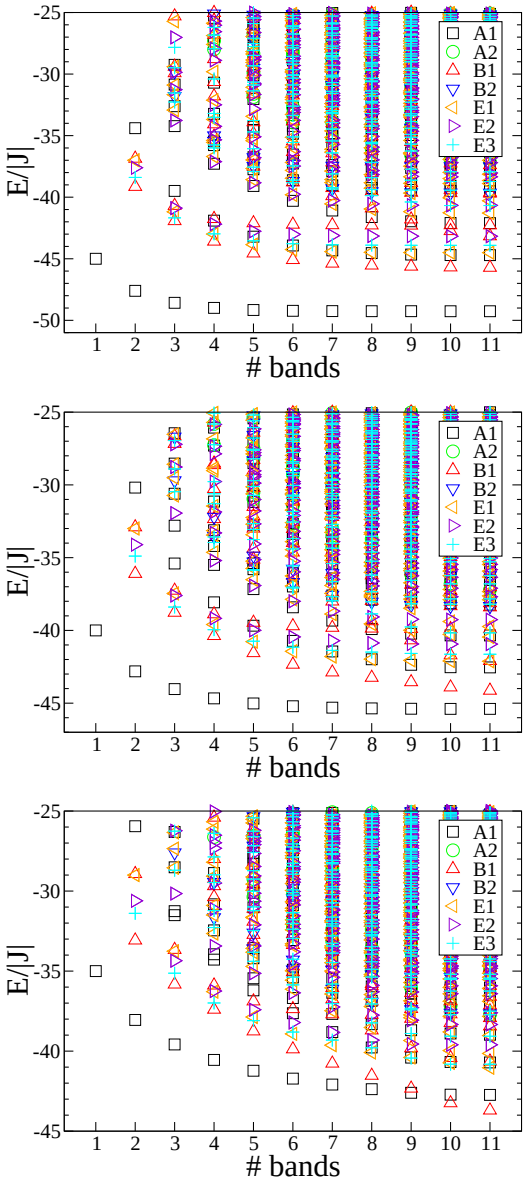

FIG. 11: (Color online) Energy levels of an a antiferromagnetic spin ring $N = 8$ with $s = 5/2$ and additional next-nearest-neighbor coupling J_{nnn} as a function of the number of occupied rotational-bands used for diagonalization in subspaces $S = 0$ with $J_{nnn}/J_{nn} = 0.2$ (top), $J_{nnn}/J_{nn} = 0.3$ (center) and $J_{nnn}/J_{nn} = 0.4$ (bottom). The states are labeled according to irreducible representations of D_8.

VI. SUMMARY

In this work we have demonstrated that the full spin-rotational symmetry can be combined with arbitrary point-group symmetries. This enables us to obtain exactly the complete energy spectrum of Heisenberg spin systems for so far unprecedented system sizes. Moreover, we have outlined a scheme to approximately diagonalize the Hamilton matrix again using the full spin-rotational

symmetry and point-group symmetries. This approximation works well for bipartite antiferromagnetic spin systems. For frustrated systems the quality reduces with increasing frustration. How such a scheme can be refined for frustrated systems will be the subject of future investigations.

Acknowledgments

Computing time at the Leibniz Computing Center in Garching is gratefully acknowledged as well as helpful advices of Dieter an Mey and Christian Terboven of High Performance Computing Center, RWTH Aachen, in setting up openMP directives. We also thank Boris Tsukerblat for fruitful discussions about the irreducible tensor operator technique and Nedko Ivanov for drawing our attention to some literature. This work was supported within a Ph.D. program of the State of Lower Saxony in Osnabrück.

---

* Electronic address: rschnall@uos.de
† Electronic address: jschnack@physik.uni-bielefeld.de

[1] D. Gatteschi and L. Pardi, Gazz. Chim. Ital. **123**, 231 (1993).
[2] J. J. Borras-Almenar, J. M. Clemente-Juan, E. Coronado, and B. S. Tsukerblat, Inorg. Chem. **38**, 6081 (1999).
[3] A. Bencini and D. Gatteschi, *Electron paramagnetic resonance of exchange coupled systems* (Springer, Berlin, Heidelberg, 1990).
[4] B. S. Tsukerblat, *Group theory in chemistry and spectroscopy: a simple guide to advanced usage* (Dover Publications, 2006), 2nd ed.
[5] B. Tsukerblat, Inorg. Chim. Acta **361**, 3746 (2008).
[6] A. S. Boyarchenkov, I. G. Bostrem, and A. S. Ovchinnikov, Phys. Rev. B **76**, 224410 (2007).
[7] I. Rousochatzakis, A. M. Läuchli, and F. Mila, Phys. Rev. B **77**, 094420 (2008).
[8] C. Raghu, I. Rudra, D. Sen, and S. Ramasesha, Phys. Rev. B **64**, 064419 (2001).
[9] C. Raghu, I. Rudra, D. Sen, and S. Ramasesha, Phys. Rev. B **68**, 029902 (2003).
[10] I. Rudra, S. Ramasesha, and D. Sen, Phys. Rev. B **64**, 014408 (2001).
[11] O. Waldmann, Phys. Rev. B **61**, 6138 (2000).
[12] C. Delfs, D. Gatteschi, L. Pardi, R. Sessoli, K. Wieghardt, and D. Hanke, Inorg. Chem. **32**, 3099 (1993), http://pubs.acs.org/doi/pdf/10.1021/ic00066a022, URL http://pubs.acs.org/doi/abs/10.1021/ic00066a022.
[13] I. G. Bostrem, A. S. Ovchinnikov, and V. E. Sinitsyn, Theor. Math. Phys. **149**, 1527 (2006).
[14] V. E. Sinitsyn, I. G. Bostrem, and A. S. Ovchinnikov, J. Phys. A-Math. Theor. **40**, 645 (2007).
[15] V. Fack, S. N. Pitre, and J. van der Jeugt, Comp. Phys. Comm. **101**, 155 (1997).
[16] V. Fack, S. N. Pitre, and J. van der Jeugt, Comp. Phys. Comm. **86**, 105 (1995).
[17] S. R. White, Phys. Rev. B **48**, 10345 (1993).
[18] M. Exler and J. Schnack, Phys. Rev. B **67**, 094440 (2003).
[19] U. Schollwöck, Rev. Mod. Phys. **77**, 259 (2005).
[20] C. Lanczos, J. Res. Nat. Bur. Stand. **45**, 255 (1950).
[21] A. W. Sandvik and J. Kurkijärvi, Phys. Rev. B **43**, 5950 (1991).
[22] A. W. Sandvik, Phys. Rev. B **59**, R14157 (1999).
[23] L. Engelhardt and M. Luban, Phys. Rev. B **73**, 054430 (2006).
[24] K. Bärwinkel, H.-J. Schmidt, and J. Schnack, J. Magn. Magn. Mater. **212**, 240 (2000).
[25] D. A. Varshalovich, A. N. Moskalev, and V. K. Khersonskii, *Quantum theory of angular momentum* (World Scientific Publishing, 1988).
[26] G. S. Griffith, Structure and Bonding **10**, 87 (1972).
[27] B. S. Tsukerblat, M. I. Belinskii, and V. E. Fainzil'berg, Sov. Sci. Rev. B Chem. **9**, 337 (1987).
[28] M. Tinkham, *Group theory and quantum mechanics* (Dover Publications, New York, 2003).
[29] E. Weisstein, *Mathworld*, URL http://mathworld.wolfram.com.
[30] A. J. Blake, R. O. Gould, C. M. Grant, P. E. Y. Milne, S. Parsons, and R. E. P. Winpenny, J. Chem. Soc.-Dalton Trans. pp. 485–495 (1997).
[31] C. P. Pradeep, D.-L. Long, P. Kögerler, and L. Cronin, Chem. Commun. pp. 4254–4256 (2007).
[32] R. Schmidt, J. Schnack, and J. Richter, J. Magn. Magn. Mater. **295**, 164 (2005).
[33] J. Schnack, R. Schmidt, and J. Richter, Phys. Rev. B **76**, 054413 (2007).
[34] J. Schnack and R. Schnalle, Polyhedron (2009), in press; doi:10.1016/j.poly.2008.10.017.
[35] D. Coffey and S. A. Trugman, Phys. Rev. B **46**, 12717 (1992).
[36] O. Waldmann, Phys. Rev. B **75**, 012415 (2007).
[37] J. Schnack and M. Luban, Phys. Rev. B **63**, 014418 (2000).
[38] O. Waldmann, Phys. Rev. B **65**, 024424 (2001).
[39] J. Schnack, M. Luban, and R. Modler, Europhys. Lett. **56**, 863 (2001).
[40] A. Lascialfari, D. Gatteschi, F. Borsa, and A. Cornia, Phys. Rev. B **55**, 14341 (1997).
[41] A. Lascialfari, D. Gatteschi, F. Borsa, and A. Cornia, Phys. Rev. B **56**, 8434 (1997).
[42] A. Caneschi, A. Cornia, A. C. Fabretti, and D. Gatteschi, Angew. Chem. Int. Edit. **38**, 1295 (1999).
[43] Y. Inagaki, T. Asano, Y. Ajiro, Y. Narumi, K. Kindo, A. Cornia, and D. Gatteschi, J. Phys. Soc. Jpn. **72**, 1178 (2003).
[44] R. Basler, C. Boskovic, G. Chaboussant, H. U. Güdel, M. Murrie, S. T. Ochsenbein, and A. Sieber, ChemPhysChem **4**, 910 (2003).

2. Cond. Mat. Phys. 12, 331 (2009)

Condensed Matter Physics, ????, Vol. ?, No ?(??), pp. 1–??

Approximate eigenvalue determination of geometrically frustrated magnetic molecules*

Roman Schnalle[1], Andreas M. Läuchli[2], Jürgen Schnack[3]

[1] Universität Osnabrück, Fachbereich Physik, D-49069 Osnabrück, Germany

[2] Max Planck Institut für Physik komplexer Systeme, Nöthnitzerstr. 38, D-01187 Dresden, Germany

[3] Universität Bielefeld, Fakultät für Physik, Postfach 100131, D-33501 Bielefeld, Germany

October 2, 2009

Geometrically frustrated magnetic molecules have attracted a lot of interest in the field of molecular magnetism as well as frustrated Heisenberg antiferromagnets. In this article we demonstrate how an approximate diagonalization scheme can be used in order to obtain thermodynamic and spectroscopic information about frustrated magnetic molecules. To this end we theoretically investigate an antiferromagnetically coupled spin system with cuboctahedral structure modeled by an isotropic Heisenberg Hamiltonian.

Key words: *Magnetic Molecules; Heisenberg Model; Geometric Frustration; Irreducible Tensor Operator Technique; Approximate Diagonalization; Cuboctahedron*

PACS: *75.10.Jm,75.50.Xx,75.40.Mg,75.50.Ee*

1. Introduction

The complete understanding of small magnetic systems such as magnetic molecules is compulsorily connected to the knowledge of their energy spectra. From the energy spectra all spectroscopic, dynamic, and thermodynamic properties of the spin systems can be obtained. Unfortunately, an exact calculation of the spectrum is often restricted due to the huge dimension of the Hilbert space even if one works within the most simple isotropic Heisenberg model. The dimension grows for a system of N spins with spin quantum number s exponentially and is $(2s+1)^N$.

In order to get insight into the properties of large magnetic molecules one can access several numerical methods which have been developed in the past. Of course, the ultimate method of choice would be an exact numerical diagonalization yielding the complete energy spectrum. In recent years there has been enormous progress on extending the range of applicability of the exact numerical diagonalization of the Heisenberg model. To this end the use of spin-rotational symmetry [1,2] in combination with point-group symmetries [3–6] can be of great advantage with respect to a reduction of computational requirements, i.e. a need of hardware resources and computation time. Apart from the exact numerical diagonalization technique the magnetism of magnetic molecules can be very well investigated using complementary methods such as Density Matrix Renormalization Group (DMRG) [7–9], Lanczos [10], or Quantum Monte Carlo (QMC) [11–13] techniques. Nevertheless, also these methods suffer from theoretical limitations, QMC for instance in systems with geometric frustration.

Currently magnetic molecules which exhibit geometric frustration are of special interest due to the richness of physical phenomena like plateaus and jumps of the magnetization for varying field as well as special features of their spectra such as low-lying singlets [14–17]. In this respect a lot of insight has been obtained by investigating molecular representations of archimedean-type spin systems [18,19], i.e. systems in which participating spins occupy the vertices of an archimedean solid. Such representations have already been synthesized several years ago and exist for example as $\{Cu_{12}La_8\}$ [20] (cuboctahedron, $s = 1/2$) and $\{Mo_{72}Fe_{30}\}$ [21,22] (icosidodecahedron, $s = 5/2$).

*rschnall@uos.de

© Roman Schnalle, Andreas M. Läuchli, Jürgen Schnack

In this context the molecular compound $\{Mo_{72}Fe_{30}\}$ is probably one of the most investigated magnetic molecules. However, a theoretical explanation of its special physical properties was so far given mostly by considering purely classical models [23,24] or directly related quantum mechanical counterparts like the rotational-band model [25,26].

In this paper we want to show how the approximate diagonalization technique which has been developed and applied to unfrustrated, i.e. bipartite, magnetic molecules in Ref. [6] can be used in order to determine the energy spectrum of geometrically frustrated magnetic molecules. The idea of this technique is to diagonalize the full Hamiltonian in a reduced basis set. The basis set itself is an eigenbasis of the rotational-band Hamiltonian. Such an ansatz was already used by Oliver Waldmann [27] in order to interpret inelastic neutron spectra of $\{Mo_{72}Fe_{30}\}$ [18]. We will demonstrate that in contrast to bipartite systems for a frustrated spin systems the rotational-band states of all non-trivially different sublattice colorings have to be taken into account in order to achieve a reliable convergence of energy levels. Throughout this paper we use a spin system with cuboctahedral structure and spin quantum numbers $s = 1$ and $s = 3/2$ as well as an antiferromagnetic coupling as an archetypical example of a frustrated magnetic spin system.

This paper is organized as follows. In Sec. 2 the general theoretical description of the system within the Heisenberg model as well as general remarks on the use of irreducible tensor operators and point-group symmetries are given. In Sec. 3 the theoretical basics of the approximate diagonalization within the isotropic Heisenberg model are briefly reviewed and specified for the cuboctahedral spin system. The convergence behaviour of the approximate diagonalization is displayed and deeply discussed as well as the specific heat and zero-field magnetic susceptibility for a cuboctahedron with $s = 3/2$. Furthermore, a numerically based finding of an approximate selection rule is reported. This paper closes with a Summary in Sec. 4.

2. Theoretical method

In order to model the physics of antiferromagnetic molecules it has been shown that an isotropic Heisenberg Hamiltonian with an additional Zeeman-term and an antiferromagnetic nearest-neighbor coupling provides the dominant terms. Such a Hamiltonian looks like

$$\underset{\sim}{H} = -\sum_{<i,j>} J_{ij} \underset{\sim}{\mathbf{s}}(i) \cdot \underset{\sim}{\mathbf{s}}(j) + g\mu_B \underset{\sim}{\mathbf{S}} \cdot \vec{B} \ . \tag{1}$$

The indices of the sum are running over all pairs $< i, j >$ of interacting spins i and j. The first part consisting of the sum over single spin operators $\underset{\sim}{\mathbf{s}}(i)$ at sites i interacting with the coupling strength $J_{ij} < 0$ refers to the Heisenberg exchange whereas the second part – the Zeeman-term – couples the total spin $\underset{\sim}{\mathbf{S}}$ to an external magnetic field $\vec{B}$.

Taking without loss of generality $J_{ij} = J$ for interacting spins the Heisenberg part assumes the following form

$$\underset{\sim}{H}_{\text{Heisenberg}} = -J \sum_{<i,j>} \underset{\sim}{\mathbf{s}}(i) \cdot \underset{\sim}{\mathbf{s}}(j), \tag{2}$$

where each coupling is counted only once. Since due to $SU(2)$ symmetry the commutation relations $\left[\underset{\sim}{H}_{\text{Heisenberg}}, \underset{\sim}{\mathbf{S}}\right] = 0$ hold, a common eigenbasis $\{|\nu\rangle\}$ of $\underset{\sim}{H}_{\text{Heisenberg}}$, $\underset{\sim}{\mathbf{S}}^2$ and $\underset{\sim}{S}_z$ can be found and the effect of an external magnetic field $\vec{B} = B \cdot \vec{e}_z$ can be included later, i.e.

$$E_\nu(B) = E_\nu + g\mu_B B M_\nu \ . \tag{3}$$

Here E_ν denotes the energy eigenvalues, $|\nu\rangle$ the eigenstates, and M_ν denotes the corresponding magnetic quantum number.

For the matrix representation of the Heisenberg Hamiltonian (2) the irreducible tensor operator technique is used [1,2,6]. The Heisenberg Hamiltonian is expressed in terms of irreducible tensor

operators and its matrix elements are evaluated using the Wigner-Eckart-theorem

$$\langle \alpha\, S\, M | \underset{\sim}{T}{}^{(k)}_q | \alpha'\, S'\, M' \rangle = (-1)^{S-M} \langle \alpha\, S || \underset{\sim}{\mathbf{T}}{}^{(k)} || \alpha'\, S' \rangle \begin{pmatrix} S & k & S' \\ -M & q & M' \end{pmatrix} . \tag{4}$$

Equation (4) states that a matrix element of the q-th component of an irreducible tensor operator $\underset{\sim}{\mathbf{T}}{}^{(k)}$ of rank k is given by the reduced matrix element $\langle \alpha\, S || \underset{\sim}{\mathbf{T}}{}^{(k)} || \alpha'\, S' \rangle$ and a factor containing a Wigner-3J symbol [28]. The basis in which the Hamilton matrix is set up is of the form $|\alpha\, S\, M\rangle$. α refers to a set of intermediate quantum numbers given by addition rules when coupling single spins $\underset{\sim}{\mathbf{s}}(i)$ to a total spin $\underset{\sim}{\mathbf{S}}$ with spin quantum number S. The underlying spin-coupling scheme directly influences the form of the irreducible tensor operator $\underset{\sim}{\mathbf{T}}{}^{(k)}$ and further on the successive calculation process of the reduced matrix elements in Eq. (4).

By using irreducible tensor operators and the Wigner-Eckart-theorem it is possible to drastically reduce the dimensionality of the problem, i.e. of the Hamilton matrices which have to be diagonalized numerically. The total Hilbert space $\mathcal{H}$ can be decomposed into subspaces $\mathcal{H}(S, M = S)$. Such a decomposition results in block factorizing the Hamilton matrix where each block can be labelled by the total spin quantum number S.

Additionally point-group symmetries lead to a further reduction of the matrices. Apart from that, states are labelled by the irreducible representation they are belonging to. This is very helpful in understanding the physics of the system. The incorporation of these symmetries results in symmetrized basis states which are constructed by the projection operator [29]

$$\mathcal{P}^{(n)} |\alpha\, S\, M\rangle = \left(\frac{l_n}{h} \sum_R \left(\chi^{(n)}(R) \right)^* \underset{\sim}{G}(R) \right) |\alpha\, S\, M\rangle \ . \tag{5}$$

Here l_n denotes the dimension of the n-th irreducible representation of the point-group $\mathcal{G}$ which is of order h. $\underset{\sim}{G}(R)$ refers to the symmetry operations of $\mathcal{G}$ and $\chi^{(n)}(R)$ denotes its character with respect to n. The effect of the symmetry operation $\underset{\sim}{G}(R)$ on basis states of the form $|\alpha\, S\, M\rangle$ is discussed in Refs. [3,5,6].

3. Approximate diagonalization for frustrated systems: the cuboctahedron

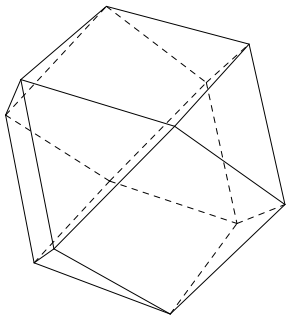

Figure 1. Geometrical structure of the cuboctahedron [30].

In this section we follow a method of calculating approximate eigenstates and eigenvalues of the Heisenberg Hamiltonian in Eq. (2) and determine approximately the energy spectrum of a spin system with cuboctahedral structure. In this system 12 spins of spin quantum number s occupy the vertices of a cuboctahedron interacting along its edges. The geometrical structure of the cuboctahedron is shown in Fig. 1. A detailed description of the approximation scheme is

given in Ref. [6] where it was successfully applied to determine approximate energy spectra and thermodynamic properties of spin rings, i.e. bipartite systems. This approximation rests on the idea to diagonalize the full Hamiltonian in a reduced basis set. The basis set itself is an eigenbasis of the rotational-band Hamiltonian which from the point of view of perturbation theory can be understood as an approximation to the full Hamiltonian. For bipartite systems this (zeroth order) approximation is already very good [25].

The Heisenberg Hamiltonian can be decomposed into two parts like

$$\underset{\sim}{H} = \underset{\sim}{H}_{\mathrm{RB}} + \underset{\sim}{H}' \ , \tag{6}$$

where $\underset{\sim}{H}_{\mathrm{RB}}$ is the rotational-band Hamiltonian [25,26,31] and $\underset{\sim}{H}'$ is an operator containing the remaining terms. The rotational-band Hamiltonian which is an effective quantum mechanical Hamiltonian based on classical assumptions looks like

$$\underset{\sim}{H}_{\mathrm{RB}} = -\frac{DJ}{2N}\left[\underset{\sim}{\mathbf{S}}^2 - \sum_{n=1}^{N_s} \underset{\sim}{\mathbf{S}}_n^2\right] \ . \tag{7}$$

Here N denotes the number of spins within the system and N_s the number of sublattices the classical ground state of the system is composed of. The prefactor $-DJ/(2N)$ can be seen as the effective coupling strength between the total spin $\underset{\sim}{\mathbf{S}}$ and the sublattice spins $\underset{\sim}{\mathbf{S}}_n$ which arise from coupling all single spins $\underset{\sim}{\mathbf{s}}(i)$ belonging to the n-th sublattice. The value of D directly depends on the system. It is chosen such that the energy of the ferromagnetic state of the system is matched; for the cuboctahedron it is $D = 6$.

The full Heisenberg Hamiltonian is now diagonalized within a reduced set $\{|\phi_i\rangle\}$, $i = 1, \ldots, n_{\mathrm{red}}$, of basis states of $\underset{\sim}{H}_{\mathrm{RB}}$ yielding approximate eigenstates and eigenvalues of $\underset{\sim}{H}$. The set of approximate basis states is energetically ordered.

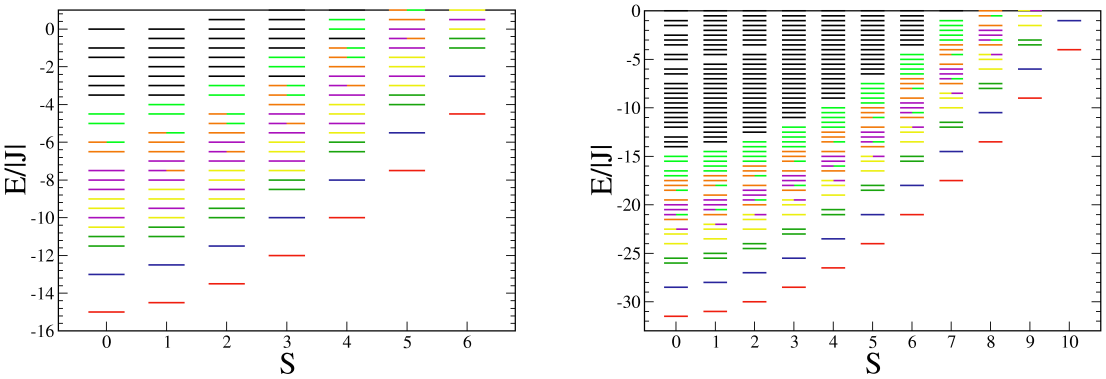

Figure 2. Part of the energy spectra of the rotational-band Hamiltonian for a cuboctahedron with twelve spins $s = 1$ (left) and $s = 3/2$ (right). Seven super-bands are colored.

Before discussing the results of our approximate diagonalization we would like to characterize the eigenbasis of $\underset{\sim}{H}_{\mathrm{RB}}$. Figure 2 shows the low-lying part of the energy spectra of $\underset{\sim}{H}_{\mathrm{RB}}$ for a cuboctahedron with $s = 1$ and $s = 3/2$ given by the rotational-band model. They exclusively consist of parabolas – so-called rotational bands. The eigenvalues $E_{\mathrm{RB}}(S_1, S_2, S_3, S)$ of $\underset{\sim}{H}_{\mathrm{RB}}$ depend only on the spin quantum numbers of the sublattice spins S_n, with $n = 1, 2, 3$, and of the total spin S. Corresponding eigenstates are trivial and analytically given as $|\alpha\, S_1\, S_2\, S_3\, S\, M\rangle$. The additional quantum number α refers to a set of intermediate spin quantum numbers which appears when coupling single spins $\underset{\sim}{\mathbf{s}}_i$ of the same sublattice to the corresponding sublattice spins $\underset{\sim}{\mathbf{S}}_i$ and further on coupling the sublattice spins to the total spin $\underset{\sim}{\mathbf{S}}$. With regard to the set of intermediate spin quantum numbers α the number of all possible ways of constructing states characterized by fixed

values of the sublattice and total spin quantum numbers determine the degeneracy of energy levels in the spectrum of the rotational-band Hamiltonian.

In the case of $s = 1$ the lowest band in Fig. 2 is given by states $|\alpha\, S_1\, S_2\, S_3\, S\, M\rangle$ with sublattice spin quantum numbers $S_1 = S_2 = S_3 = S_{\max} = 4 \cdot 1 = 4$ while the second band is given by a deviation of one sublattice spin of 1, i.e. $|\alpha\, (S_{\max} - 1)\, S_{\max}\, S_{\max}\, S\, M\rangle$ and permutations thereof. The other bands can then be constructed by introducing additional deviations of the sublattice spin quantum numbers. The energy spectrum with $s = 3/2$ shown in Fig. 2 can be constructed accordingly.

Additionally several energy levels in Fig. 2 are colored. This coloring refers to so-called super-bands. A super-band consists of those rotational bands for which the sum of sublattice spin quantum numbers is the same. In contrast to bipartite systems (see Ref. [6]) the spectrum of the rotational-band Hamiltonian for the cuboctahedron is much denser at low energies and only the first three super-bands are well separated from the others.

The classical ground state of the system plays the key role within the approximate diagonalization. The better the quantum mechanical system can be approximated by a classical picture of the ground state the more effectively the approximate diagonalization works, i.e. the faster the approximate energy eigenvalues converge towards the exact values. From a purely classical point of view the ground state of a cuboctahedron exhibits a three-sublattice structure and is infinitely degenerate since there coexist coplanar and non-coplanar vector orientations [32]. Here it should be emphasized that within the approximate diagonalization, i.e. within a quantum mechanical treatment, coplanarity of the classical ground state does not play a role, but the coloring of the classical ground state does, since there is a direct impact on the set of intermediate spin quantum numbers α in the rotational-band states $|\alpha\, S_1\, S_2\, S_3\, S\, M\rangle$ which are taken into account as basis states in the approximate diagonalization.

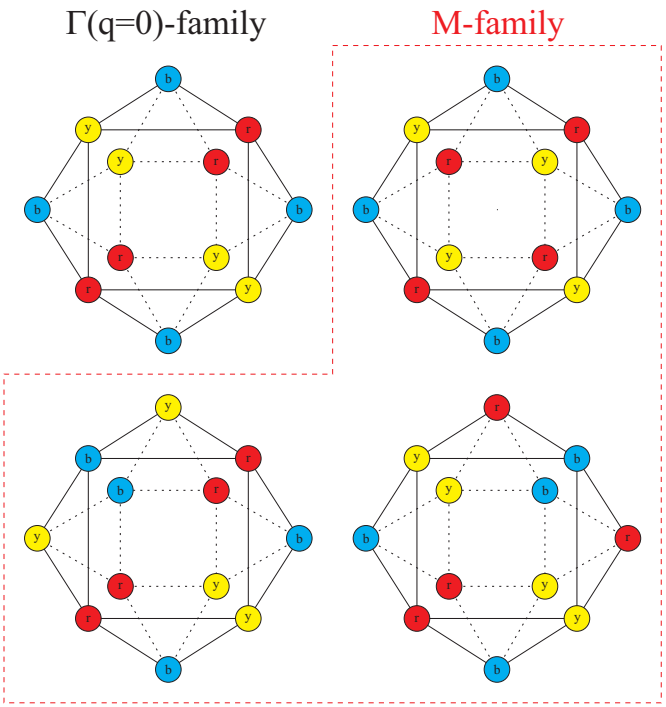

Figure 3. Families of the classical ground state of the cuboctahedron. Coloring of the $\Gamma(q = 0)$-family (upper left). Coloring of the three equivalent states of the M-family (upper right and bottom). The drawing is only schematic and not perspectively correct. The labels correspond to y: yellow, r: red, and b: blue.

The classical ground state of the cuboctahedron exhibits 24 colorings of the spins which can be

– by group theoretical considerations – decomposed into two families that are invariant under operation of the full point-group symmetry O_h [19]. Following Ref. [19] these families will be denoted as $\Gamma(q = 0)$-family and M-family. It has also been shown that those irreducible representations of O_h which form the $\Gamma(q = 0)$- and M-families are found in the low-lying part of the spectrum of the quantum cuboctahedron with half-integer spins $s = 1/2, 3/2, 5/2$ [19]. Figure 3 shows the colorings of the different classical ground state families of the cuboctahedron. In a classical picture each color refers to a sublattice with all spins pointing into the same direction. The angle between classical spins belonging to different sublattices is 120°.

In order to calculate the approximate spectrum of the system one is now left with the construction of basis states of the form $|\alpha\, S_1\, S_2\, S_3\, S\, M\rangle$, i.e. quasi-classical states. Therefore spins belonging to the same sublattice have to be coupled to yield the total sublattice spins $\underset{\sim}{\mathbf{S}}_1$, $\underset{\sim}{\mathbf{S}}_2$ and $\underset{\sim}{\mathbf{S}}_3$. Afterwards these total sublattice spins are coupled to the total spin $\underset{\sim}{\mathbf{S}}$. The underlying coupling scheme is given by a classical ground state, i.e. a coloring from Fig. 3 and incorporated in the quantum number α. In the following the resulting basis states will be labelled with respect to the classical reference state. To this end one has to distinguish between basis states of the form $|\gamma\, S_1\, S_2\, S_3\, S\, M\rangle_\Gamma$, $|\mu_1\, S_1\, S_2\, S_3\, S\, M\rangle_{M_1}$, $|\mu_2\, S_1\, S_2\, S_3\, S\, M\rangle_{M_2}$ and $|\mu_3\, S_1\, S_2\, S_3\, S\, M\rangle_{M_3}$. The notation of the set of intermediate quantum numbers and the subscript of the states now directly point to the classical ground state colorings, i.e. the underlying coupling scheme. It is important to note, that each of these four basis sets spans the same Hilbert space $\mathcal{H}(S, M)$.

In the case of the M-family three different colorings exist. When diagonalizing the Hamiltonian approximately while additionally using point-group symmetries one has to restrict to those symmetry groups where the symmetry operations do not alter the sublattice structure. A symmetry operation has no impact on the sublattice structure if the corresponding spin permutation results in recoloring of spins where all spins of a given sublattice maintain the same color, i.e. subscript (r: red, y: yellow, b: blue). For example an operation which leads to a cyclic permutation of colorings like

$$r \to y \to b \to r \tag{8}$$

has no impact on the sublattice structure.

While the sublattice structure of the $\Gamma(q = 0)$-family is left invariant under all symmetry operations of O_h, the sublattice structure (i.e. coloring) of the M-family is not. In order to restore the sublattice invariance of the classical ground state belonging to the M-family the basis states for the approximate diagonalization can be constructed from a usually overcomplete set M of basis states by an orthonormalization procedure. This set consists of rotational-band eigenstates from each coloring of the M-family, i.e. is given by

$$M = \left\{|\mu_1\, S_1\, S_2\, S_3\, S\, M\rangle^i_{M_1}\right\} + \left\{|\mu_2\, S_1\, S_2\, S_3\, S\, M\rangle^i_{M_2}\right\} + \left\{|\mu_3\, S_1\, S_2\, S_3\, S\, M\rangle^i_{M_3}\right\}\ , \tag{9}$$

while the index i is taking the values $1, \ldots, n_{\mathrm{red}}$. Here n_{red} reflects the overall number of states contained in the incorporated rotational bands which is independent of the choice of the coupling scheme.

Since the underlying coupling scheme is different regarding the chosen coloring these states have to be converted into an – in general – arbitrary reference scheme A before calculations can be performed. A transition between states belonging to different coupling schemes can be calculated using general recoupling coefficients [33,34]. For the transition of a basis state $|\mu_1\, S\, M\rangle_{M_1}$ referring to a coloring M_1 of the M-family into the scheme A one yields

$$|\mu_1\, S\, M\rangle_{M_1} = \sum_{\alpha, S_1, S_2, S_3} {}_A\langle\alpha\, S\, M|\mu_1\, S\, M\rangle_{M_1}\, |\alpha\, S\, M\rangle_A\ , \tag{10}$$

where the summation indices indicate that the summation is running over all valid combinations of values for the intermediate spin quantum numbers α as well as for the sublattice spin quantum numbers. The transitions between states of colorings M_2 and M_3 into the scheme A can be obtained analogously.

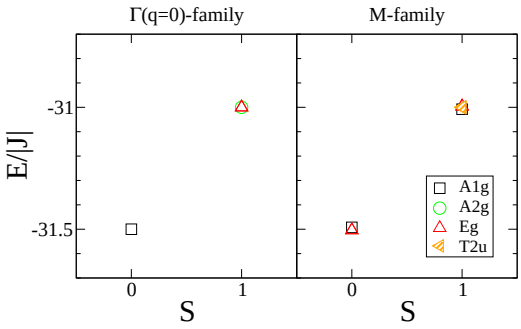

Figure 4. Classification by irreducible representations of O_h of the quasi-classical states with lowest energies of the $\Gamma(q = 0)$-family and M-family within $S = 0$ and $S = 1$ subspaces. The given energies refer to a diagonalization of the Heisenberg Hamiltonian exclusively within these quasi-classical states in the system with $s = 3/2$.

Figure 4 shows the classification of the quasi-classical states with lowest energies within $S = 0$ and $S = 1$ subspaces according to irreducible representations of O_h. It corresponds to an approximate diagonalization of $\underset{\sim}{H}_{\text{Heisenberg}}$ using only a reduced basis set of states from the lowest rotational band in the system with $s = 3/2$. Obviously the classification of the quasi-classical states is independent of the single spin quantum number s. Solely, the energies are changed when approximately diagonalizing the Hamiltonian of a system with different single spin quantum numbers. Based on a classical ground state belonging to the $\Gamma(q = 0)$-family the states belong to the irreducible representations A_{1g} ($S = 0$) and A_{2g}, E_g (S=1). Taking the M-family as a starting point for the construction of basis states the states belong to A_{1g}, E_g (S=0) and A_{1g}, E_g, T_{2u} (S=1) where the T_{2u}-state has apart from its intrinsic degeneration, i.e. the dimension of the irreducible representation T_{2u}, a twofold multiplicity.

The difference in the geometric properties of the lowest states of the chosen ground-state family, expressed by their decomposition into different irreducible representations, should directly lead to a convergence behaviour which depends on the choice of the underlying coloring. Since the approximate basis set contains energetically ordered states (from lowest to higher), low-lying states are expected to converge faster with growing number of basis states used for the approximate diagonalization [6].

3.1. Convergence of individual colorings

In Fig. 5 the approximate eigenvalues of a cuboctahedron with $s = 1$ and $s = 3/2$ in dependence on the number of incorporated bands within the $S = 0$ subspaces are shown. As underlying classical ground states for each system the $\Gamma(q = 0)$-family as well as one member of the M-family have been chosen. In every subfigure the last column refers to results from a complete diagonalization within $\mathcal{H}(S = 0)$. Since the $\Gamma(q = 0)$-family is invariant under O_h, the full point-group symmetry of a cuboctahedron (O_h) was used in order to classify the states. As mentioned before the individual members of the M-family are not invariant under O_h but under D_2. Thus, in this case the D_2 point-group symmetry was applied.

Looking at Fig. 5 it becomes apparent that the convergence is directly dependent on the choice of the underlying classical ground states. In agreement with theoretical expectations states which correspond to low-lying eigenstates of the rotational-band model converge faster than higher-lying states. Additionally, by comparing the spectra of $s = 1$ and $s = 3/2$ it can be seen that the ground state energy converges more rapidly with increasing single spin quantum number s. Nevertheless, apart from some states which exhibit a quite regular and fast convergence behaviour the convergence is – overall – rather poor. Especially the so-called low-lying singlet[1], which appears in the

[1] Here: the lowest E_g-state in the system with $s = 3/2$ based on a classical ground state coloring of the $\Gamma(q = 0)$-family.

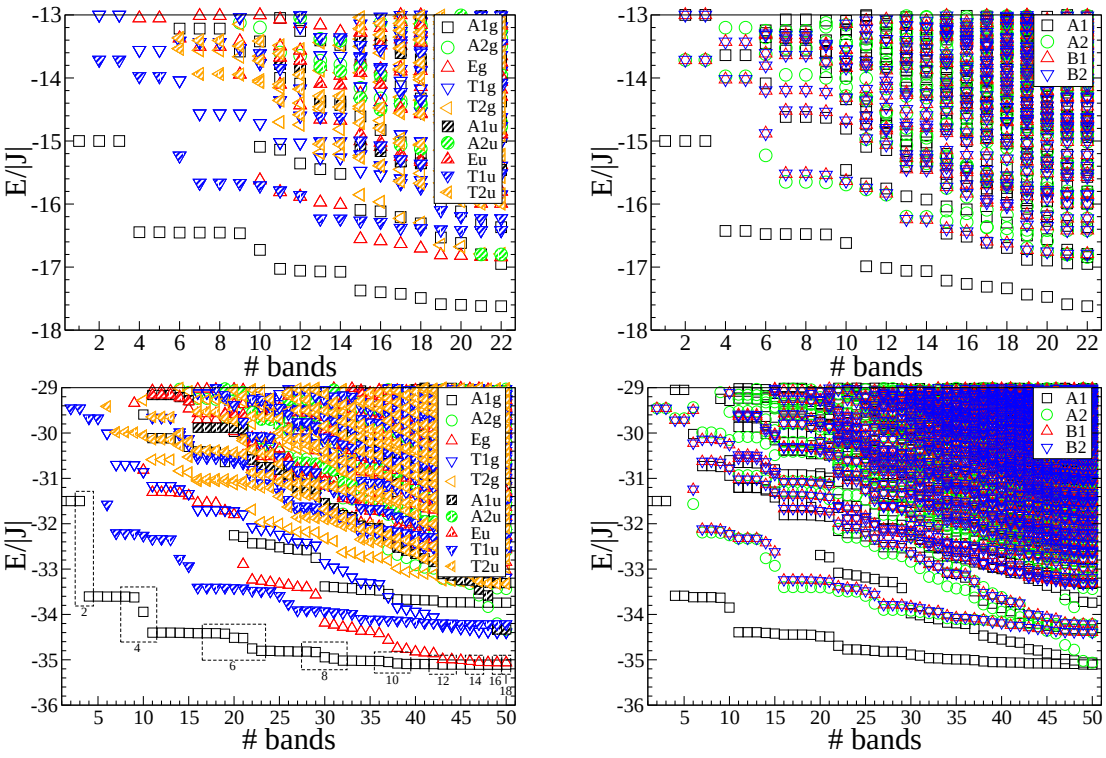

Figure 5. Low-lying energy spectra of a cuboctahedron with $s = 1$ (upper row) and $s = 3/2$ (lower row) within $S = 0$ subspaces using an increasing number of bands (states). The underlying classical ground states belong to the $\Gamma(q = 0)$-family (left) and to one coloring of the M-family (right) while O_h (left) and D_2 (right) point-group symmetries were used in order to classify the states. The dashed boxes in the lower left figure indicate regions, i.e super-bands, in which the energy of the ground state is considerably lowered. The numbers refer to the number of magnons of the super-bands.

case of half-integer spins s below the first triplet contributions, converges very slowly. This means that it is poorly approximated by one or a few eigenstates of the rotational-band Hamiltonian, but instead is a superposition of very many basis states.

One significant property which becomes evident when tracing single energy levels is that the convergence is stepwise – at least in the low-lying part of the spectra. Regions in which the ground state is considerably lowered are exemplarily marked with dashed boxes in the case of a cuboctahedron $s = 3/2$ assuming a classical reference state of the $\Gamma(q = 0)$-family. The numbers below the boxes refer to the number of magnons existing in the states of those rotational bands which are incorporated within the marked regions. Obviously the ground state energy is lowered whenever super-bands with an even number of magnons are incorporated in the approximate diagonalization. The observation of a stepwise convergence leads to a helpful additional approximation given by an approximate selection rule which is discussed below (see Sec. 3.4). It should be mentioned here that qualitatively the same convergence behaviour can be observed within subspaces of $S > 0$. However, additional information cannot be extracted from graphical visualizations of the convergence in these subspaces, thus they will not be presented here.

3.2. Convergence of combined colorings

In order to improve the convergence of the energy levels in comparison to the behaviour shown in Fig. 5 the decomposition of the quasi-classical states in Fig. 4 directly leads to the starting point. Since the quasi-classical states, that result from different colorings, can be classified according to

irreducible representations of $2A_{1g}$ and E_g, it is a straightforward task to use linear combinations of rotational-band eigenstates of the $\Gamma(q=0)$-family as well as of the M-family as basis states for the approximate diagonalization. The set of basis states results from an extension of M in Eq. (9) to

$$\begin{aligned} G = &\left\{|\mu_1\, S_1\, S_2\, S_3\, S\, M\rangle^i_{M_1}\right\} + \left\{|\mu_2\, S_1\, S_2\, S_3\, S\, M\rangle^i_{M_2}\right\} \\ &+ \left\{|\mu_3\, S_1\, S_2\, S_3\, S\, M\rangle^i_{M_3}\right\} + \left\{|\gamma\, S_1\, S_2\, S_3\, S\, M\rangle^i_{\Gamma}\right\} \end{aligned} \tag{11}$$

and subsequent orthonormalization of the incorporated states.

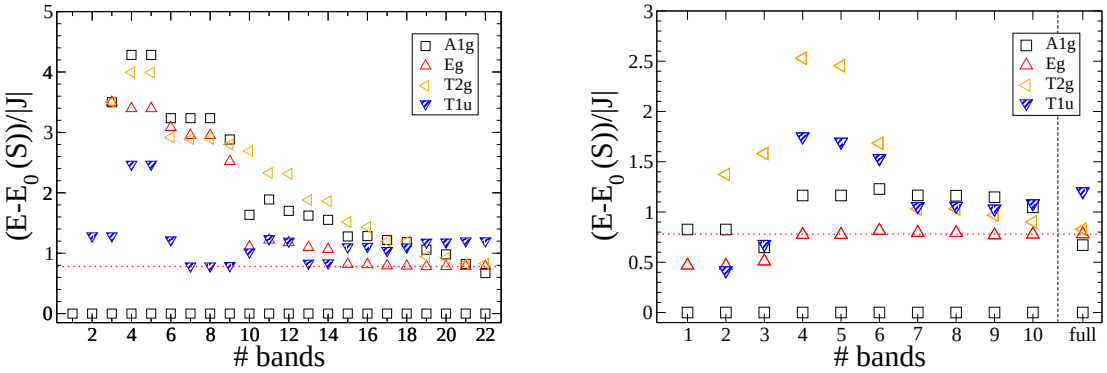

Figure 6. Energy difference to the ground state of selected low-lying energy levels of the cuboctahedron $s = 1$ within $S = 0$ subspace in dependence on the number of incorporated rotational bands. The reduced set of basis states is taken from rotational-band states of the $\Gamma(q = 0)$-family only (left) and from linear combinations of states of all four colorings (right). The classification is according to O_h point-group symmetry. The dotted red line refers to the exact difference to the E_g-state.

In Fig. 6 the energy difference between selected low-lying energy levels and the ground state of the system is displayed for a cuboctahedron $s = 1$ within $S = 0$ subspace. The difference is shown in dependence on the number of incorporated rotational bands. The last column refers in both subfigures to the exact values, taken from a complete diagonalization. The dotted red line indicates the energy difference to the E_g-state.

In the first case (left subfigure) only rotational-band states of the $\Gamma(q = 0)$-family are taken into account for the approximate diagonalization. In the second case (right subfigure) linear combinations of states of all four colorings are used. The first noticeable difference is that when taking basis states of all colorings into account the low-lying levels start and remain in close proximity to their final (true) value. This is especially obvious when comparing the convergence of the lowest E_g-state in both subfigures. The second difference is that when using linear combinations of states of all four colorings the convergence is smoother and more rapidly. This can be traced back to the fact that the different colorings contribute to low-lying states of different irreducible representations which in the other families would only be available as high-lying states. Therefore, it is advantageous to use fewer bands but basis states of all classical colorings for the approximate diagonalization.

A short explanation might be appropriate in order to understand why the energy differences sometimes increase when taking more states into account. This is due to the fact that the ground state in such cases converges more rapidly than the excited states. Although all approximate eigenvalues improve on an absolute scale the differences get worse for a moment.

3.3. Results

In this section we like to present how good thermodynamic observables can be approximated. Figure 7 shows the specific heat $C(T, B)$ (left) and the magnetic susceptibility dM/dB (right) for zero field $B = 0$ of a cuboctahedron $s = 3/2$. The energy spectrum of this system can be completely

calculated using irreducible tensor operator technique in combination with a D_2 point-group symmetry [35]. In Fig. 7 the exactly calculated specific heat and the susceptibility are compared with results from an approximate diagonalization using only states of the lowest rotational band in each coloring in order to set up the basis. We also show how these observables look like if evaluated with only the lowest rotational band (L-band) of $\underset{\sim}{H}_{\mathrm{RB}}$ (red colored energy levels in Fig. 2).

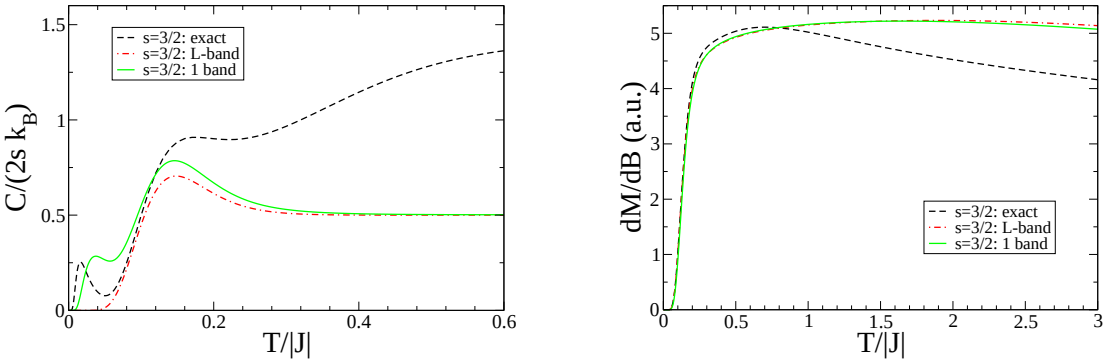

Figure 7. Comparison of approximate and exact specific heat $C(T, B)$ (left) and zero-field susceptibility dM/dB (right) for a cuboctahedron $s = 3/2$. The L-band refers to magnetic properties evaluated with the lowest band of the rotational-band Hamiltonian. For the approximate diagonalization only the states of the lowest rotational band but of each coloring are taken into account.

As one can see the low-temperature specific heat is very sensitive to the structure of low-lying levels. In the rotational-band model the lowest band (L-band) is gaped and describes a rotor. Therefore, the specific heat is suppressed at small temperatures and and higher temperatures approaches $3/2$ k_B. The approximate diagonalization, although only taking the lowest (L-band) states of all four coloring into account, achieves already an improvement for low-temperatures. The little Schottky-peak is the result of low-lying singlets and rearranging triplets. At higher temperatures this approximation displays the same behavior as the pure L-band which is expected since only L-band like states are incorporated.

In contrast to the specific heat which directly reflects the density of states within a certain energy interval the magnetic susceptibility reflects the density of magnetic states. To that end it is not surprising that the magnetic susceptibilities calculated from the approximate spectra do not considerably differ. Since the exact spectrum also possesses a rotational-band like behaviour at the lower edge the contributions from the approximate diagonalization and from the L-band reproduce the steep rise of the susceptibility for low temperatures very well. Obviously, the exact thermodynamical properties cannot be reproduced properly in the case of increasing temperature because the approximate spectra only contain a fraction of the energy levels of the full Hilbert space $\mathcal{H}$.

3.4. Approximate selection rule

As mentioned before (Sec. 3.1) the stepwise convergence behaviour leads to an approximate selection rule. Using this selection rule the computational effort when setting up the Hamilton matrices can be further reduced. In Fig. 5 it was shown that when diagonalizing in the $\Gamma(q = 0)$-family, regions can be marked in which single energy levels are affected by taking into account additional rotational-band states. The same can be done for the M-family. As it was already mentioned, the marked regions coincide with the incorporation of rotational-band states belonging to the same super-band.

Looking at Fig. 5 the approximate energy eigenvalues of the ground state are lowered whenever states $|\gamma\, S_1\, S_2\, S_3\, S\, M\rangle$ are additionally included which belong to a super-band with an even number of magnons. Since the convergence behaviour is state-sensitive the energy of the lowest states

belonging to the 3-dimensional irreducible representation T_{1u}, for example, is considerably lowered whenever super-bands with an odd number of magnons are included. This relation between the incorporation of super-bands and the immediate affection on the energies of certain approximate eigenstates can also be observed if the classical ground state belongs to the M-family.

As a result of the aforementioned observations a simple rule can be conjectured for low-lying energy levels $|S_{1,b}\, S_{2,b}\, S_{3,b}\, S\, M\rangle$. The matrix elements $\langle S_{1,a}\, S_{2,a}\, S_{3,a}\, S\, M|\underset{\sim}{H}|S_{1,b}\, S_{2,b}\, S_{3,b}\, S\, M\rangle$ connecting these states with other states $|S_{1,a}\, S_{2,a}\, S_{3,a}\, S\, M\rangle$ are one magnitude (or more) bigger than other matrix elements if

$$|n_a - n_b| \mod 2 = 0\ , \tag{12}$$

where $n_a = \sum_{i=1}^{3} S_{i,\max} - \sum_{i=1}^{3} S_{i,a}$ and n_b (similarly evaluated), denote the number of magnons of the super-bands the states are belonging to. The Hamilton matrices approximately split up according to Eq. (12). Thus, simultaneously computation time is saved and the dimensionality of the problem is reduced.

4. Summary

In this paper an approximate diagonalization scheme was proposed and used in order to determine the energy spectra of geometrically frustrated spin systems. As an example the cuboctahedron was discussed. It was shown that the convergence is clearly dependent on the coloring of the underlying classical ground state, i.e on the coupling scheme. Therefore, the approximation can be improved by using an adapted set of basis states that origin from rotational-band states of all possible sublattice colorings. Furthermore, it was shown that the approximate diagonalization is useful in order to study the low-temperature thermodynamics of geometrically frustrated systems, even in its simplest form when only states from one rotational band within each coloring are taken into account.

Although the necessary calculations are rather involved, especially for huge frustrated systems, the approximate diagonalization can be a valuable method. Numerically the evaluation of recoupling coefficients constitutes the strongest challenge, i.e. calculations are rather limited by runtime than by available memory. However, recent developments show that highly parallelized program code or public resource computing can help to overcome this barrier.

Acknowledgements

Computing time at the Leibniz Computing Centre in Garching is greatfully acknowledged as well as helpful advices of Mohammed Allalen. We also thank Boris Tsukerblat for fruitful discussions about the irreducible tensor operator technique. This work was supported within a Ph.D. program of the State of Lower Saxony in Osnabrück.

References

1. D. Gatteschi, L. Pardi, Gazz. Chim. Ital. **123** (1993) 231
2. J. J. Borras-Almenar, J. M. Clemente-Juan, E. Coronado, B. S. Tsukerblat, Inorg. Chem. **38** (1999) 6081
3. O. Waldmann, Phys. Rev. B **61** (2000), 9 6138
4. I. G. Bostrem, A. S. Ovchinnikov, V. E. Sinitsyn, Theor. Math. Phys. **149** (2006) 1527
5. V. E. Sinitsyn, I. G. Bostrem, A. S. Ovchinnikov, J. Phys. A-Math. Theor. **40** (2007), 4 645
6. R. Schnalle, J. Schnack, Phys. Rev. B **79** (2009), 10 104419
7. S. R. White, Phys. Rev. B **48** (1993) 10345
8. M. Exler, J. Schnack, Phys. Rev. B **67** (2003) 094440
9. U. Schollwöck, Rev. Mod. Phys. **77** (2005) 259
10. C. Lanczos, J. Res. Nat. Bur. Stand. **45** (1950) 255
11. A. W. Sandvik, J. Kurkijärvi, Phys. Rev. B **43** (1991) 5950
12. A. W. Sandvik, Phys. Rev. B **59** (1999) R14157

13. L. Engelhardt, M. Luban, Phys. Rev. B **73** (2006) 054430
14. J. Schulenburg, A. Honecker, J. Schnack, J. Richter, H.-J. Schmidt, Phys. Rev. Lett. **88** (2002) 167207
15. C. Schröder, H.-J. Schmidt, J. Schnack, M. Luban, Phys. Rev. Lett. **94** (2005) 207203
16. R. Schmidt, J. Schnack, J. Richter, J. Magn. Magn. Mater. **295** (2005) 164
17. J. Schnack, R. Schmidt, J. Richter, Phys. Rev. B **76** (2007) 054413
18. V. O. Garlea, S. E. Nagler, J. L. Zarestky, C. Stassis, D. Vaknin, P. Kögerler, D. F. McMorrow, C. Niedermayer, D. A. Tennant, B. Lake, Y. Qiu, M. Exler, J. Schnack, M. Luban, Phys. Rev. B **73** (2006) 024414
19. I. Rousochatzakis, A. M. Läuchli, F. Mila, Phys. Rev. B **77** (2008) 094420
20. A. J. Blake, R. O. Gould, C. M. Grant, P. E. Y. Milne, S. Parsons, R. E. P. Winpenny, J. Chem. Soc.-Dalton Trans. (1997) 485
21. A. Müller, S. Sarkar, N. Shah, H. Bögge, M. Schmidtmann, S. Sarkar, P. Kögerler, B. Hauptfleisch, A. X. Trautwein, V. Schünemann, Angew. Chem., Int. Ed. **38** (1999) 3238
22. A. Müller, M. Luban, C. Schröder, R. Modler, P. Kögerler, M. Axenovich, J. Schnack, P. C. Canfield, S. Bud'ko, N. Harrison, Chem. Phys. Chem. **2** (2001) 517
23. M. Axenovich, M. Luban, Phys. Rev. B **63** (2001) 100407
24. C. Schröder, R. Prozorov, P. Kögerler, M. D. Vannette, X. Fang, M. Luban, Phys. Rev. B **77** (2008) 224409
25. J. Schnack, M. Luban, Phys. Rev. B **63** (2000) 014418
26. J. Schnack, M. Luban, R. Modler, Europhys. Lett. **56** (2001) 863
27. O. Waldmann, Phys. Rev. B **75** (2007) 012415
28. D. A. Varshalovich, A. N. Moskalev, V. K. Khersonskii, *Quantum theory of angular momentum*, World Scientific Publishing (1988)
29. M. Tinkham, *Group theory and quantum mechanics*, Dover Publications, New York (2003)
30. E. Weisstein, *Mathworld*, URL `http://mathworld.wolfram.com`
31. O. Waldmann, Phys. Rev. B **65** (2001)
32. H.-J. Schmidt, M. Luban, J. Phys. A: Math. Gen. **36** (2003) 6351
33. V. Fack, S. N. Pitre, J. van der Jeugt, Comp. Phys. Comm. **86** (1995) 105
34. V. Fack, S. N. Pitre, J. van der Jeugt, Comp. Phys. Comm. **101** (1997) 155
35. J. Schnack, R. Schnalle, Polyhedron, doi:10.1016/j.poly.2008.10.017

3. Polyhedron 28, 1620 (2009)

Frustration effects in antiferromagnetic molecules: the cuboctahedron

Jürgen Schnack*,[a], Roman Schnalle[b]

[a] *Universität Bielefeld, Fakultät für Physik, D-33501 Bielefeld, Germany*
[b] *Universität Osnabrück, Fachbereich Physik, D-49069 Osnabrück, Germany*

Abstract

Frustration of magnetic systems which is caused by competing interactions is the driving force of several unusual phenomena such as plateaus and jumps of the magnetization curve as well as of unusual energy spectra with for instance many singlet levels below the first triplet state. The antiferromagnetic cuboctahedron can serve as a paradigmatic example of certain frustrated antiferromagnets. In addition it has the advantage that its complete energy spectrum can be obtained up to individual spin quantum numbers of $s = 3/2$ (16,777,216 states).

Key words: Magnetic Molecules, Heisenberg model, Antiferromagnets, Frustration, Energy spectrum
PACS: 75.50.Ee, 75.10.Jm, 75.50.Xx, 75.40.Mg, 24.10.Cn

1. Introduction

The magnetism of antiferromagnetically coupled and geometrically frustrated spin systems is a fascinating subject due to the richness of phenomena that are observed [1, 2]. Realizations of such systems exist in one, two, and three dimensions; the most famous being the two-dimensional kagome lattice [2, 3, 4, 5, 6, 7] and the three-dimensional pyrochlore antiferromagnet [8, 9, 10, 11, 12, 13, 14, 15, 16].

It is very interesting and from the point of theoretical modeling appealing that similar but zero-dimensional spin systems – in the form of magnetic molecules [17, 18, 19, 20, 21] – exist that potentially could show many of the special features of geometrically frustrated antiferromagnets. Figure 1 displays the zero-dimensional "little brothers" of the kagome antiferromagnet: the cuboctahedron which consists of squares surrounded by triangles and the icosidodecahedron which consists of pentagons surrounded by triangles. Such finite size antiferromagnets offer the possibility to discover and understand properties that are shared by the infinitely extended lattices. An example is the discovery of localized independent magnons [6, 22], which explain the unusual magnetization jump at the saturation field. Also the plateau at 1/3 of the saturation magnetization that appears in systems built of corner sharing triangles could be more deeply investigated by looking at the cuboctahedron and the icosidodecahedron [23, 24].

In this article we continue investigations along this line. We focus on two points. First we discuss the physics of the regular cuboctahedron as a function of the single spin quantum number $s = 1/2, 1, 3/2$. For these cases all energy eigenvalues could be obtained with the help of Irreducible Tensor Operator (ITO) techniques [25, 26, 27] and by application of point group symmetries. As a second point we investigate irregular cuboctahedra. This study is motivated by recent magnetization measurements of the icosidodecahedral molecules $\{Mo_{72}Fe_{30}\}$ [18] and $\{Mo_{72}Cr_{30}\}$ [20] published in Ref. [28] which could successfully be interpreted by a *classical* Heisenberg model with random antiferromagnetic exchange couplings between the paramagnetic ions.

*Tel: ++49 521 106-6193; fax -6455; jschnack@uni-bielefeld.de

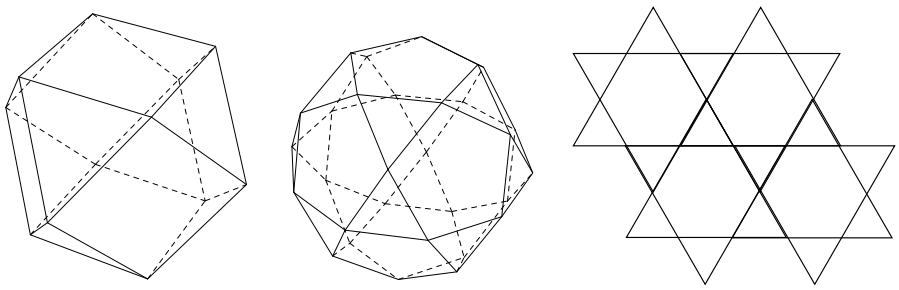

Figure 1: Cuboctahedron, icosidodecahedron, and (part of the) kagome lattice

2. Theoretical model

The physics of many of the mentioned spin systems can be well understood with the help of the isotropic Heisenberg model,

$$\underset{\sim}{H} \quad = \quad -2 \sum_{u<v} J_{uv}\, \underset{\sim}{\vec{s}}(u) \cdot \underset{\sim}{\vec{s}}(v) \ . \tag{1}$$

Here the sum runs over pairs of spins given by spin operators $\underset{\sim}{\vec{s}}$ at sites u and v. A negative value of the exchange interaction J_{uv} corresponds to antiferromagnetic coupling. We refer to a regular body, e.g. cuboctahedron, if there are only nearest neighbor couplings of constant size J. In the case of an irregular coupling the nearest-neighbor couplings can assume values according to the chosen distribution.

Since the Hamiltonian commutes with the total spin, we can find a common eigenbasis $\{\,|\,\nu\,\rangle\}$ of $\underset{\sim}{H}$, $\underset{\sim}{S}^2$, and $\underset{\sim}{S}_z$ and denote the related eigenvalues by E_ν, S_ν, and M_ν, respectively. The eigenvalues of (1) are evaluated in mutually orthogonal subspaces $\mathcal{H}(S,M)$ of total spin S and total magnetic quantum number M using Irreducible Tensor Operator (ITO) techniques [25, 26, 27]. In addition point group symmetries have been applied for the regular cuboctahedron.

3. The regular cuboctahedron

The regular cuboctahedron belongs to the class of geometrically frustrated antiferromagnets built of corner-sharing triangles. Such systems possess an extended magnetization plateau at 1/3 of the saturation magnetization $\mathcal{M}_{\rm sat}$ caused by dominant up-up-down contributions [23, 24], an unusually high jump of the magnetization at the saturation field due to independent magnons [22, 6] as well as low-lying singlets below the first triplet level [29, 30, 24]. These features are shared for instance by the icosidodecahedron and by the kagome lattice.

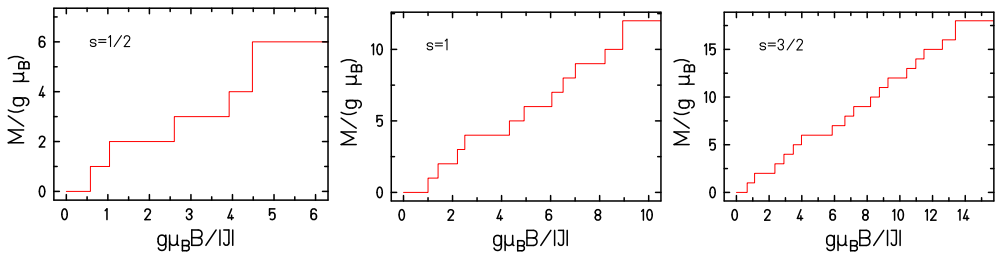

Figure 2: Magnetization as a function of applied field at $T = 0$ for the regular cuboctahedron with $s = 1/2$, $s = 1$, and $s = 3/2$. The extended plateau at $\mathcal{M}_{\rm sat}/3$ is clearly visible.

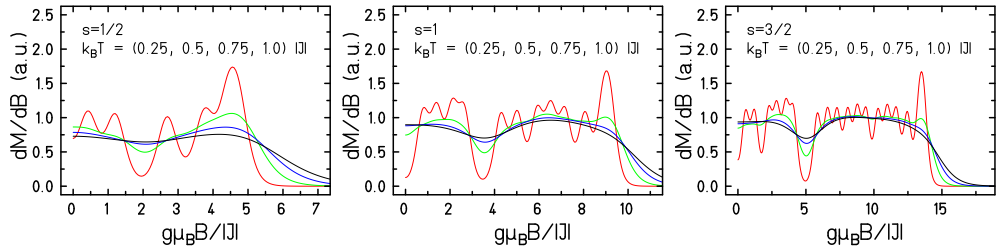

Figure 3: Differential susceptibility as a function of applied field at $k_BT/|J| = 0.25, 0.5, 0.75, 1.0$ for the regular cuboctahedron with $s = 1/2$, $s = 1$, and $s = 3/2$. The smoother the curve, the higher the temperature.

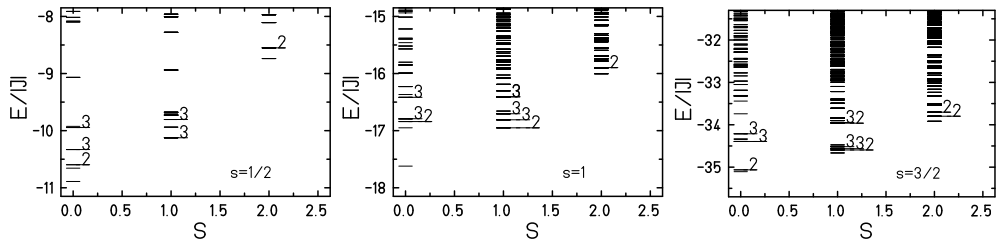

Figure 4: Low-lying energy levels for the regular cuboctahedron with $s = 1/2$, $s = 1$, and $s = 3/2$. Numbers attached to selected levels denote their multiplicities d_S; unlabeled levels below the highest labeled level have $d_S = 1$.

Figure 2 shows the magnetization curves at $T = 0$ for the regular cuboctahedron with $s = 1/2$, $s = 1$, and $s = 3/2$. These curves show besides the plateau at $\mathcal{M}_{\rm sat}/3$ a jump to saturation of height $\Delta M = 2$. Both features are reflected by the differential susceptibility function which is displayed in Fig. 3. Each step in Fig. 2 corresponds to a peak in Fig. 3. One notices that the peaks are washed out for higher temperatures, but that the minimum that corresponds to the plateau at $\mathcal{M}_{\rm sat}/3$ persists up to temperatures of the order of the exchange coupling.

As a function of the intrinsic spin s the differential susceptibility $\mathrm{d}\mathcal{M}/\mathrm{d}B$ exhibits two properties. With increasing spin quantum number s the individual peaks oscillate more and more with smaller relative amplitude, but the minimum at 1/3 is actually sharpened. It is known that in the classical limit, i.e. for $s \to \infty$, the differential susceptibility is practically flat below the saturation field except for the dip at 1/3 [23].

For zero field Fig. 4 shows the low-lying energy levels. In the case of $s = 1/2$ (l.h.s. of Fig. 4) one notices the low-lying singlets below the first triplet. These states are a cornerstone of geometric frustration and as well present in the kagome lattice and the icosidodecahedron with $s = 1/2$ [29]. It is interesting to note that with increasing s, i.e. towards a more classical behavior, the number of these states decreases. For $s = 1$ (middle of Fig. 4) the first excited singlet level is already (slightly) above the lowest triplet level. For $s = 3/2$ (r.h.s. of Fig. 4) a doubly degenerate excited singlet level remains below the lowest triplet, the others have disappeared. This behavior, i.e. no excited singlets below the lowest triplet for integer spins and a doubly degenerate excited singlet below the lowest triplet, does not change anymore for higher spin quantum numbers as can be checked e.g. by Lanczos methods.

The rather high symmetry of the cuboctahedron leads to many degenerate energy levels. As examples we label some low-lying energy levels in Fig. 4 by their multiplicity d_S, i.e. by the degeneracy of the whole multiplet. The full degeneracy including the multiplicity of the magnetic sublevels d_M is then $d = d_S \times d_M$. Clearly, such high multiplicities have an important impact on the magnetocaloric behavior since they increase the entropy for low temperatures [30, 31]. In the following we would like to discuss the impact of low-lying singlets below the first triplet which in the case of extended lattices are supposed to condense in infinite number onto the ground state.

Figure 5 compares the heat capacity (l.h.s.) and the zero-field susceptibility (r.h.s.) for the regular cuboctahedron with $s = 1/2$, $s = 1$, and $s = 3/2$. The heat capacity shows a pronounced double peak

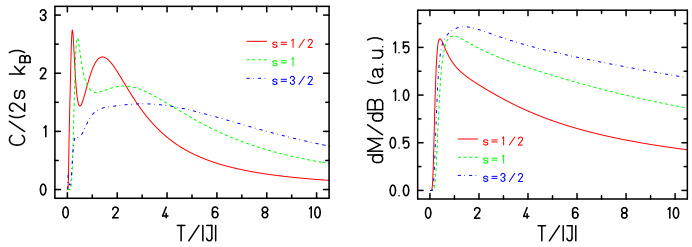

Figure 5: Heat capacity (l.h.s.) and zero-field susceptibility (r.h.s.) for the regular cuboctahedron with $s = 1/2$, $s = 1$, and $s = 3/2$.

structure for $s = 1/2$ and $s = 1$ which dissolves into a broad peak with increasing spin quantum number. The broad peak also moves to higher temperatures with increasing s. The reason for the first sharp peak is twofold. Since there are several gaps between the low-lying levels the density of states has a very discontinuous structure which results in the double peak structure. For $s = 1/2$ the low-lying singlets provide a very low-lying non-magnetic density of states which is responsible for the fact that the first sharp peak is at such low temperatures. For $s = 1$ the first sharp peak results from both excited singlet as well as lowest triplet levels. For $s = 3/2$ a remnant of the first sharp peak is still visible; it is given by the low-lying singlets, but since they are so few, also influenced by the lowest triplet levels.

The behavior of the heat capacity is contrasted by the susceptibility on the r.h.s. of Fig. 5 which reflects mostly the density of states of magnetic levels and is only weakly influenced by low-lying singlets. Therefore, the first sharp peak, or any other structure at very low temperatures, is absent .

4. The irregular cuboctahedron

In this section we investigate how the magnetic properties of the cuboctahedron change if random variations of the exchange coupling parameters are introduced. This study is motivated by recent magnetization measurements of the icosidodecahedral molecules $\{Mo_{72}Fe_{30}\}$ [18] and $\{Mo_{72}Cr_{30}\}$ [20] published in Ref. [28], which were interpreted by assuming random distributions of exchange parameters in a classical Heisenberg model description.

We introduce variations of the exchange parameters of the Hamiltonian (1) by replacing the common nearest neighbor exchange parameter $J_{uv} = J$ with values of a flat random distribution $J - 0.5\Delta \leq J_{uv} \leq J + 0.5\Delta$. Thus the mean exchange parameter is kept to be J. In order to gain sufficient statistical certainty we use ensembles of 10,000 spectra for realizations of the irregular cuboctahedron with $s = 1/2$; the results do not deviate from those for 1,000 realizations. For larger s the production of sufficiently large ensembles is hindered by prohibitively many diagonalizations of larger matrices.

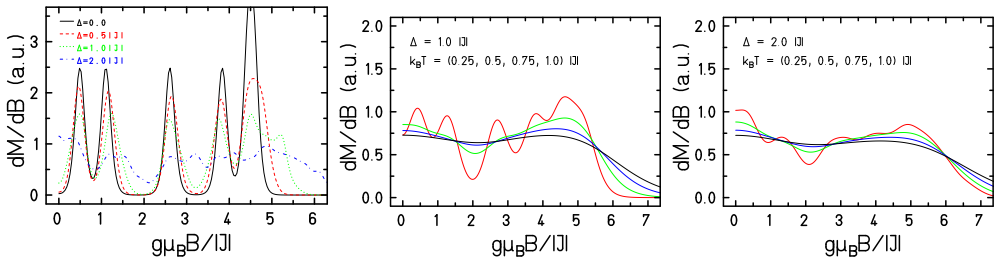

Figure 6: Differential susceptibility as a function of applied field for the irregular cuboctahedron with $s = 1/2$. L.h.s.: dependence on the width Δ of the random distribution. Middle: dependence on the temperature $k_BT/|J| = 0.25, 0.5, 0.75, 1.0$ for $\Delta = 1.0|J|$. R.h.s.: same as middle for $\Delta = 2.0|J|$.

Figure 6 shows the differential susceptibility that results from averages using distributions with various Δ. The figure on the l.h.s. compares $\mathrm{d}\mathcal{M}/\mathrm{d}B$ at the rather low temperature of $k_BT = 0.1|J|$ for $\Delta = 0$, i.e. the regular cuboctahedron, with $\Delta = 0.5|J|$, $\Delta = 1.0|J|$, and $\Delta = 2.0|J|$. One clearly sees that the pattern which mainly originates from ground state level crossings does not change much for $\Delta = 0.5|J|$ and $\Delta = 1.0|J|$. It needs a variation as large as $\Delta = 2.0|J|$, i.e. ferromagnetic interactions occur, to qualitatively change the differential susceptibility function. The reason is that smaller variations do no alter the structure of low-lying energy gaps. The singlet-triplet gap, which is approximately $0.765|J|$, does not vary very much for the ensembles with smaller Δ, and so does the singlet-triplet crossing which is determined by the singlet-triplet gap. It needs an appreciable variance of the exchange parameter distribution in order to impose large variations of the level crossing fields.

The middle and the r.h.s. of Fig. 6 display $\mathrm{d}\mathcal{M}/\mathrm{d}B$ for temperatures $k_BT/|J| = 0.25, 0.5, 0.75, 1.0$ and $\Delta = 1.0|J|$ and $\Delta = 2.0|J|$, respectively. As already explained, there is only very little difference between the behavior of an irregular cuboctahedron with $\Delta = 1.0|J|$ (middle) and the regular one. For $\Delta = 2.0|J|$ (r.h.s.) the differential susceptibility is much more smeared out which includes an appreciable broadening at the saturation field. Considering the irregular cuboctahedron we can conclude that the magnetic properties are rather stable against random fluctuations of the exchange parameters. This means that the striking behavior especially of the experimental differential susceptibility of $\{Mo_{72}Fe_{30}\}$ and $\{Mo_{72}Cr_{30}\}$ which shows no signs of level crossings at all [28] needs further theoretical exploration of the microscopic origin.

Acknowledgment

Computing time at the Leibniz Computer Center in Garching is greatly acknowledged as well as helpful openMP advices by Dieter an Mey and Christian Terboven of High Performance Computing, RWTH Aachen University. We thank Boris Tsukerblat for motivating discussions about the Irreducible Tensor Operator technique.

References

[1] A. P. Ramirez, Annu. Rev. Mater. Sci. **24** (1994) 453
[2] J. Greedan, J. Mater. Chem. **11** (2001) 37
[3] H. Diep, editor, *Magnetic systems with competing interactions*, World Scientific, Singapore (1994)
[4] Y. Narumi, K. Katsumata, Z. Honda, J.-C. Domenge, P. Sindzingre, C. Lhuillier, Y. Shimaoka, T. C. Kobayashi, K. Kindo, Europhys. Lett. **65** (2004) 705
[5] M. E. Zhitomirsky, Phys. Rev. Lett. **88** (2002) 057204
[6] J. Schulenburg, A. Honecker, J. Schnack, J. Richter, H.-J. Schmidt, Phys. Rev. Lett. **88** (2002) 167207
[7] J. L. Atwood, Nat. Mater. **1** (2002) 91
[8] O. Tchernyshyov, R. Moessner, S. L. Sondhi, Phys. Rev. Lett. **88** (2002), 6 067203
[9] R. Moessner, Can. J. Phys. **79** (2001) 1283
[10] S. T. Bramwell, M. J. P. Gingras, Science **294** (2001) 1495
[11] E. Berg, E. Altman, A. Auerbach, Phys. Rev. Lett. **90** (2003) 147204
[12] K. Penc, N. Shannon, H. Shiba, Phys. Rev. Lett. **93** (2004) 197203
[13] J.-H. Chung, M. Matsuda, S.-H. Lee, K. Kakurai, H. Ueda, T. J. Sato, H. Takagi, K.-P. Hong, S. Park, Phys. Rev. Lett. **95** (2005) 247204
[14] C. L. Henley, Phys. Rev. Lett. **96** (2006) 047201
[15] H.-J. Schmidt, J. Richter, R. Moessner, J. Phys. A: Math. Gen. **39** (2006) 10673
[16] M. E. Zhitomirsky, H. Tsunetsugu, Phys. Rev. B **75** (2007) 224416
[17] A. J. Blake, R. O. Gould, C. M. Grant, P. E. Y. Milne, S. Parsons, R. E. P. Winpenny, J. Chem. Soc.-Dalton Trans. (1997) 485
[18] A. Müller, S. Sarkar, S. Q. N. Shah, H. Bögge, M. Schmidtmann, S. Sarkar, P. Kögerler, B. Hauptfleisch, A. Trautwein, V. Schünemann, Angew. Chem., Int. Ed. **38** (1999) 3238
[19] A. Müller, A. M. Todea, J. van Slageren, M. Dressel, H. Bögge, M. Schmidtmann, M. Luban, L. Engelhardt, M. Rusu, Angew. Chem., Int. Ed. **44** (2005) 3857
[20] A. M. Todea, A. Merca, H. Bögge, J. van Slageren, M. Dressel, L. Engelhardt, M. Luban, T. Glaser, M. Henry, A. Müller, Angew. Chem. Int. Ed. **46** (2007) 6106
[21] C. P. Pradeep, D.-L. Long, P. Kögerler, L. Cronin, Chem. Commun. (2007) 4254
[22] J. Schnack, H.-J. Schmidt, J. Richter, J. Schulenburg, Eur. Phys. J. B **24** (2001) 475
[23] C. Schröder, H. Nojiri, J. Schnack, P. Hage, M. Luban, P. Kögerler, Phys. Rev. Lett. **94** (2005) 017205

[24] I. Rousochatzakis, A. M. Läuchli, F. Mila, Phys. Rev. B **77** (2008) 094420
[25] D. Gatteschi, L. Pardi, Gazz. Chim. Ital. **123** (1993) 231
[26] J. J. Borras-Almenar, J. M. Clemente-Juan, E. Coronado, B. S. Tsukerblat, Inorg. Chem. **38** (1999) 6081
[27] O. Waldmann, Phys. Rev. B **61** (2000) 6138
[28] C. Schröder, R. Prozorov, P. Kögerler, M. D. Vannette, X. Fang, M. Luban, A. Matsuo, K. Kindo, A. Müller, A. M. Todea, Phys. Rev. B **77** (2008) 224409
[29] R. Schmidt, J. Schnack, J. Richter, J. Magn. Magn. Mater. **295** (2005) 164
[30] J. Schnack, R. Schmidt, J. Richter, Phys. Rev. B **76** (2007) 054413
[31] A. Honecker, M. E. Zhitomirsky, J. Phys. Conf. Ser., in print; arXiv:0809.4414v1